Liquid-liquid microreactors for phase transfer catalysis

Liquid-liquid Microreactors for Phase Transfer Catalysis

PROEFSCHRIFT

ter verkrijging van de graad van doctor aan de

Technische Universiteit Eindhoven, op gezag van de

rector magnificus, prof.dr.ir. C.J. van Duijn, voor een

commissie aangewezen door het College voor

Promoties in het openbaar te verdedigen

op dinsdag 14 december 2011 om 14.00 uur

door

Jovan Jovanović

geboren te Beograd, Joegoslavië

Dit proefschrift is goedgekeurd door de promotor:

prof.dr.ir. J.C. Schouten

Copromotor:

dr. ir. T.A. Nijhuis

"What I cannot create, I do not understand."

Richard P. Feynman

Summary

Over the last decade microreactors have emerged as an attractive alternative to the conventional batch reactors commonly found in the chemical industry. The sub-millimeter inner diameter channels allow for surface-to-volume ratios above 10000 m^2/m^3, resulting in a significant intensification of the mass and heat transfer. Furthermore, the small volumes and laminar flow operation allow for reaction control otherwise unachievable in conventional stirred tank reactors. Consequently, higher product yields are achieved while the small size or microreactors allows for an increase in the process safety. Although significant research has been performed on single phase and gas-liquid systems in microreactors, relatively few studies exist on the liquid-liquid microreactor systems. One of the liquid-liquid chemical processes that would significantly benefit from microreactor application are those which are based on phase transfer catalysis. They employ catalysts which have the ability to penetrate the interface between two immiscible (liquid) phases, allowing for reactions to take place between otherwise nonreactive components. Consequently, phase transfer catalysis has found broad application in fine chemical, polymer and pharmaceutical industry.

Today, most of the phase transfer catalyzed reactions are performed in conventional stirred tank reactors. Conversion and selectivity of phase transfer catalyzed reactions in stirred tank reactors depend, among other things, on the interfacial area of the liquid drops in the mixed suspension in the reactor. These liquid drops have a wide range of size distribution as the result of an inhomogeneous energy dissipation induced by the mechanical stirring of the suspension. Consequently, the conversion and selectivity varies from drop to drop, lowering the product quality and incurring additional separation costs to eliminate unwanted byproducts. The high degree of reaction control achievable in microreactors, allows for highly selective synthesis. Therefore, the combination of phase transfer catalysis and microreactor technology could reduce mass transfer limitations and increase the selectivity and product yield. The goal of this thesis was to gain insight on the impact of flow on the reaction, thus allowing to develop liquid-liquid microreactors for phase transfer catalysis applications. The research was mainly focused on the capillary microreactor which, with four stable operating flow patterns and a throughput range from g/h to kg/h, presents an attractive alternative to chip-based and microstructured reactors for lab and pilot scale applications. The developed microreactors were applied for selective synthesis, kinetics study and chemical production via phase transfer catalysis.

In order to develop microreactors for phase transfer catalysis, first the hydrodynamics of the liquid-liquid flow in microchannels had to be understood. Furthermore, optimal flow patterns for reaction applications had to be identified. In chapter 2 the extraction of 2-butanol from toluene under different flow patterns in a water/toluene flow in a 250 µm inner-diameter capillary microreactors was studied. Four stable flow patterns were identified: annular, parallel, slug and bubbly flow. The influence of the capillary length, flow rate and aqueous-to-organic volumetric flow ratio on the flow pattern hydrodynamics was investigated. Weber number dependant flow maps were composed, which were used

to interpret the flow pattern formation in terms of surface tension and inertia forces. The flow patterns were evaluated in terms of stability, surface-to-volume ratio, achieved throughput and extraction efficiency. Slug and bubbly flow operation yielded 100 % thermodynamic extraction efficiency, while by increasing the aqueous-to-organic volumetric ratio to 9 allowed for 99 % 2-butanol extraction. The parallel and annular flow operational windows were limited by the capillary length, thus yielding maximal 2-butanol extraction of 30 and 47 %, for the parallel and annular flow, respectively.

The evaluation of flow patterns in chapter 2 showed that slug and bubbly flow pattern are most promising for reaction applications, due to large surface-to-volume ratios and extraction efficiencies. Slug flow was appropriate for low throughput applications, where long reaction times (>1 min) were required, while the bubbly flow was applicable in high throughput reaction systems with mass transfer limitations, which required short reaction times.

In chapter 3, the hydrodynamics and the pressure drop of liquid-liquid slug flow in capillary microreactor were studied on the example of water-toluene and ethylene glycol/water-toluene flows. The slug lengths of the alternating continuous and dispersed phases were measured as a function of the slug velocity, the volumetric flow ratio, and the capillary microreactor internal diameter. The pressure drop was modeled as the sum of two contributions: the frictional and the interface pressure drop. Two models were presented, viz. the stagnant film model and the moving film model, both accounting for the presence of a thin liquid film between the dispersed phase slug and the capillary wall. The stagnant film model was found to accurately predict the liquid-liquid slug flow pressure drop. The influence of inertia and the consequent change of the slug cap curvature are accounted for by modifying Bretherton's curvature parameter in the interface pressure drop equation. The stagnant film model was in good agreement with experimental data with a mean relative error of less than 7 %.

The high degree of control over the aqueous and organic slug interfacial area in a microchannel slug flow provides an attractive means to optimize yield and productivity of a phase transfer catalyzed reaction. In chapter 4 the selective alkylation of phenyl-acetonitrile to the monoalkylated product in a microchannel of 250 μm internal diameter operated continuously and solvent free in the slug flow regime was studied. The conversion of phenylacetonitrile increased from 40 % to 99 % as a result of 97 % larger slug surface-to-volume ratio when the volumetric aqueous-to-organic phase flow ratio was raised from 1.0 to 6.1 at the same residence time. The larger surface-to-volume ratio decreases selectivity due to the simultaneous increase of the rate of the consecutive reaction to the dialkylated product. Therefore, an optimum flow ratio with a maximal productivity was found, while achieving selectivity of 98 %. Conversion and selectivity in the microchannel reactor were both significantly larger than in a stirred reactor.

In chapter 5 the precise control over the slug lengths in a microreactor was employed to study a complex system of liquid-liquid phase transfer catalyzed alkylation of phenylacetonitrile in a basic medium. The influence of the surface-to-volume ratio, the reactant molar ratios, base and phase transfer catalyst concentrations on the reaction were

investigated in order to observe the reaction on the liquid-liquid interface. The interfacial reaction was interpreted with two proposed mechanisms existing in the literature: the Starks extraction and Makosza interfacial mechanisms. The kinetic study showed a strong indication that the reaction proceeds via the interfacial mechanism. Microreactor kinetic study allowed for a degree of surface-to-volume ratio control unachievable in stirred tank reactors, which was used to measure of the observed interfacial reaction rate constant.

The application of bubbly flow for phase transfer catalyzed production of benzyl benzoate was studied in chapter 6. An interdigital mixer - redispersion capillary reactor assembly was developed to prevent the liquid-liquid bubbly flow coalescence in microreactors. The application of constrictions to prevent coalescence resulted in a reproducibility increase by a factor of 6, achieving 33.4 % conversion in 10 s, compared to the 18.8 % in a capillary without the constrictions. By controlling the total flow rate and the aqueous-to-organic ratio the bubbly flow surface-to-volume ratio could be increased up to 230700 m^2/m^3, more than 100 times higher than in conventional stirred tank reactors. The increase of the redispersion capillary inner-diameter to 0.75 mm, allowed for the increase of the residence time to 67 s, resulting in a product yield of 98 %.

The developed process allowed for ton per annum benzyl benzoate production. Compared to the conventional phase transfer catalyzed esterification, the continuous operation in the interdigital-redispersion capillary assembly eliminated the use of solvents and bases, removing an energy intensive step of distillation, while increasing process safety.

Table of contents

Chapter 1. Introduction

1.1 Liquid-liquid reaction systems

Reactions involving two immiscible liquid phases can be found in all chemical industries, from petrochemical to fine chemical, pharmaceutical and biotechnology industry. Notable examples of liquid-liquid reaction systems that are widely used include Friedel-Crafts alkylation[1], aromatic nitration[2], ester hydrolysis[3], oxidations[4], phase transfer catalysis[5] and emulsion polymerization[6].

In a liquid-liquid reactor, the reaction rate is mainly controlled by three parameters: the mass transfer rate of the chemical species between the two immiscible liquid phases, chemical reaction in the bulk of the liquids and the reaction on the phase interface. Furthermore, in a typical liquid-liquid reaction system the overall reaction depends on the combination of the aforementioned parameters. The kinetics of these reactions often includes several parallel or consecutive reactions, affecting the yield and the purity of the final product. In the fine chemical and pharmaceutical processes, where high value, low volume products are used, the lower yield and the purity of the product often results in increased separation costs.

In the last 50 years one of the fastest growing number of liquid-liquid applications was in phase transfer catalysis (PTC) reactions, which has by 1994 grown to a market of 10 billion dollars per annum[7], with current processes operating with throughputs as high at 100000 t/annum[8]. PTC employs chemical compounds (e.g. quaternary ammonium salts) which are soluble in both the aqueous and organic phase, which induce reactions between otherwise immiscible and non reacting reactants. PTC technology enables the use of mild aqueous bases, such as sodium hydroxide, in where normally aggressive bases, such as metalhydrides, would be required[9,10]. Furthermore, conversion[11] and selectivity[12] are

significantly increased compared to traditional methods while limiting side reactions[10]. Consequently, significant reductions in material costs are achieved, allowing for the effective competition of Western producers with the low cost fine chemical producers from China and India.These advantages make PTC a widely applied method in the fine chemicals industry, for alkylation, arylation, condensation and carbene addition reactions[10,13]. Today, phase transfer catalyzed reactions are carried out in stirred tank reactiors, a non ideal solution which often brings about drawbacks such as loss of selectivity and catalyst deactivation due to the inefficient agitation.

1.2 Liquid-liquid reactions in stirred tanks

Liquid-liquid heterogeneous reactions are most commonly carried out in mechanically stirred tank reactors, while to a lesser extent in packed, agitated or spray columns and static mixers[14]. The stirred tank reactor can be operated in batch, semi batch or continuous mode. The most common reactor employed in the fine chemical and pharmaceutical industry is the batch reactor. The wide application of the batch reactor stems from its flexibility, as gases, liquids and solids can be employed without significant reactor modification. In liquid-liquid reaction systems the reaction rate is highly dependent on the interfacial area as both the liquid-liquid extraction and interfacial reaction rate are highly dependent on it. Depending on the reactor volume and type of mechanical agitator the industrial stirred tank reactors can achieve interfacial areas from 100 to 1000 m^2/m^3 [15]. Often the agitation is not sufficiently increasing the interfacial area of the generated liquid-liquid dispersions, resulting in long reaction times needed to complete the reaction. Alternatives such as impinging-streams[16] and rotating disk contactors[17] were developed; however the fine chemical and pharmaceutical industry is rather conservative to accept them. To this date one of the most common technical solutions for the low interfacial areas achieved in batch reactors is the surfactant addition[18] which often leads to increased separation costs.

One of the main drawbacks of the stirred tank reactors is the inhomogeneous mixing induced by the stirrer, resulting in temperature and concentration gradients (Figure 1). Furthermore, the stirrer generates dispersions with a wide droplet size distribution which often differs from one batch to another. Systems where an intermediate product is desired or where parallel reactions occur often are not suitable for stirred tank batch reactors[19] as the product quality will vary at the end of each batch campaign, therefore increasing the separation costs. Last, due to the inhomogeneous mixing hotspots can occur, resulting in runaway reactions severely decreasing the safety of operation[20].
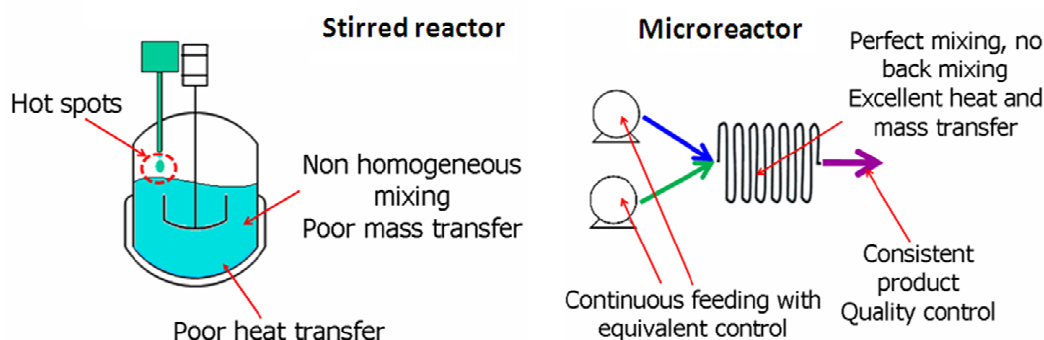
Figure 1: Stirred tank reactor vs. the continuous microreactor

In recent years microreactors have been put in the spotlight as emerging technology that could replace the batch reactor and potentially revolutionize the fine chemical and pharmaceutical industry[21].

1.3 Microreactors: state of the art

Microreactors gained much attention as a promising alternative to conventional reactors, allowing for higher mass transfer and product yield as well as increase in the process safety[22]. With decreasing linear dimensions significant increase of the surface-to-volume ratio is achieved. For the channel diameter from tens to hundreds of micrometers, the surface-to-volume ratio in the range of 10000 to 50000 m^2/m^3 is achieved[23]. Consequently, significant intensification of mass and heat transfer can be achieved, resulting in considerable reduction in operation times[24]. Additionally, microreactors can be operated at high pressures (up to 600 bar in stainless steel microreactors), therefore opening a path to novel process windows[25] where a significant intensification of the reaction rate can be achieved by operating at high pressures and temperatures[26] or in explosive regimes[27]. Microreactors were successfully applied in extraction[28], chemical synthesis[29] and biotechnology[30]. Furthermore, laminar flow operation and interface control allow for a level of reaction control otherwise unachievable in conventional stirred tank reactors[31]. Consequently, the performance of microreactors was found to outperform the structured reactors such as monolith, fixed bed and solid foams as shown in examples of methanol-steam reforming[32] and Fischer-Tropsch synthesis[33].

The microreactor research today utilizes a wide range of technical solutions which include: mesh[34], catalyst-trap[35], micro-packed bed[36], falling film[37], and meandering channel[38] microreactors. Although there are a large number of variations, most of the microreactors can be roughly classified according to their structure and throughput to: chip, capillary, microstructured and industrial microreactors (Figure 2).
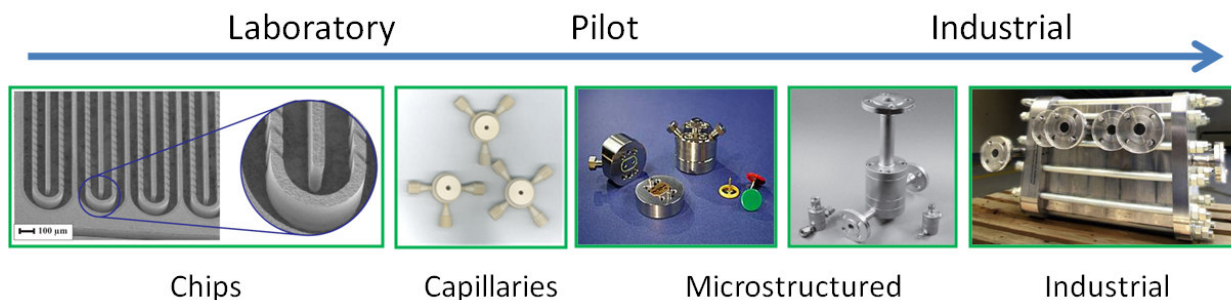
Figure 2: Four main classes of microreactors: chip[39], capillary, microstructured[40] and industrial microreactors[41]

A comparison of estimated surface-to-volume ratios, characteristic internal dimensions and throughput ranges of the four aforementioned classes of microreactors is shown in Figure 3. Chip and capillary microreactors are commonly found with channel diameters below 250 µm, therefore allowing them to achieve surface-to-volume above 50000 m^2/m^3. Chip based microreactors are usually made of glass[29], silicon[42], PDMS (Polydimethylsiloxane)[28] and PMMA (Polymethyl methacrylate)[43]. The designs of the chip microreactors can range from simple Y or T shapes to complex microstructures as shown in Figure 2. Due to their material properties, the chips often have to be operated at low pressures[44-46], thus limiting their industrial application. A promising alternative to the chips is the application of low cost T and Y couples and capillaries as microreactor systems[47,48]. The couples and capillaries can be made from stainless steel or chemically resistant high performance polymers such as PEEK, thus allowing pressure operation up to 450 bar. Moreover, the couples come in a range of geometries, such as T, Y or X thus eliminating the need for on-chip mixers. The main drawback of capillary microreactors lays their scale-up. Unlike chips, where multiple parallel channels can be etched on a single chip, scale-up of capillaries requires the employment of a large number of capillaries and manifolds.

Microstructured reactors are usually made of glass, stainless steel or highly resistant alloys such as Hastelloy. They employ more complex mixing elements than the T or Y geometries, such as the interdigital[49] or "split and recombine"[50] mixer. Combining small internal dimensions with specially designed mixers, allows for surface-to-volume ratios above 10000 m^2/m^3 for liquid-liquid extraction, with throughput in the l/h range[51]. Stainless steel, alloy and glass industrial microreactors have already found their place in chemical production in a number of companies such as DSM[52], Lonza[53], Degussa and Bayer[54].
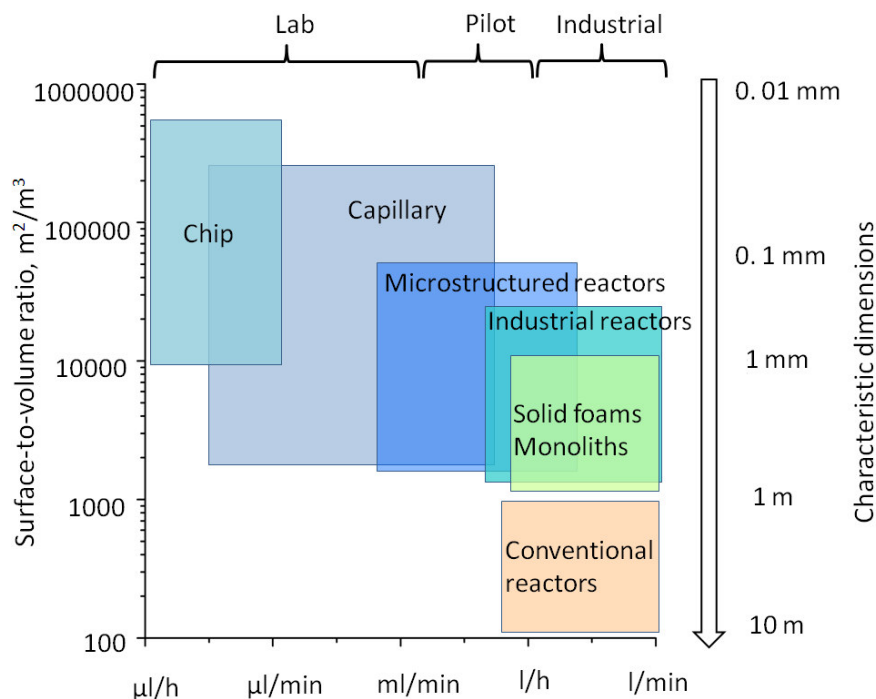
Figure 3: Surface-to-volume ratio, characteristic internal dimensions and throughput ranges of the chip, capillary, microstructured and industrial microreactors when compared to the solid foam, monolith and conventional reactors.

Scale-up of the microreactors is an ongoing challenge, as two approaches exist:

- Parallelization, whereby large number of identical microchannels are employed (Figure 4 a).
- Internal scale-up, whereby a combination of microsturctured reactor design and conventional dimension scale-up is applied (Figure 4 b).

Parallelization was demonstrated as an efficient method in the case of single phase or gas-solid reaction systems. Ohio based Velosys, has been one of the pioneers of microreactor parallelization concept for GTL applications[57]. Internal scale-up, is highly promising although not widely employed approach, with most application reports coming from the Swiss company Lonza[53].

Last, the small sizes of microreactors, excellent safety profile coupled with their high performance have been touted as one of the future tools of modular chemical production. Consequently, a quick modification of production capacity would be possible, allowing the producer to adapt to both periods of demand growth and demand destruction (Figure 5).

a.   **b.**
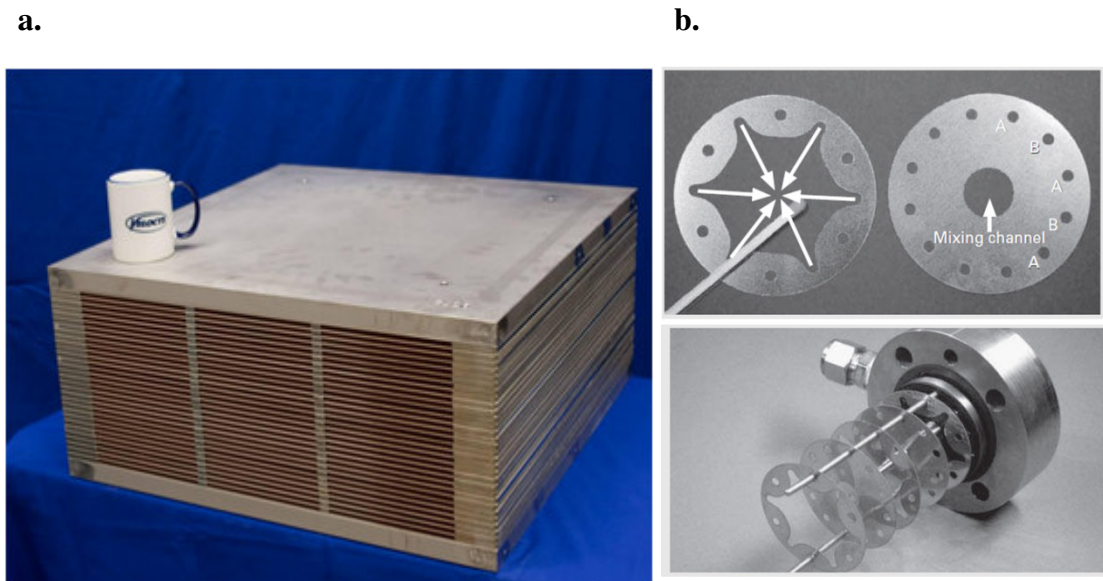
*Figure 4: Scale-up by parallelization (Velocys GTL microreactor[55]) (**a.**) and internal scaling-up (IMM StarLaminator[56]) (**b.**)*
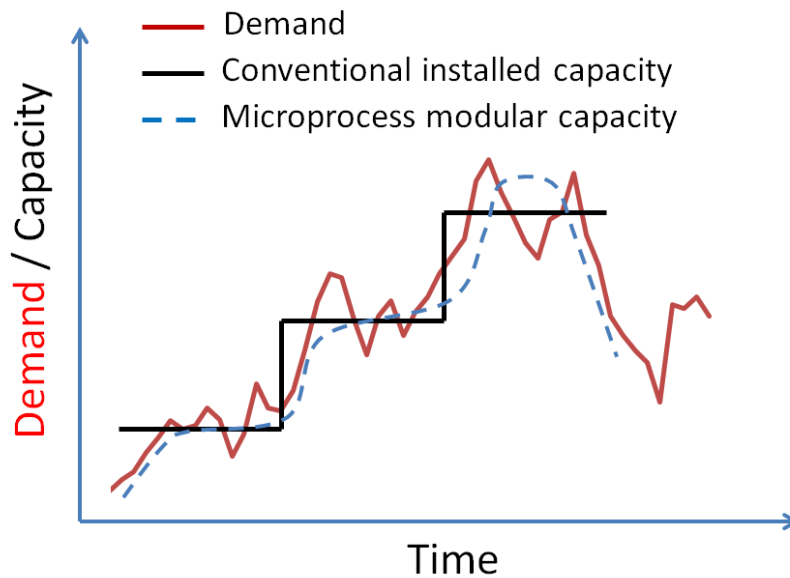
Figure 5: Modular microprocess production allows for addition and removal of production capacity, thus enabling a quick response for change in product demand compared to conventional production.

Table 1: Overview of industrially relevant liquid-liquid microreactor studies found in literature.

Reaction	Remarks
Hydrodehalogenation[61,62]	Yields from 69 to 100 % achieved at residence times from 8 to 10 s. The use of microreactor resulted in 30 % increase in selectivity compared to the batch process.
Acylation of amines[63]	Combinatorial chemistry allowing for parallel synthesis. The yields were in the range from 80 to 95 %.
Nitration of aromatics[64,65]	Yields of 60-94 % comparable to conventional production methods. Lower temperature and increased safety of operation. Residence times more than 5 times shorter than in conventional production.
Diazo coupling[66]	Conversion (>99 %) is higher than in any macroscopic system at residence times of 2.3 s. Improved selectivity and safety of the process.
Isomerization of allyl alcohols[67]	Yields comparable to those in conventional batch reactor. Depending on the alcohol used (C_4-C_8), the yields range from 1 to 61 %.
Photocyanation of aromatics[68]	Yields from 28 to 73 %. Two operation regimes investigated: oil-water and water-oil-water. Residence times from 70 to 210 s.
Nitration of aliphatics[69]	Yields from 75 to 90 % with selectivity up to 100 %.
Dihydro addition[70]	Yields up to 80 % achieved using a microgrid for dispersing the phases coupled with a micromixer
Heck reaction[71]	Heck reaction rates of reactions performed in microreactors were higher than in conventional reaction flasks. Two flow regimes were investigated: laminar and segmented flow. By operating in segmented flow regime the reaction yields were increased by more than 10 %.
Malonic ester methylation[72]	The segmented flow regime achieved by alternating pumping resulted in reaction yields from 19.8 to 28.2 %. The batch reaction yield for the same reaction times was 23 %.
Phase transfer alkylation[73]	Yields were from 75-96 % in a microreactor vs. 49 % in a conventional batch reactor. The residence times employed were 2-10 min.
Indigo synthesis[74]	Operation in a bubbly flow regime prevented the clogging of the microreactor by the precipitating reaction product. The maximum yields obtained were 87-97 %.
Strecker reaction[75]	Reaction yields from 43 to 67 %. The in situ production of HCN coupled with small volume processing greatly increases the safety of this reaction system.

1.4 Liquid-liquid microreactors

Unlike the gas-liquid[58-60] and single phase microreactor systems, relatively few studies were done on liquid-liquid systems in microchannels. Hydrodynamic studies performed in gas-liquid and liquid-liquid systems, showed the existence of a number of flow patterns such as the slug, bubbly, parallel and annular flow. Although a number of flow patterns were identified, no classification was made in terms of mass transfer characteristics and reaction application. An overview of industrially relevant liquid-liquid microreactor studies is shown in Table 1. Most attention was given to slug flow, where it was successfully demonstrated in the case of industrially significant nitrations[64,65,69] and alkyations[73].

Furthermore, extensive studies have been performed on the slug flow size control and the numerous reports were made of the significant improvements in yield in slug flow, yet little effort was made to understand the link between the slug hydrodynamics and reaction control. Few pressure drop studies on the liquid-liquid slug flow were performed, with no accurate models for the hydrodynamic resistance in a two phase flow. Therefore, the understanding of liquid-liquid flow hydrodynamics in microchannels, flow pattern interfacial areas and pressure drop is essential for the design of liquid-liquid microreactors. Finally, scale-up via parallelization in multiphase systems represents a challenge as flow maldistributions are common[76].

1.5 Scope and outline

The research was carried out within the NWO/CW TOP project "Smart structured reactors". The goal of the project was to develop new types of microstructured multiphase reactors, with full control over the interfacial areas and with an optimal balance between pressure drop, mass transfer, and catalytic reactivity. These new reactors would render major yield and selectivity improvements by complete control of the interaction of physical transport and reaction processes. The improvements were demonstrated on the examples of phase transfer catalyzed reactions employed in the synthesis, kinetic study and chemical production applications. The research was focused on the capillary and microstructured reactors. The achievable throughputs range from g/h to kg/h, therefore presenting an attractive alternative to chip-based reactors for lab and pilot scale applications. As a result, novel processes for fine chemical and pharmaceutical industry were developed resulting in optimal space-time yields and minimum waste production.

In order to design a multiphase microreactor, first the hydrodynamic flow patterns have to be analyzed. In chapter 2, the results of a liquid-liquid flow pattern study in capillary microreactor are presented. The flow patterns were evaluated in terms of stability, surface-to-volume ratio, achieved throughput and efficiency of the desired product from one phase into another. The flow maps were composed using Weber number as coordinates, thus allowing the interpretation of the flow pattern formation in terms of surface tension and

inertia forces. The influence of the capillary length, flow rate and aqueous-to-organic volumetric flow ratio on the slug, bubbly, parallel and annular flow hydrodynamics was investigated. Furthermore, the extraction of 2-butanol under different flow patterns was studied.

The hydrodynamics and the pressure drop of liquid-liquid slug flow in round capillary microreactor are further investigated in chapter 3. Two liquid-liquid flow systems are considered, the water-toluene and ethylene glycol/water-toluene flow. The slug lengths of the alternating continuous and dispersed phases were measured as a function of the slug velocity, the volumetric flow ratio, and the capillary internal diameter. The pressure drop was modeled as the sum of two contributions: the frictional and the interface pressure drop. The influence of inertia and the consequent change of the slug cap curvature were accounted for by modifying Bretherton's curvature parameter in the interface pressure drop equation.

In chapter 4, an emerging methodology in microreactor research, "fluidic reaction control" is investigated. As a result, precise control over the interfacial area of aqueous and organic slugs in segmented flow in a microchannel reactor providing an attractive means to optimize yield and productivity of a phase transfer catalyzed reaction. The selective alkylation of phenylacetonitrile to the monoalkylated product in a microchannel of 250 μm internal diameter operated continuously and solvent free in the slug flow regime was studied. Optimum flow conditions for maximal productivity and comparison with the conventional batch reactor are discussed.

Chapter 5 describes the application of capillary microreactors as tools for kinetics studies. The fluidic control over the interfaces in a microreactor was employed to study a complex system of liquid-liquid phase transfer catalyzed alkylation of phenylacetonitrile in a basic medium. The influence of the surface-to-volume ratio, the reactant molar ratios, hydroxide and phase transfer catalyst concentrations on the reaction were investigated in order to observe the reaction on the liquid-liquid interface. The interfacial reaction was interpreted with two proposed mechanisms existing in the literature: the Starks extraction and Makosza interfacial mechanisms. The interfacial mechanism was modified in order to observe the interfacial reaction, allowing for the measurement of the observed interfacial reaction rate constant.

Chapter 6 focuses on the scale-up of the capillary microreactor system to t/annum scale, by employing an internal scale-up principle. A novel interdigital mixer - redispersion capillary reactor assembly was developed. The system was tested on the phase transfer catalyzed esterification to produce benzyl benzoate. The bubbly flow generated by the interdigital mixer-redispersion capillary assembly was studied as a function of capillary length and flow rates. The benefits of the novel process compared to the conventional phase transfer catalyzed esterification process in terms of yield, safety and waste reduction are discussed. Finally, the main conclusions and recommendations are presented in chapter 7.

References

(1)   Ladnak, V.; Hofmann, N.; Brausch, N.; Wasserscheid, P. Continuous, Ionic Liquid-Catalysed Propylation of Toluene in a Liquid-Liquid Biphasic Reaction Mode using a Loop Reactor Concept. *Adv. Synth. Catal.* 2007, *349*, 719.

(2)   Zaldivar, J.M.; Molga, E.; Alos, M.A.; Hernandez, H.; Westerterp, K.R. Aromatic nitrations by mixed acid. Fast liquid-liquid reaction regime, *Chem. Eng. Process.* 1996, *35*, 91.

(3)   Brockmann, R.; Demmering, G.; Kreutzer, U.; Lindemann, M.; Plachenka, J.; Steinberger, U. Fatty acids in Ullmann's Encyclopedia of Industrial Chemistry, Wiley-VCH Verlag GmbH & Co. KGaA, 2002.

(4)   Ballini, R.; Petrini, M. Recent synthetic developments in the nitro to carbonyl conversion (Nef reaction), *Tetrahedron* 2004, *60*, 1017.

(5)   Starks, C.; Liotta, C.; Halpern, M. Phase-transfer catalysis: fundamentals, applications and industrial perspectives. Chapman&Hall, London, 1994.

(6)   Gilbert, R. G. Emulsion Polymerization: a Mechanistic Approach, Academic Press, London, 1996.

(7)   Halpern, M. Practical Phase Transfer Catalysis, *PTC Comm.*, 1999, *2*, 167.

(8)   Halpern, M. Increasing Plant Profits by Phase-Transfer Catalysis Retrofit, *PTC Comm.*, 1996, *2*, 1.

(9)   March, J. Advanced organic chemistry: reactions, mechanisms and structure, 4th ed., Wiley-Interscience, New York, 1992.

(10) Makosza, M. Two-phase reactions in the chemistry of carbanions and halocarbenes: a useful tool in organic synthesis. *Pure Appl. Chem.* 1975, *43*, 439.

(11) Makosza, M.; Jagusztyn-Grochowska, M.; Ludwikow, M.; Jawdosiuk, M. Reactios of organic anions: reactions of phenylacetonitrile derivatives with aromatic nitrocompounds in basic media. *Tetrahedron* 1974, *30*, 3723.

(12) Naik, S.D.; Doraiswamy, L.K. Phase transfer catalysis: chemistry and engineering. *AIChE J.* 1998, *44*, 612.

(13) Freedman, H.H. Industrial applications of phase transfer catalysis (PTC): past, present and future. *Pure Appl. Chem.* 1986, *58*, 857.

(14) Trambouze, P.; Euzen, J.P. Chemical Reactors: From Design to Operation. Editions Technip, Paris, 2004.

(15) Perry, R. H.; Green, D. W. Perry's Chemical Engineers Handbook, 7th ed., McGraw-Hill, New York, 1997.

(16) Dehkordi, A. M. Liquid–Liquid Extraction with an Interphase Chemical Reaction in an Air-Driven Two-Impinging-Streams Reactor: Effective Interfacial Area and Overall Mass-Transfer Coefficient. *Ind. Eng. Chem. Res.* 2002, *41*, 4085.

(17) Sarker, S.; Mumford, C. J.; Phillips, C.R. Liquid-Liquid Extraction with Interphase Chemical Reaction in Agitated Columns. 2. Hydrodynamics and Mass Transfer in Rotating Disk and Oldshue Rushton Contactors. *Ind. Eng. Chem. Process Des. Dev.* 1980, *19*, 672.

(18) Lele, S.S.; Bhave, R.R.; Sharma, M.M. Fast liquid-liquid reactions: role of emulsifiers. *Ind. Eng. Chem. Process Des. Dev.* 1983, *22*, 73.

(19) de Bellefon, C.; Caravieilhes, S.; Joly-Vuillemin, C.; Schweich, D.; Berthod, A. A liquid-liquid plug-flow continuous reactor for the investigation of catalytic reactions: The centrifugal partition chromatograph, *Chem. Eng. Sci.* 1998, *53*, 71.

(20) Steensma, M.; Westerterp, K.R. Thermally safe operation of a semibatch reactor for liquid-liquid reactions-fast reactions. *Chem. Eng. Technol.* 1991, *14*, 367.

(21) Roberge, D. M.; Ducry, L.; Bieler, N.; Cretton, P.; Zimmermann B. Microreactor Technology: A Revolution for the Fine Chemical and Pharmaceutical Industries? *Chem. Eng. Technol.* 2005, *28*, 318.

(22) Heugebaert, T.S.A.; Roman, B. I.; De Blieck, A.; Stevens, C. V. A safe production method for acetone   cyanohydrin, *Tetrahedron Lett.* 2010, *51*, 4189.

(23) Hessel, V.; Hardt, S.; Löwe, H. Chemical Micro-process Engineering – Fundamentals, Modeling and Reactions, Wiley-VCH, Weinheim, 2004.

(24) Lomel, S.; Falk, L.; Commenge, J. M.; Houzelot, J. L.; Ramdani, K. The microreactor. A systematic and efficient tool for the transition from batch to continuous process? *Chem. Eng. Res. Des.* 2006, *84*, 363.

(25) Illg, T.; Lob, P.; Hessel, V. Flow chemistry using milli- and microstructured reactors-From conventional to novel process windows, *Bioorg. Med. Chem.* 2010, *18*, 3707.

(26) Razzaq, T.; Kappe, C.O. Continuous flow organic synthesis under high-temperature/pressure conditions, *Chem. Asian J.* 2010, *5*, 1274.

(27) Voloshin, Y.; Halder, R.; Lawal, A. Kinetics of hydrogen peroxide synthesis by direct combination of H_2 and O_2 in a microreactor. *Catal. Today* 2007, *125,* 40.

(28) Fries, D. M.; Voitl, T.; von Rohr, P. R.; Liquid extraction of vanillin in rectangular microreactors. *Chem. Eng. Technol.* 2008, *31*, 1182.

(29) Garcia-Egido, E.; Spikmans, V.; Wong, S. Y. F.; Warrington, B.H. Synthesis and analysis of combinatorial libraries performed in an automated micro reactor system. *Lab Chip* 2003, *3*, 73.

(30) Anderson, R. C.; Su, X.; Bogdan, G. J.; Fenton, J. A miniature integrated device for automated multistep genetic assays. *Nucleic Acids Res.* 2000, *28*, 1.

(31) Jovanović, J.; Rebrov, E.V.; Nijhuis, T. A.; Hessel, V.; Schouten, J.C. Phase-Transfer Catalysis in Segmented Flow in a Microchannel: Fluidic Control of Selectivity and Productivity. *Ind. Eng. Chem. Res.* 2010, *49*, 2681.

(32) Delsman, E.R.; Laarhoven, B.J.P.F.; de Croon, M.H.J.M.; Kramer, G.J.; Schouten, J.C. Comparison Between Conventional Fixed-Bed and Microreactor Technology for a Portable Hydrogen Production Case, *Chem. Eng. Res. Des.* 2005, *83*, 1063.

(33) Almeida, L.C.; Echave, F.J.; Sanz, O.; Centeno, M.A.; Arzamendi, G.; Gandia, L.M.; Sousa-Aguiar, E.F.; Odriozola, J.A.; Montes, M. Fischer-Tropsch synthesis in microchannels, *Chem. Eng. J.* 2010, *126*, 536.

(34) Amador, C.; Wenn, D.; Shaw, J.; Gavriilidis, A.; Angeli, P. Design of a mesh microreactor for even flow distribution and narrow residence time distribution, *Chem. Eng. J.* 2008, *135*, S259.

(35) Huang, J.; Weinstein, J.; Besser, R.S. Particle loading in a catalyst-trap microreactor: Experiment vs. simulation, *Chem. Eng. J.* 2009, *155*, 388.

(36) Su, Y.; Zhao, Y.; Chen, G.; Yuan, Q. Liquid-liquid two-phase flow and mass transfer characteristics in packed microchannels, *Chem. Eng. Sci.* 2010, *65*, 3947.

(37) Ziegenbalg, D.; Lob, P.; Al-Rawashdeh, M.; Kralisch, D.; Hessel, V.; Schonfeld, F. Use of "smart interfaces" to improve the liquid-sided mass transport in a falling film microreactor, *Chem. Eng. Sci.* 2010, *65*, 3557.

(38) Fries, D. M.; von Rohr, P.R. Liquid mixing in gas-liquid two-phase flow by meandering microchannels, *Chem. Eng. Sci.* 2009, *64*, 1326.

(39) Ehrfeld, W.; Gärtner, C.; Golbig, K.; Hessel, V.; Konrad, R.; Löwe, H.; Richter, T.; Schulz, C. Fabricationof components and systems for chemical and biological microreactors, *Proc. of the 1st Int. Conf. on Microreaction Technology* 1997, 72.

(40) http://www.imm-mainz.de/index.php?id=2670

(41) http://www.dsm.com/en_US/downloads/media/backgrounder_micro_reactor.pdf

(42) Henriksen, T.R; Olsen, J.L; Vesborg, P.; Chorkendorff, I.; Hansen, O. Highly sensitive silicon microreactor for catalyst testing. *Rev. Sci. Instrum.* 2009, *80*, 124101-1.

(43) Ahmed-Omer, B.; Barrow, D.; Wirth, T. Effect of segmented fluid flow, sonication and phase transfer catalysis on biphasic reactions in capillary microreactors. *Chem. Eng. J.* 2008, *135S*, S280.

(44) Gray, B.L.; Jaeggo, D.; Mourlas, N.J.; van Drieënhuizen, B.P.; Williams, K.R.; Maluf, N.I.; Kovacs, G.T.A. Novel interconnection technologies for integrated microfluidic systems, *Sens. Actuators*, *A* 1999, *77*, 57.

(45) Andersson, H.; van der Wijngaart, W.; Enoksson, P.; Stemme, G. Micromachined flow-through filter-chamber for chemical reactions on beads, *Sens. Actuators, B* 2000, *67*, 203.

(46) Chiou, C.H.; Lee, G.B.; Hsu, H.T.; Chen, P.W.; Liao, P.C. Micro devices integrated with microchannels and electrospray nozzles using PDMS casting techniques, *Sens. Actuators, B* 2000, *86* , 280.

(47) Dummann, G.; Quittmann, U.; Groschel, L.; Agar, D. W.; Worz, O.; Morgenschweis, K. The capillary-microreactor: a new reactor concept for the intensification of heat and mass transfer in liquid-liquid reactions, *Catal. Today* 2003, *79*, 433.

(48) Nielsen, C.A.; Chrisman, R.W.; LaPointe, R.E.; Miller, T.E. Novel Tubing Microreactor for Monitoring Chemical Reactions. *Anal. Chem.* 2002, *74*, 3112.

(49) Hessel, V.; Hardt, S.; Löwe, H.; Schönfeld F. Laminar mixing in different interdigital micromixers: I. Experimental characterization. *AIChE J.* 2003, *49*, 566.

(50) Zuidhof, K. T.; de Croon, M. H. J. M.; Schouten J. C. Beckmann rearrangement of cyclohexanone oxime to ε-caprolactam in microreactors. *AIChE J.* 2010, *56*, 1297.

(51) Benz, K.; Jäckel, K.P.; Regenauer, K.J.; Schiewe, J.; Drese, K.; Ehrfeld, W.; Hessel, V.; Löwe H. Utilization of Micromixers for Extraction Processes. *Chem. Eng. Technol.* 2001, *24*, 11.

(52) Lerou, J.J.; Tonkovich, A.L.; Silva, L.; Perry, S.; McDaniel, J. Microchannel reactor architecture enables greener processes, *Chem. Eng. Sci.* 2010, *65*, 380.

(53) Kockmann, N.; Gottsponer, M.; Roberge, D. M. Scale-up concept of single-channel microreactors from process development to industrial production*, Chem. Eng. J.* 2011, *167*, 718.

(54) Hessel, V.; Knobloch, C.; Löwe, H. Review on patents in microreactor and micro process engineering. *Recent Patents on Chemical Engineering* 2008, *1*, 1.

(55) http://www.velocys.com/docs/NGCS_Presentation_3-Jun-10_redacted.pdf

(56) http://www.imm-mainz.de/fileadmin/IMM-upload/Flyer-Katalog_etc/Catalogue09_StarLam.pdf

(57) Deshmukh, S.R.; Tonkovich,A. L. Y.; Jarosch, K.T.; Schrader, L.; Fitzgerald, S.P.; Kilanowski, D.R.; Lerou, J.J.; Mazanec, T.J. Scale-Up of Microchannel Reactors For Fischer−Tropsch Synthesis. *Ind.Eng.Chem.Res.* 2010, *49*, 10883.

(58) Chen, I.Y.; Yang, K.S.; Wang, C.C. An empirical correlation for two-phase frictional performance in small diameter tubes. *Int. J. Heat Mass Transf.* 2002, *45*, 3667.

(59) Chung, P.M.Y.; Kawaji, M.; The effect of channel diameter on adiabatic two-phase flow characteristics in microchannels. *Int. J. Multiphas. Flow* 2004, *30*, 735.

(60) Warnier, M.J.F.; de Croon, H.J.M; Rebrov, E.V.; Schouten, J.C. Pressure drop of gas-liquid Taylor flow in round microcapillaries for low to intermediate Reynolds numbers. *Microfluid. Nanofluid.* 2009, *8*, 33.

(61) Floyd, T. M.; Jensen, K. F.; Schmidt, M. A.; Towards integration of chemical detection for liquid phase microchannel reactors. *Proceedings of the 4th International Conference on Microreaction Technology* 2000, 461.

(62) Herweck, T.; Hardt, S.; Hessel, V.; Löwe, H.; Hofmann, C.; Weise, F.; Dietrich, T.; Freitag, A. Visualization of flow patterns and chemical synthesis in transparent microreactors, *Proceedings of the 5th International Conference on Microreaction Technology* 2001, 215.

(63) Kikutani, Y.; Hisamoto, H.; Tokeshi, M.; Kitamori, T. Fabrication of a glass microchip with three-dimensional microchannel network for 2 x 2 parallel synthesis, *Lab. Chip* 2002, *2,* 188.

(64) Burns, J. R.; Ramshaw, C.; Development of a microreactor for chemical production, *Trans. Inst. Chem. Eng.* 1998, *77*, 206.

(65) Ducry, L.; Roberge, D. M. Controlled autocatalytic nitration of phenol in a microreactor *Angew. Chem.* 2005, *117*, 8186.

(66) Hisamoto, H.; Saito, T.; Tokeshi, M.; Hibara, A.; Kitamori, T. Fast and high conversion phase-transfer synthesis exploiting the liquid-liquid interface formed in a microchannel chip. *Chem. Commun.* 2001, *24*, 2662.

(67) de Bellefon, C.; Tanchoux, N.; Caravieilhes, S.; Grenoullet, P.; Hessel, V. Microreactors for dynamic, high-throughput screening of fluid/liquid molecular catalysis. *Angew. Chem., Int. Ed.* 2000, *39*, 3442.

(68) Ueno, K.; Kitagawa, F.; Kitamura, N. Photocyanation of pyrene across an oil/water interface in a polymer microchannel chip. *Lab. Chip* 2002, *2*, 231.

(69) Antes, J.; Turcke, T.; Kerth, J.; Marioth, E.; Schnurer, F.; Krause, H. H.; Lobbecke, S. Application of microreactors for the nitration of ureas. *32nd International Annual Conference of ICT (Energetic Materials)* 2001, 146.

(70) Wiles, C.; Watts, P.; Haswell, S.J.; Pombo-Villar, E.; 1,4-Addition of enolates to α,β -unsaturated ketones within a micro reactor. *Lab. Chip* 2002, *2*, 62.

(71) Ahmed, B.; Barrow, D.; Wirth, T. Enhancement of reaction rates by segmented fluid flow in capillary scale reactors. *Adv. Synth. Catal.* 2006, *348*, 1043.

(72) Okamoto, H. Effect of alternating pumping of two reactants into a microchannel on a phase transfer reaction. *Chem. Eng. Technol.* 2006, *29*, 504.

(73) Ueno, M.; Hisamoto, H.; Kitamori, T.; Kobayashi, S. Phase-transfer alkylation reactions using microreactors. *Chem. Commun.* 2003, *8*, 936.

(74) Poe, S.L.; Cummings, M.A.; Haaf, M.P.; McQuade, D.T. Solving the clogging problem: precipitate-forming reactions in flow. *Angew. Chem.* 2006, *45*, 1544.

(75) Acke, D.R.J.; Stevens, C.V. A HCN -based reaction under microreactor conditions: industrially feasible and continuous synthesis of 3,4-diamino-1H-isochromen-1-ones. *Green Chem.* 2007, *9*, 386.

(76) Yue, J.; Boichot, R.; Luo, L.; Gonthier, Y.; Chen, G.;Yuan, Q. Flow distribution and mass transfer in a parallel microchannel contactor integrated with constructal distributors *AIChE J.* 2010, *56*, 1547.

Chapter 2. Liquid-liquid flow patterns in a capillary microreactor: stability, surface-to-volume ratios, and extraction performance

Abstract

The capillary microreactor, with four stable operating flow patterns and a throughput range from g/h to kg/h, presents an attractive alternative to chip-based and microstructured reactors for lab and pilot scale applications. In this chapter the extraction of 2-butanol from toluene under different flow patterns in a water/toluene flow in long capillary microreactors is presented. The influence of the capillary length (0.2-2.2 m), flow rate (0.1-12 ml/min) and aqueous-to-organic volumetric flow ratio (0.25-9) on the slug, bubbly, parallel and annular flow hydrodynamics was investigated. Weber number dependant flow maps were composed for capillary lengths of 0.4 and 2 m, which are used to interpret the flow pattern formation in terms of surface tension and inertia forces. By decreasing the capillary length from 2 to 0.4 m, the transition of annular to parallel flow was observed. The capillary length had little influence on the slug and bubbly flows. The flow patterns were evaluated in terms of stability, surface-to-volume ratio, achieved throughput and extraction efficiency. Slug and bubbly flow operation yielded 100 % thermodynamic extraction efficiency, while by increasing the aqueous-to-organic volumetric ratio to 9 allowed for 99 % 2-butanol extraction. The parallel and annular flow operational windows were limited by the capillary length, thus yielding maximal 2-butanol extraction of 30 and 47 %, for the parallel and annular flow, respectively.

2. 1 Introduction

When operating on a lab scale, chips and capillaries are commonly employed as microreactors[1, 2]. In comparison to chips, there exist several advantages of capillary systems, apart from low-cost building blocks: First, residence time can be varied over a wide range without changing flow patterns. Usually in the microreactor based reaction studies, the residence time is changed by altering the flow rates[3]. In multiphase systems varying the flow rate to alter the residence time will result in change of flow patterns[4,5], consequently changing the reaction conditions (Figure 1). It is much better to change residence time by changing the reactor length at a constant flow rate. On chip, longer channels may be difficult to fabricate, a limitation that does not hold for capillaries, which are easily longer than 10 m as shown in chapter 4. Second, the transparency of the capillary is easily achieved by employing fused silica or PTFE capillaries. Last, the capillary microreactor system can be easily assembled and modified, thus allowing one assembly to perform a function for which multiple chips would be needed.

Detailed knowledge about the hydrodynamics that are occurring in multiphase reactors are of crucial importance as different flow patterns influence the mass transfer and axial dispersion, which each directly impact the conversion and selectivity of the reaction. Compared to the large number of liquid-liquid hydrodynamic studies in performed in microchips[4-11] there exist relatively few studies of the different flow patterns in a capillary microreactor system[12]. Depending on the total flow rate and the volumetric flow ratio, several liquid-liquid flow patterns are achievable in microchannels, such as: annular, parallel, bubbly or slug flow[13]. In literature most attention has been given to the liquid-liquid slug flow [12,14,15] while the studies of other flow patterns are scarce. Furthermore, there are no studies reported in the literature on the influence of microchannel length on the hydrodynamics of liquid-liquid flow patterns.

Increase flow

Change the slug size

Transition to parallel flow
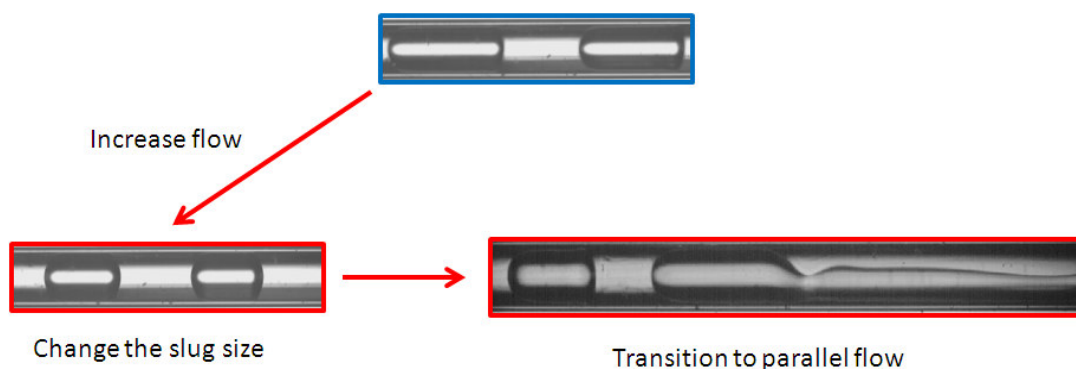
Figure 1: Multiphase studies in chips: increase of flowrate in order to change the residence time, results in flow pattern transition.

This study is focused on the extraction of 2-butanol from toluene under different flow patterns in a water/toluene flow in long capillary microreactors. While significant improvements in mass transfer are achieved in microreactors, the extraction efficiency has only been studied under slug and parallel flow [4, 16]. In this study the influence of the

capillary length, flow rate and volumetric flow ratio on the flow pattern hydrodynamics has been investigated. A Y-mixer was used due its ability to form reproducible flow patterns[12]. The flow patterns were evaluated in terms of stability, surface-to-volume ratio, achieved throughput and extraction efficiency.

2.2 Experimental

Chemicals. All chemicals used in this work are commercially available GC grade and were obtained from Sigma-Aldrich. The organic phase consisted of 18.0 wt% solution 2-butanol in toluene. Decahydronaphthalene was used as the internal standard in the organic phase for the GC analysis, at a concentration of 0.57 mol/L. The aqueous phase was demineralized water.

Physical Properties. The interfacial surface tension between the aqueous and organic phases was measured via a Krüss K11 tensiometer at 20 °C. The viscosity was measured with a Brookfield LVDV-I Prime viscometer at 20 °C. The physical properties of the liquids used in the experiments are shown in Table 1. The contact angles were measured by taking high resolution pictures of drops on a fused silica plate immersed in toluene and demineralized water, for demineralized water and toluene drops, respectively. The values of the contact angles were measured by analyzing the high resolution images with the Matlab[TM] software.

Table 1: Physical properties of the studied system

Mixture	Density, kg/m^3	Viscosity, Pa·s	Surface tension, N/m
2-butanol/toluene	0.867[a]	$5.9 \cdot 10^{-4}$ [a]	$3.85 \cdot 10^{-2}$ [a]
Demineralized H$_2$O	0.998[b]	10^{-3} [b]	-

a-experimental
b-taken from Perry et al. (1997)

Experimental setup. A schematic view of the experimental set-up is given in Figure 2. The system consists of two HPLC pumps (Shimadzu LC-20AD) which feed the organic and aqueous phases to a stainless steel Y-mixer. In order to eliminate any flow disturbances caused by the HPLC pump pulsation, 1 m long PEEK constrictions with a 150 µm inner diameter were used in both lines. The internal diameter of the Y-mixer inlets and outlet was 250 µm, with an angle of 110° between the two inlet lines. A transparent fused silica microcapillary with an internal diameter of 250 µm was connected to the Y-mixer. In the experiments, the length of the fused silica microcapillary was varied from 0.2 to 2.2 m. Experiments were performed at flow rates of 0.05 – 8.0 ml/min, and organic-to-aqueous flow ratios of 1.0 – 9.0.

The liquid-liquid flow was visualized under a microscope (Zeiss Axiovert) and recorded by a high speed camera (Redlake MotionPro CCD) at 2500 frames per second. The calculation of the slug lengths and the interfacial surface areas was performed via image analysis using the Matlab^{TM} software.

Analysis. The organic phase was quantitatively analyzed using a Varian CP-3800 gas chromatograph equipped with a 30 m x 0.25 mm CP-Sil 5 CB column and a FID detector.

Mass transfer in the sampling zone. The overall mass transfer in the microreactor system includes the contributions from the Y-mixer, capillary, and the receiving container. The mass transfer in the mixer and capillary cannot be physically decoupled, thus they are measured together[17]. Furthermore, due to the large differences in flow rates of the individual flow patterns (from 0.1 to 12 ml/min), separate sampling methods were employed.

The slug flow was studied at flow rates from 0.1 to 0.6 ml/min. A 4 mm inner diameter glass tube with a thin PTFE tape bottom was used to minimize the contact time in the sampling vessel. The aqueous phase was removed by a syringe via the PTFE bottom, thus limiting the mass transfer time to no longer than 5 s. Organic phase samples of 5 μl were taken by a syringe via the PTFE bottom and analyzed via the gas chromatograph.

Stable dispersions were formed in the sampling vessel under bubbly flow. The washing of the dispersion with toluene induced phase separation. The sampling was performed in a 2 ml vial containing 0.7 ml of toluene and 0.7 ml of demineralized water. The capillary outlet was placed near the phase interface, thus allowing quick separation. Each sample was collected for 2 s.

The efficiency of the sampling under slug and bubbly flows was tested by directing the aqueous and organic feed lines in the sampling vessel. The measurements showed average deviations of the organic inlet concentration of 5.4 % and 6.2 % for the slug and bubbly flows, respectively. Those were deemed sufficient for the extraction experiments.

The high total flow rates (3-12 ml/min) corresponding to annular and parallel flows caused aqueous and organic phase redispersion and interface disruptions in the sampling vessel, creating significant mass transfer during sampling. In order to ensure the validity of the measured data, the mass transfer in the sampling vessel was measured. The sampling vial was modeled as a constant volume semibatch system with mass transfer, described as:

$$\frac{dC_{org}}{dt} = -k_L a \left(C_{org} - K_{2-BuOH} C_{aq} \right) + \frac{F_{org} C_{org,0}}{V_{org}} \tag{1}$$

where C_{org} and C_{aq} are the organic and aqueous concentrations, respectively; F_{org} is the organic flow rate (1.5-6 ml/min); V_{org} is the organic phase volume in the vial (0.3 ml); K_{2-BuOH} is the partition coefficient (0.94 at the AO ratio of 1) and $k_L a$ is the vial mass transfer coefficient. Samples of 10 μl were collected at different time intervals in order to estimate the average mass transfer coefficient in the vessel (Figure 3), which was determined from

Eq. 1, via the least square method. In order to verify the k_La values from vial mass transfer model, the vial mass transfer coefficient was determined by using the Eq. 9 from the results section. The mean difference between the k_La values acquired via the Eq.1 and Eq.9 was 6.5 %. Therefore the k_La results were deemed sufficient for the calculation of the organic concentration at the capillary outlet via Eq.1. For all annular and parallel flow mass transfer measurements, the sampling time was 2 s.

Emulsion stability. The stability of emulsions generated by the bubbly flow was analyzed by aging 20 ml emulsion samples in 50 ml vials at 20 °C and 40 °C. The aging was performed in a Heraeus Instruments T-6120 oven.

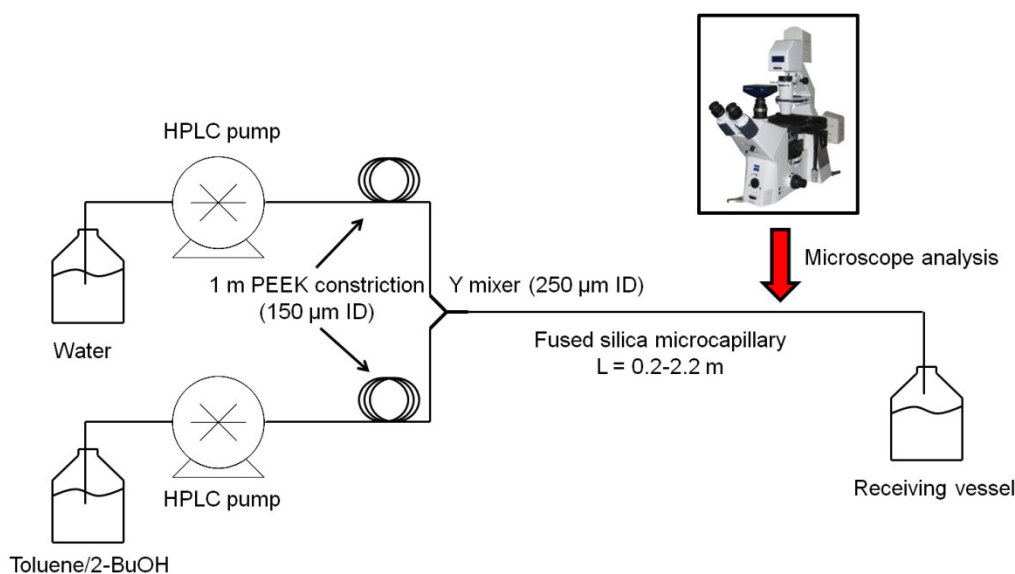*Figure 2: Experimental setup: stainless steel Y-mixer coupled with a 250 µm internal-diameter fused silica capillary. Supply of the organic and aqueous mixtures was provided by two HPLC pumps (Shimadzu LC-20AD).*
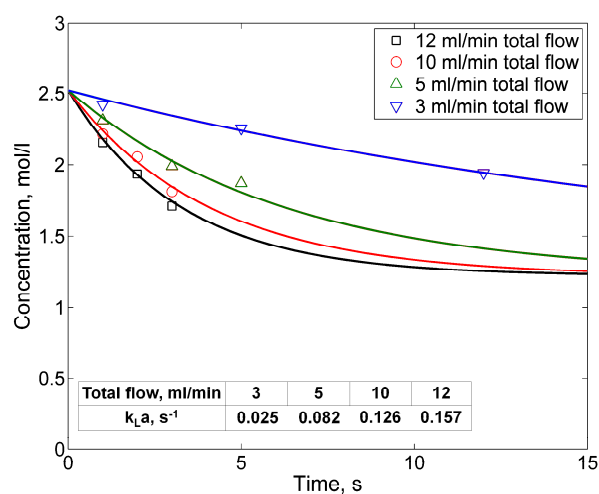

Figure 3: Modeling (solid lines) and experimental measurements (points) of the mass transfer in the sampling vial at total flow rates from 3 to 12 ml/min and the AO ratio of 1.

2.3 Results

2.3.1 Hydrodynamics

The flow patterns achievable in the Y mixer capillary microreactor were studied at aqueous and organic flow rates from 0.05 to 8.0 ml/min. In order to observe the influence of the capillary length on the flow patterns, the capillary length was varied from 0.2 to 2.2 m.

The minimum surface energy in the studied system is obtained when the aqueous phase wets the wall. Consequently, given enough time to evolve, all flow rate combinations ended up at this energetic minimum. Two types of startup conditions were studied, with the aqueous and the organic phases wetting the capillary wall, which resulted in flow patterns where the continuous phase was the aqueous phase (Figure 4 a-e) and the organic phase (Figure 4 f-h), respectively. Four distinct flow patterns were identified: annular, bubbly, parallel and slug flow (Figure 4 a-e). Furthermore, three inverted flow patterns were observed, in which the organic phase partially wetted the capillary wall (Figure 4 f-h). Those were unstable with the exception of the inverted bubbly flow, and quickly reverted to the flow pattern with the aqueous phase as the continuous phase. Last, the transitional intermittent flow pattern was observed in the transition region between flow patterns. The stability of the flow patterns can be explained by the difference in the wetting properties of the two phases used. The contact angle of the aqueous and organic phases on the fused silica was 53.1° and 139.2°, respectively. Dreyfus et al. (2003) showed that in the case when the continuous phase is partially wetting the capillary walls, unstable disordered flow patterns were observed[6]. The flows with the continuous aqueous phase were studied in the mass transfer experiments due to their reproducibility and stability.

The flow maps of the identified flow patterns as a function of the organic and aqueous flow rates are shown in Figure 5. The liquid properties and the relevant dimensionless numbers for the observed flow patterns are listed in Tables 1 and 2. It can be seen from the Reynolds (Re) and Capillary (Ca) number values that the inertia and surface tension are dominating over the viscous stresses for all the flow patterns. Zhao et al. (2006) proposed the use of Weber (We) number for mapping of flow patterns as it expresses the ratio of the two most dominant stresses in the system, the surface tension and inertia[13]. The flow maps, replotted using We numbers, are shown in Figure 6. Several regions can be distinguished:

- At small Weber numbers for both phases, formation of slugs happens immediately at the inlet, i.e. flow perturbations grow faster than they can be convected away. Both in the short capillary and the long capillary, slug flow is found, in which the continuous phase wets the channel and the discontinuous phase forms the drops. The low We numbers indicate that it is a surface tension dominating region, in which surface tension generates regular interfaces of alternating continuous and discontinuous slugs.

- At higher flow rates of the organic phase, the absolute instability that leads to drop formation becomes a convective instability, i.e. perturbations at the feed are convected away from the inlet faster than they can grow against the flow. The crossover to this regime occurs at a Weber number of the organic phase of about unity, in agreement with observations reported in the literature[18]. As a result, a parallel flow is observed in the beginning of the capillary, and it takes significant length for the disturbances to grow. The range of flow rates that exhibit parallel flow region gets smaller with length. The influence of the capillary length on the flow patterns was studied by varying the length from 0.2 to 2.2 m. In the range of capillary lengths from 0.4 to 2.2 m, the flow map remained unchanged, while the reporducibility of the annular flow is decreased yielding wavy annular flow at lengths lower than 1.5 m (Figure 4 e). At capillary lengths of 0.4 m and lower, the flow pattern map changes, with wavy annular flow transforming into parallel flow. No significant influence on the flow patterns was observed at the capillary lengths of 0.2 -0.4 m. The flow pattern maps at capillary lengths of 0.4 and 2 m are shown in Figures 5 and 6.

- At high flow rates with Weber numbers larger than unity for both phases, droplet (bubbly) flows are observed. Here, the more abundant phase is the continuous one; when the flow rate of organic phase is more than 5 times higher than that of the aqueous phase, then small aqueous droplets are dispersed in the organic phase. This is in contrast to what happens at lower flowrates, where minimization of surface energy always put the aqueous phase on the wall. Clearly, at We>>1, the contribution of surface terms to the energy of the system is not as important. Droplets form because the inertial stresses, of order ρv^2, easily overcome the surface stresses, of order γ/d, that resist breakup.

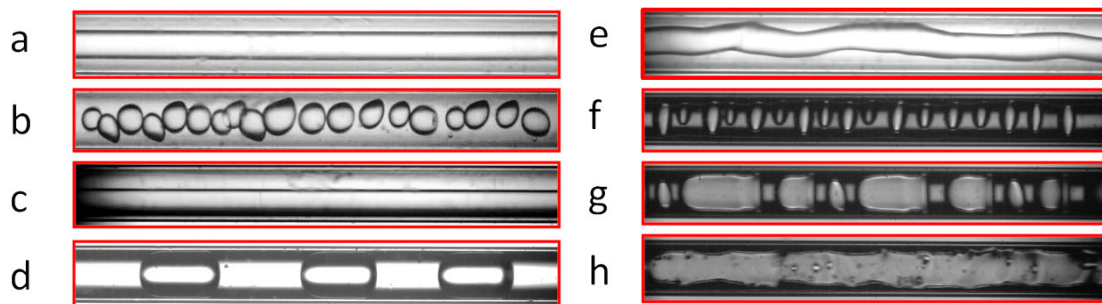- An intermittent flow was observed in flowrate ranges between droplet flow and slug flow.

Figure 4: Flow patterns: a. annular, b. bubbly, c. parallel, d. slug, e. wavy annular, f. inverted bubbly, g. inverted slug, h. inverted annular.
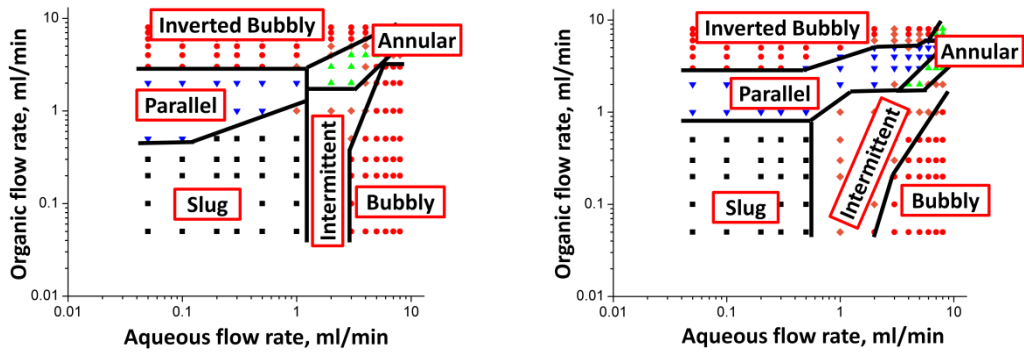
*Figure 5: Flow maps based on the aqueous and organic flow rates at: **a.** 2 m long capillary, **b.** 0.4 m long capillary.*
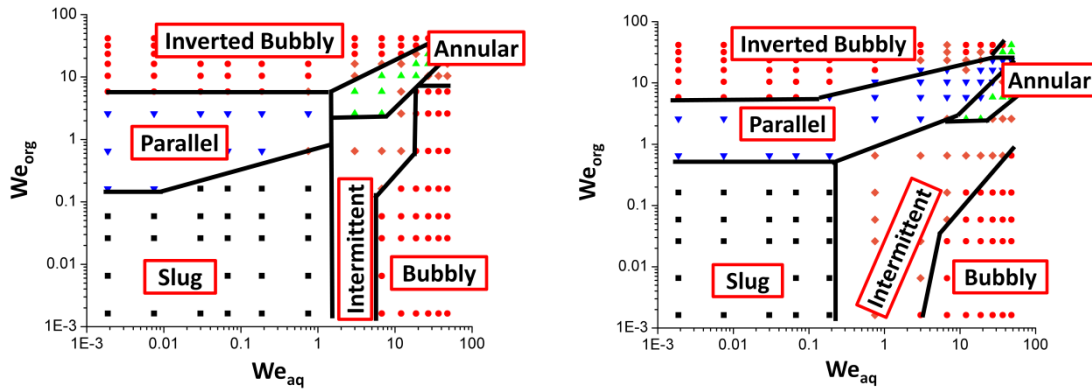
*Figure 6: Flow maps based on the aqueous and organic We numbers at: **a.** 2 m long capillary, **b.** 0.4 m long capillary.*

Table 2: Re, Ca and We number flow pattern ranges for the organic and aqueous phases

Flow pattern	Re_{org}	Re_{aq}	Ca_{org}	Ca_{aq}	We_{org}	We_{aq}
2 m capillary						
Slug	12.5 – 62.4	4.2 – 84.2	$5.0 \cdot 10^{-4}$ – $2.6 \cdot 10^{-3}$	$4.0 \cdot 10^{-4}$ – $8.8 \cdot 10^{-3}$	$6.5 \cdot 10^{-3}$ – $1.6 \cdot 10^{-1}$	$1.9 \cdot 10^{-3}$ – $7.5 \cdot 10^{-1}$
Bubbly	6.2 – 999	4.2 – 678	$3.1 \cdot 10^{-2}$ – $4.2 \cdot 10^{-4}$	$1.8 \cdot 10^{-2}$ – $5.3 \cdot 10^{-2}$	23.4 – 41.7	3.0 – 27.0
Annular	377 – 999	169.7 – 678	$1.6 \cdot 10^{-2}$ – $4.2 \cdot 10^{-4}$	$1.8 \cdot 10^{-2}$ – $7.1 \cdot 10^{-2}$	5.9 – 41.7	3.0 – 47.9
Parallel	62.4 – 374	4.2 – 84.8	$2.6 \cdot 10^{-3}$ – $1.6 \cdot 10^{-2}$	$4.0 \cdot 10^{-4}$ – $8.8 \cdot 10^{-3}$	$1.6 \cdot 10^{-1}$ – 5.90	$1.9 \cdot 10^{-3}$ – $7.5 \cdot 10^{-1}$
0.4 m capillary						
Slug	6.2 – 62.4	4.2 – 42.4	$3.0 \cdot 10^{-3}$ – $2.6 \cdot 10^{-3}$	$4 \cdot 10^{-4}$ – $4.4 \cdot 10^{-3}$	$1.6 \cdot 10^{-3}$ – $1.6 \cdot 10^{-1}$	$1.9 \cdot 10^{-3}$ – $1.9 \cdot 10^{-1}$
Bubbly	127 – 1022	25.5 – 593	$5.0 \cdot 10^{-3}$ – $4.2 \cdot 10^{-2}$	$2.6 \cdot 10^{-3}$ – $6.2 \cdot 10^{-2}$	$6.5 \cdot 10^{-1}$ – 41.7	$6.7 \cdot 10^{-2}$ – 36.7
Annular	249 – 999	339 – 678	$1.0 \cdot 10^{-2}$ – $4.2 \cdot 10^{-2}$	$3.5 \cdot 10^{-2}$ – $7.1 \cdot 10^{-2}$	2.6 – 41.7	12.0 – 48.0
Parallel	249 – 749	169 – 509	$1.0 \cdot 10^{-2}$ – $3.1 \cdot 10^{-2}$	$1.8 \cdot 10^{-2}$ – $5.3 \cdot 10^{-2}$	2.6 – 23.4	3.00 – 27.0

2.3.2 Slug flow

The slug flow was observed at organic and aqueous Ca numbers below 10^{-2} and We numbers below 1. These Ca and We number values indicate that the surface tension is the dominating force, being stronger than the viscous and inertial forces. Of all flow patterns, only slug flow allows to control the residence time, slug size and surface to volume ratio by adjusting the flow rates. The total flow rate has little influence on the slug size in the range from 0.1 to 0.6 ml/min (Figure 7 a). The slug size depends on the ratio of the aqueous and organic flow rates (AO ratio). By increasing the AO ratio from 0.25 to 9.0, the dispersed slug size decreases from above 1000 µm to approximately 250 µm. Consequently, the slug surface-to-volume ratio increases significantly, from 3000 m^2/m^3 to above 35000 m^2/m^3 (Figure 7 b). It should be pointed out that in the computation of the slug flow surface-to-volume ratios, only slug cap surface area was used, as the thin film (<7 µm) surrounding the slug does not play a role in liquid-liquid mass transfer due to its quick saturation[19]. Depending on the continuous phase Ca number there exist three regimes for the slug formation[15,20,21]: squeezing (10^{-4}<Ca<0.0058), dripping (0.013<Ca<0.1) and transitional (0.0058<Ca<0.013). As the Ca number was below $2.6 \cdot 10^{-4}$, the slugs were formed via the squeezing regime, where the surface tension fully dominated over the viscous and inertial forces. Garstecki et al. (2006)[15] postulated the following linear scaling law for the dispersed phase slug size in the squeezing regime:

$$\frac{L_{slug}}{D} = A + B \frac{F_d}{F_c} \tag{2}$$

where L_{slug} is the slug length; D is the diameter of the capillary; F_d is the dispersed (organic) phase flow rate and F_c the continuous (aqueous) flow rate; while A and B are the parameters which are determined by the geometry of the system[22]. Eq. 2 described the slug size with an R^2 of 0.94 (Figure 7 a).

2.3.3 Bubbly flow

Bubbly flow was observed at the AO ratio above 4, where the continuous aqueous phase disperses the organic phase into smaller bubbles. Inverted bubbly flow was observed at the AO ratio below 0.2.

The bubbly flow was found at Ca numbers smaller than 0.1 and continuous phase We numbers higher than 1, indicating that the inertia of the fluids are the dominating stresses. The generated bubbles are not ideally spherical (Figure 4 b), confirming that surface tension cannot keep the droplets spherical in the face of significant inertial stress.
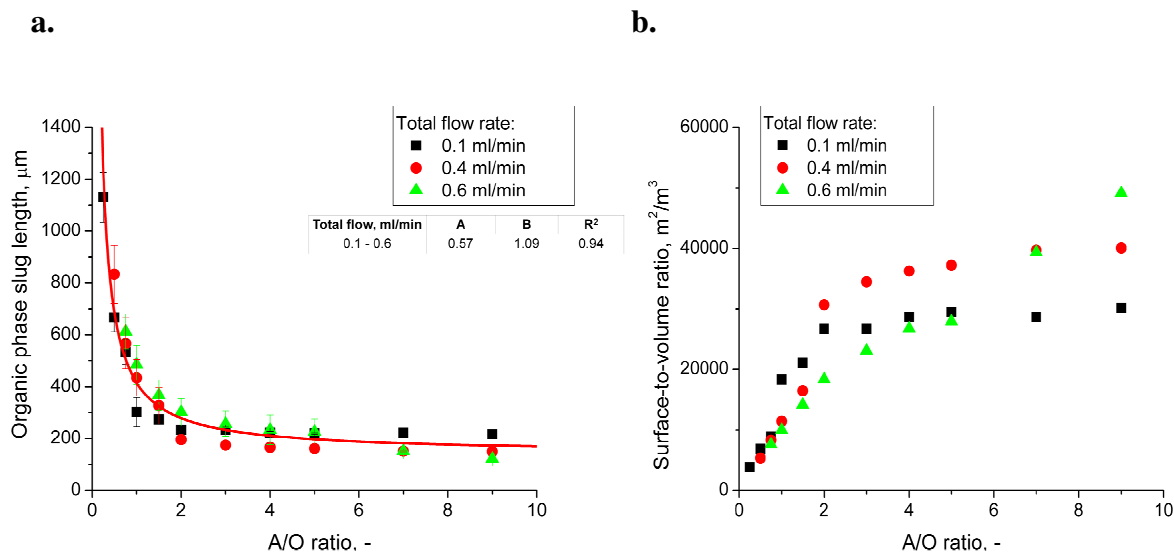
a.

b.

*Figure 7: Scaling law modeling of the dispersed, organic slug size (**a.**) and surface-to-volume ratio (**b.**) as a function of the AO ratio at 0.1, 0.4 and 0.6 ml/min total flow rates and capillary length of 0.4 m.The scaling law modeling yielded values of 0.57 and 1.09 for the geometry dependent parameter A and B, respectively.*

The bubble sizes were studied in a 0.4 m capillary at a total flow rate from 5 to 10 ml/min and at two AO ratios of 5 and 10. With increasing flow rate the mean bubble diameter decreases (Figure 8 a) resulting in significant increase of the surface-to-volume ratio from 50000 to above 150000 m^2/m^3 (Figure 8 b). It can be seen that the mean bubble diameter virtually does not depend on the AO ratio. In the bubbly flow, a wide range of dispersed phase bubble sizes is generated, with diameters ranging from tens to hundreds of µm. Therefore, in order to obtain a complete analysis of the bubble sizes generated, one must observe the bubble size distribution rather than the mean bubble diameter.

In order to study the influence of the flow rate and AO ratio on the bubble size, the bubble size distribution was analyzed at the flow rates of 7 and 10 ml/min for the AO ratios of 5 and 10 (Figure 9). The size of the generated bubbles is largely determined by the energy spent on their break up. By observing the We numbers (Figure 6), it is clear that the breakup is caused by the continuous phase inertial force. By increasing the AO ratio the We number of the organic phase (i.e. the inertial force provided by the organic flow) decreases while the We number of the aqueous phase increases. The result is a very slight change in the size distribution. The influence of the flow rate on the distribution was more pronounced than the AO ratio. With increasing flow rates, smaller bubble sizes and narrower size distributions were achieved, for both AO ratios. The smallest bubbles were found in the case of the 10 ml/min flow rate at an AO ratio of 5, with a narrow distribution of bubble sizes in the range of 5-60 µm. Under those conditions both the organic and aqueous phase We numbers are larger than 1 (Figure 9 c), indicating that the inertia is dominating in both flows. It can be concluded that the smallest size can be achieved under the conditions of fully developed inertia (i.e. We>1). Last, these results show the importance of the inertial contribution of both flows. At a throughput of 10 ml/min, the

bubbly flow in a capillary microreactor shows the same average bubble size diameter of approximately 40 µm the as the interdigital microreactor[23].

The highly dispersed organic phase droplets generated by the bubbly flow pattern result in the formation of stable emulsions. In order to test their stability, the emulsions were aged at temperatures of 20 °C and 40 °C as described in the experimental section. At 40 °C full separation was achieved after 24 hours, while at 20°C the full separation was achieved after 8 days. The emulsion was easily broken by the addition of toluene at 20°C. After washing with demineralized water the emulsion stability was reduced from 8 days to approximately 3 hours.

a.
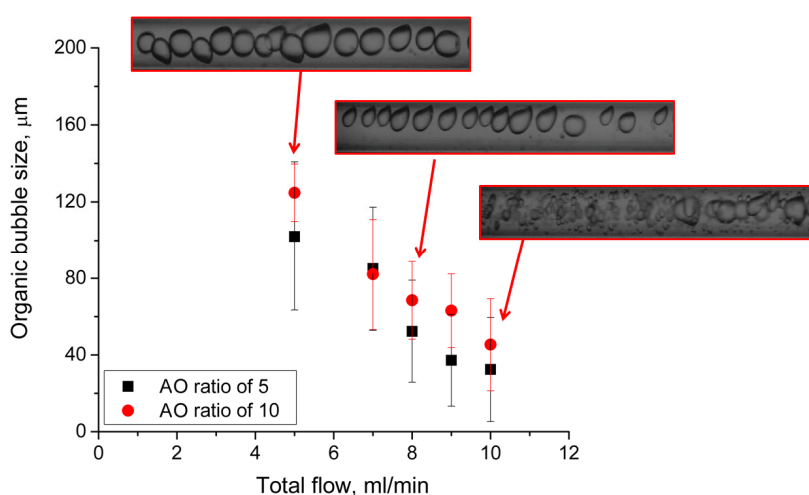
b.
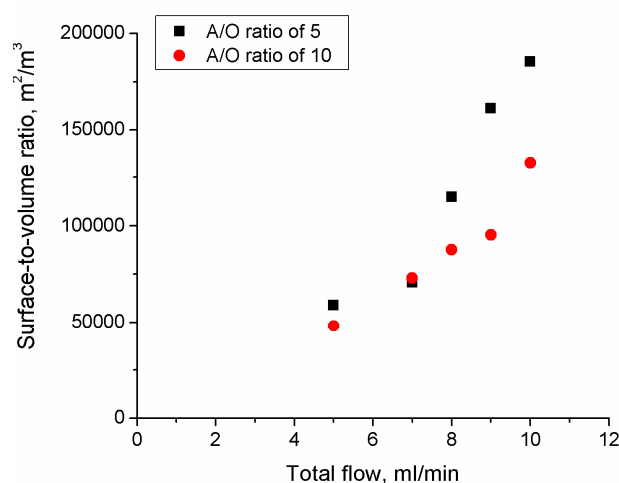
*Figure 8: Bubble size (**a.**) and surface-to-volume ratio (**b.**) as a function of the total flow rate at AO ratios of 5 and 10, and capillary length of 0.4 m.*
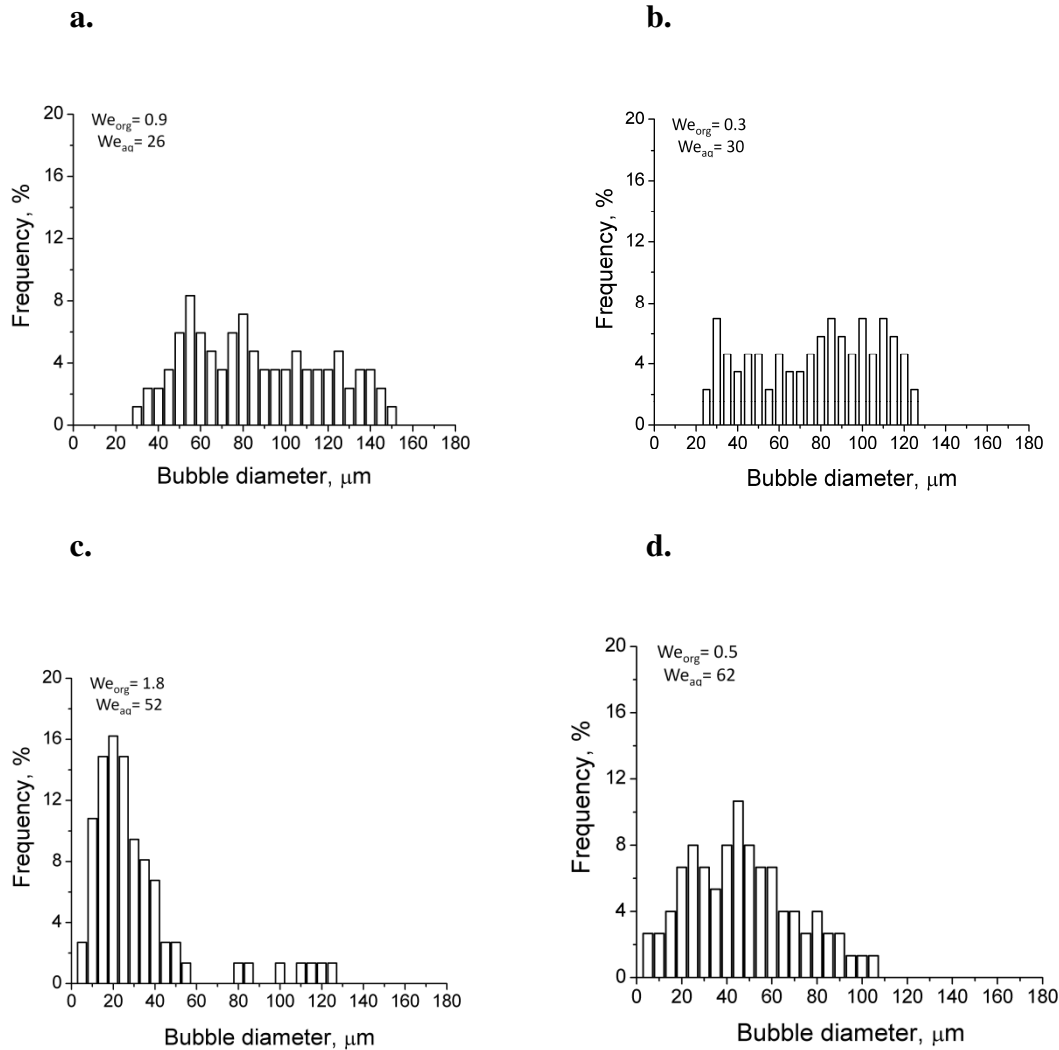
Figure 9: Bubble size distribution for: **a.** *7 ml/min and AO ratio of 5,* **b.** *7 ml/min and AO ratio of 10,* **c.** *10 ml/min and AO ratio of 5,* **d.** *10 ml/min and AO ratio of 10.*

2.3.4 Annular and parallel flow

Unlike the slug and bubbly flows, the annular and parallel flows offer a limited degree of interface surface area control by changing either the flow rate or the AO ratio. The annular and parallel flows are achieved at an AO ratio of 1, while changing the AO ratio destabilizes the flow. Parallel flow is achieved at lengths below 0.4 m, while stable annular flow is created at the length above 1.5 m. During the transition between these flow patterns, wavy annular flow is observed for the capillary lengths between 0.4 and 1.5 m (Figure 4 e). The hydrodynamics were studied only in fully developed and reproducible parallel and annular flows.

The microscope observations showed that the parallel and annular flows consisted of an inner organic phase jet surrounded by the continuous aqueous phase. The microscope observations of the annular to parallel flow transitions indicated that the shape of the

organic jet was cylindrical. Therefore, for the estimation of the surface-to-volume ratios, the shape of the organic jet was assumed to be ideally cylindrical. The diameter of the organic phase jet was measured as a function of flow rate at the capillary length of 0.4 and 2 m for annular and parallel flow, respectively. As the total flow rate increases, the organic jet diameter of the parallel flow increases by 5.0 %, while in the annular flow, the organic jet diameter decreases by 16 % (Figure 10 a). Consequently the parallel surface-to-volume ratio decreases by 4.9 %, while the annular flow surface-to-volume ratio increases by 19 % (Figure 10 b). It is important to note that at total flow rates above 10 ml/min, disturbances in the parallel flow interface occur, which include twisting of the organic jet (Figure 11 a) and wavy parallel interface (Figure 11 b). These disturbances confirmed the assumption of the cylindrical shape of the organic jet. Moreover, at flow rate of 12 ml/min the dispersion of the aqueous phase inside of the organic jet of the parallel flow (Figure 11 c) was observed. Although it was not possible to quantify the disturbances, it is clear that in the unstable parallel flow, the surface-to-volume ratio increases significantly.

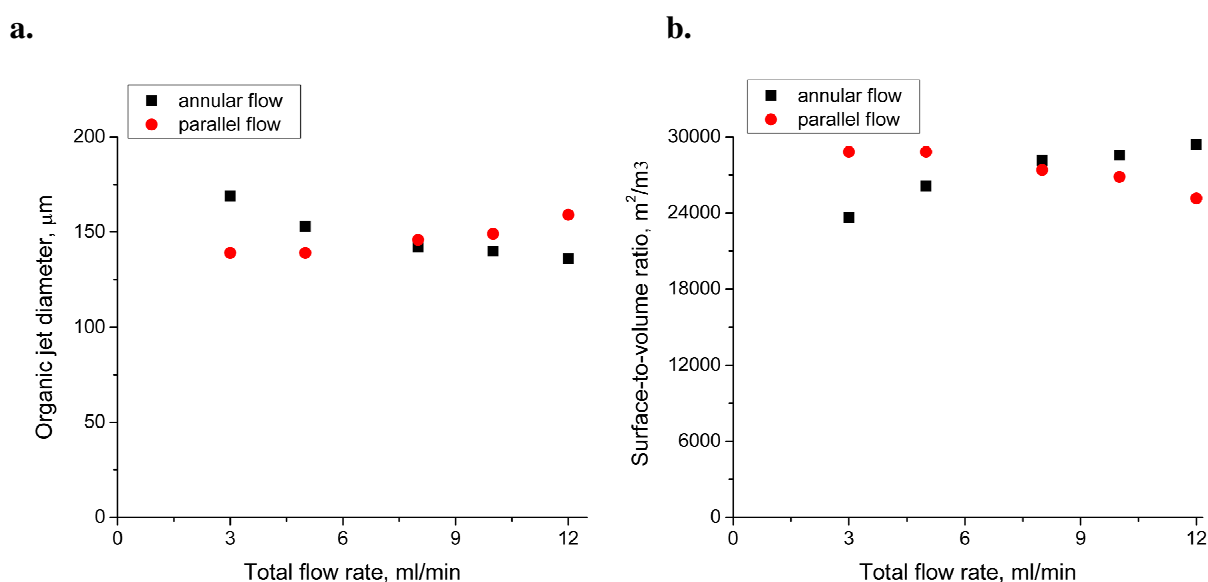*Figure 10: The organic jet diameter (**a.**) and surface-to-volume ratio (**b.**) of the annular and parallel flows as a function of total flow rate at the AO ratio of 1. The capillary length was 0.4 and 2 m for the parallel and annular flow, respectively.*
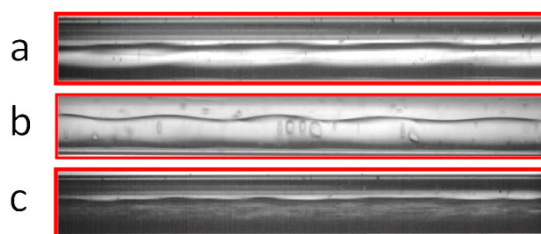

*Figure 11: Parallel flow instabilities: **a.** twisting of the organic jet, b. wavy interface and c. dispersion of the continuous, aqueous phase in the organic jet.*

2.4 Mass transfer results

2.4.1 Equilibrium operation: slug and bubbly flow

Extraction experiments in the slug and bubbly flow regimes were performed at the capillary length of 0.4 m. The variation of the total flow rates of the slug and bubbly flows showed that the organic concentration was independent of the residence time, thus indicating that the system was operating at equilibrium conditions (Figure 12). The equilibrium concentrations were measured at AO ratios from 0.25 to 9. The comparison of the slug and bubbly flow results with the equilibrium organic concentrations at different AO ratios confirmed that the slug and bubbly flows operate at thermodynamic equilibrium. The results show a high mass transfer rate is occurring in slug and bubbly flow, which can be explained by the high surface-to-volume ratios (Figures 7 b and 8 b). Additionally, in the slug flow the presence of the internal circulations in the slugs further intensify the mass transfer rate [24, 25]. Similarly, in the bubbly flow, the inertial deformation of the bubbles results in internal circulations. Furthermore, bubbly flow can achieve surface-to-volume ratios above 150000 m^2/m^3, thus significantly intensifying the mass transfer. The slug flow residence time was in the range of 2-12 seconds, 20 to 50 times longer than in the case of the bubbly flow (0.11 - 0.24 seconds).

The partition coefficient was calculated as a function of the organic and aqueous concentrations:

$$K_{2-\text{BuOH}} = \frac{C_{org}}{C_{aq}}$$ (3)

The partition coefficient was determined from the bubbly and slug flow experiments for the case of different aqueous-to-organic flow ratios. Moreover, the partition coefficient was determined via equilibrium measurements in vials for different aqueous-to-organic ratios. The partition coefficient was found to decrease with increasing AO ratio (Figure 13). With increasing AO ratio, the aqueous phase volume increases while the organic phase volume decreases. Consequently, the amount of extracted 2-butanol increases, thus lowering the concentration of 2-butanol in the organic phase.

When a liquid-liquid system is in a thermodynamic equilibrium the following condition is fulfilled[26] :

$$\gamma^{org}_{2-\text{BuOH}} x^{org}_{2-\text{BuOH}} = \gamma^{aq}_{2-\text{BuOH}} x^{aq}_{2-\text{BuOH}}$$ (4)

where γ and x are the activity coefficients and molar fractions of 2-butanol in the aqueous and organic phases. Combining Eqs. 3 and 4 yields:

$$K_{2-\text{BuOH}} = \frac{\gamma^{org}_{2-\text{BuOH}} M^{aq} \rho^{org}}{\gamma^{aq}_{2-\text{BuOH}} M^{org} \rho^{aq}}$$ (5)

The activity coefficients are highly dependent on the concentration, therefore the partition coefficient will change with changing concentration in the system. The partition

coefficients were modeled by using the NRTL equation of state, as it is most suitable for liquid-liquid equilibrium systems[27]. The NRTL equation of state predicted the partition coefficients with a mean relative error of 82 % (Figure 13). The poor prediction results of the NRTL model can be explained by the fact that the interactions between the hydrocarbons and alcohols have not been properly accounted for in the currently available equation of state models[28]. In the water-toluene/2-butanol system numerous intermolecular interactions exist. These intermolecular interactions include dispersion, induction, dipole-dipole and hydrogen bonding interactions[29] which further complicate the equation state based modeling of the liquid-liquid equilibrium. Therefore, the experimentally derived partition coefficients were used in the modeling of the mass transfer.
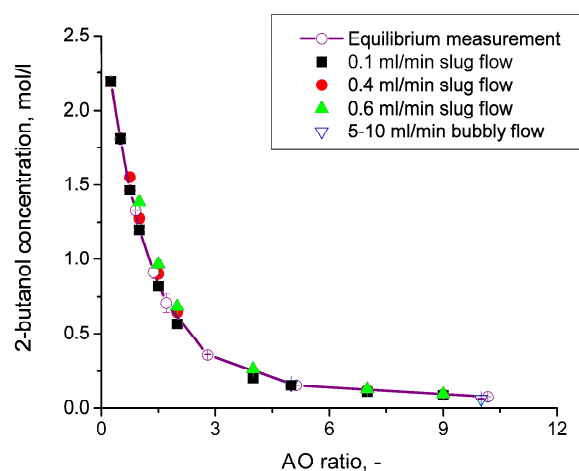

Figure 12: Concentration of 2-butanol in the organic phase for the slug flow, bubbly flow and equilibrium experiments as a function of the AO ratio.
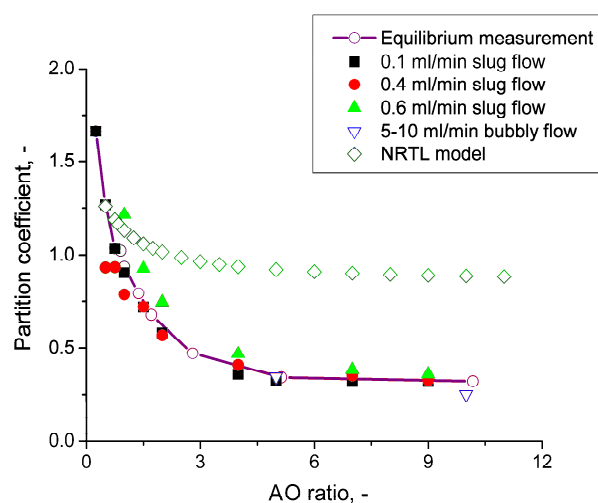

Figure 13: Partition coefficient in the slug flow, bubbly flow, equilibrium experiments and the NRTL model as a function of the AO ratios.

2.4.2 Non-equilibrium operation: parallel and annular flow

Compared to the slug and bubbly flow, at stable parallel and annular flow conditions, there are little or no internal circulations caused by the dispersed phase movement. Consequently, thermodynamic equilibrium is not reached in the capillary, which allows for the measurement of the global mass transfer coefficient. The mass transfer coefficients were calculated by measuring the decrease of the concentration in the organic phase. The organic phase concentrations were corrected for the mass transfer in the sampling zone via Eq. 1 and are shown in Figure 14.

The mass transfer of 2-butanol from the organic phase into the aqueous phase can be written as:

$$\frac{dC_{org}}{dt} = -k_L a \left(C_{org} - K_{2-\text{BuOH}} C_{aq} \right) \tag{6}$$

The mass balance of the 2-butanol yields the aqueous concentration:

$$C_{aq} = \frac{F_{org}(C_{org,0} - C_{org})}{F_{aq}} = \frac{(C_{org,0} - C_{org})}{AO} \tag{7}$$

Since the mass transfer in parallel and annular flows was studied at an AO ratio of 1, Eq. 6 becomes:

$$\frac{dC_{org}}{dt} = -k_L a \left(C_{org}(1 + K_{2-\text{BuOH}}) - K_{2-\text{BuOH}} C_{org,0} \right) \tag{8}$$

Integration of Eq. 8 yields the global mass transfer coefficient:

$$k_L a = \frac{1}{t(1 + K_{2-\text{BuOH}})} \ln \left| \frac{C_{org,0}}{C_{org}(1 + K_{2-\text{BuOH}}) - K_{2-\text{BuOH}} C_{org,0}} \right| \tag{9}$$

The $k_L a$ values as a function of the capillary length are shown in Figure 15. As the capillary length decreases, the flow pattern transforms from stable annular to wavy annular and then to the parallel flow. Furthermore, by increasing the flow rate above 10 ml/min, the parallel flow becomes unstable. Consequently the $k_L a$ values of the four operating regimes were measured: stable annular, unstable annular, unstable parallel and stable parallel flow. In the stable annular flow regime, by increasing the flow rate from 3 to 12 ml/min, the surface-to-volume ratio increases by 19 % (Figure 9 b), and consequently the $k_L a$ increases.

The surface-to-volume ratio increases in both the unstable annular and parallel flow regimes as a result of the deformation and breakup of the liquid-liquid interface. Consequently, the mass transfer coefficient increases as compared to that in stable flow (Figure 15). In the stable parallel flow no influence of the flow rate was found. Last, by

increasing the flow rate from 5 to 10 ml/min the stable parallel flow transforms to unstable parallel flow, with small struts of organic liquid penetrating the aqueous phase. Similar pattern was observed by Zhao et al. (2006)[13]. The thin liquid struts increase the surface-to-volume ratio, and consequently the mass transfer coefficient.

Thermodynamic extraction efficiency[21] was used to compare the amount of extracted 2-butanol to the thermodynamic limit (Eq. 10). Figure 16 shows the 2-butanol thermodynamic extraction efficiency under parallel and annular flow regimes as a function of the residence time. For both flow patterns the extraction efficiency increases with residence time, yielding the maximal efficiencies of 60 and 90 %, for parallel and annular flow, respectively. The change of the extraction efficiency is proportional to the interface surface area increase due to instability. This accounts for higher efficiency found at 12 ml/min parallel flow when compared to 10 ml/min.

$$E\% = \left| \frac{C_{org} - C_{org,0}}{C_{org,eq} - C_{org,0}} \right| \cdot 100\% \qquad (10)$$

*Figure 14: Concentration of 2-butanol in the organic phase as a function of residence time for the parallel (**a.**) and annular flow (**b.**) at total flow rates from 3 to 12 ml/min and the AO ratio of 1.*
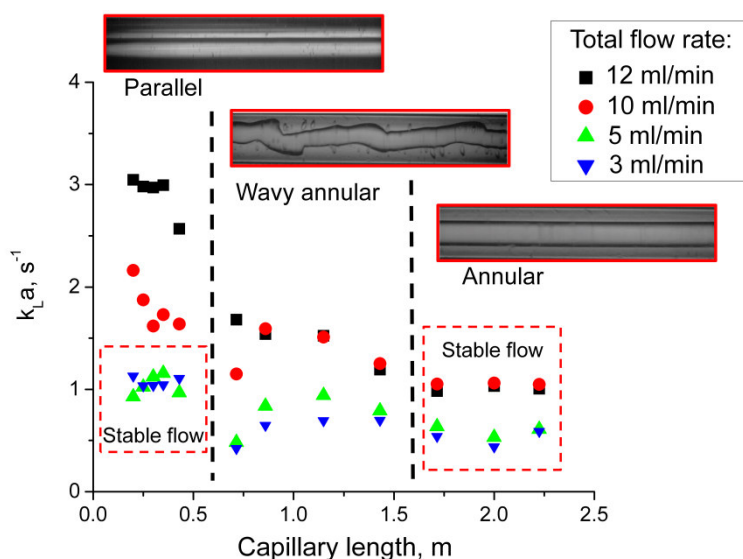
Figure 15: Liquid-liquid mass transfer coefficient as a function of the capillary length, at total flow rates from 3 to 12 ml/min and the AO ratio of 1.

*Figure 16: Extraction efficiency as a function of residence time for the parallel (**a.**) and annular flow (**b.**) at total flow rates from 3 to 12 ml/min and the AO ratio of 1.*

2.4.3 Flow pattern comparison and potential applications

The extraction application potential of the studied flow patterns was evaluated by measuring the amount of extracted 2-butanol. The slug and bubbly flow regimes operate at the thermodynamic equilibrium, therefore the removal of 2-butanol was studied as a function of the AO ratio. By increasing the AO ratio, the volume of the aqueous phase increases, and with it, the number of moles of 2-butanol that can be removed from the organic phase. Consequently, by controlling the AO ratio, the extraction can be increased up to 99 % (Figure 17). Although, parallel and annular flow have similar surface-to-volume ratios as the slug flow (Table 3), the thermodynamic equilibrium could not be

reached, which limits the thermodynamic extraction efficiency to 60 and 90 % for the parallel and annular flow regimes, respectively. Their surface-to-volume ratios cannot be controlled by changing the flow ratio, thus limiting the flow patterns to a narrow window of operation. In stable parallel and annular flow there are no internal circulations caused by the flow which intensify the mass transfer as in the case of the slug and bubbly flow. Consequently, the maximal extraction of 2-butanol was 30 % and 47 % (Figure 18), for the parallel and annular flow, respectively. Last, the residence time of the annular flow could not be extended by increasing the length of the capillary, as the maximal pressure (400 bar) of the pumps was reached. Narrow windows of operation coupled with low extraction efficiencies and short residence times severely limit the extraction application of the parallel and annular flow regimes. Therefore, the best performance in terms of extraction application in the capillary microreactor is in the slug and bubbly flow regimes.

Figure 17: Extraction of 2-butanol in slug and bubbly flow as a function of the AO ratio.

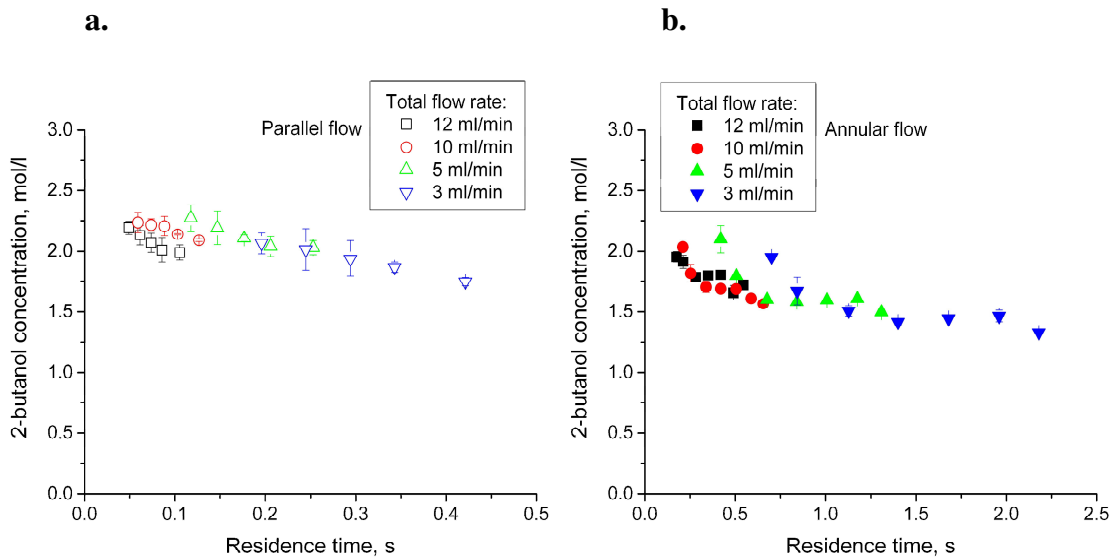**a.**   **b.**

*Figure 18: Extraction of 2-butanol as a function of residence time for the parallel (**a.**) and annular flow (**b.**) at total flow rates from 3 to 12 ml/min and the AO ratio of 1.*
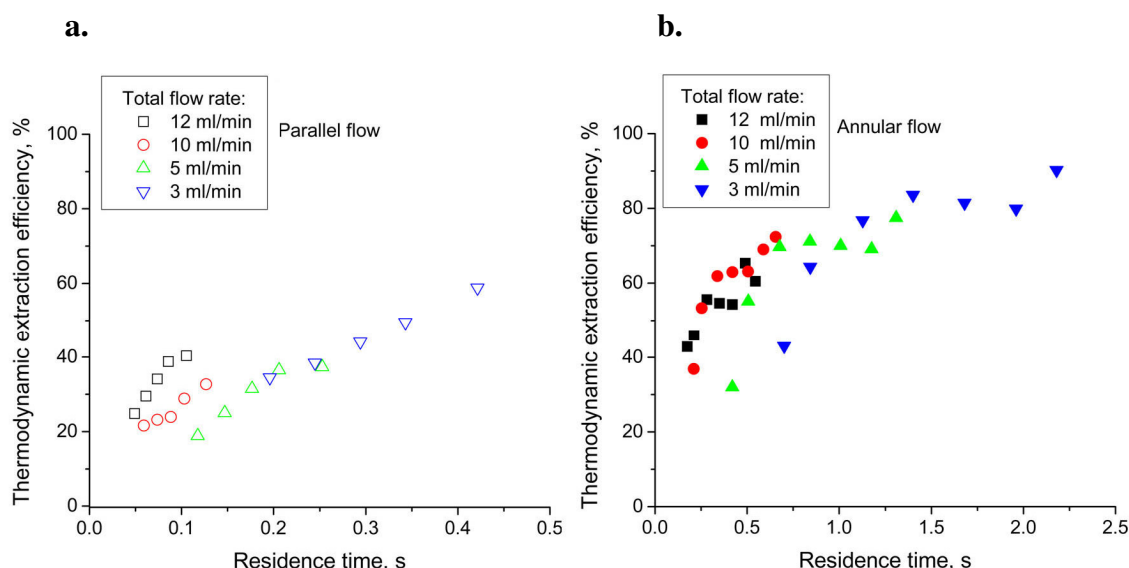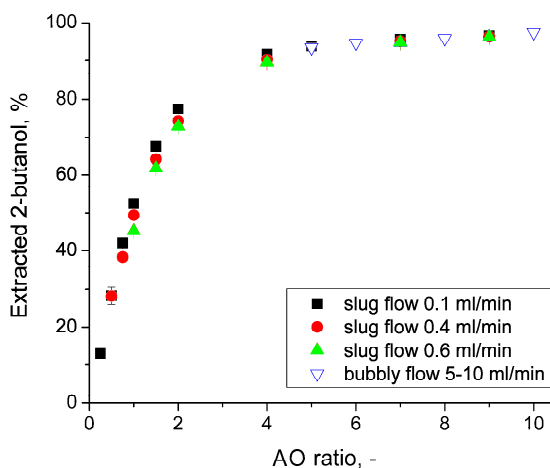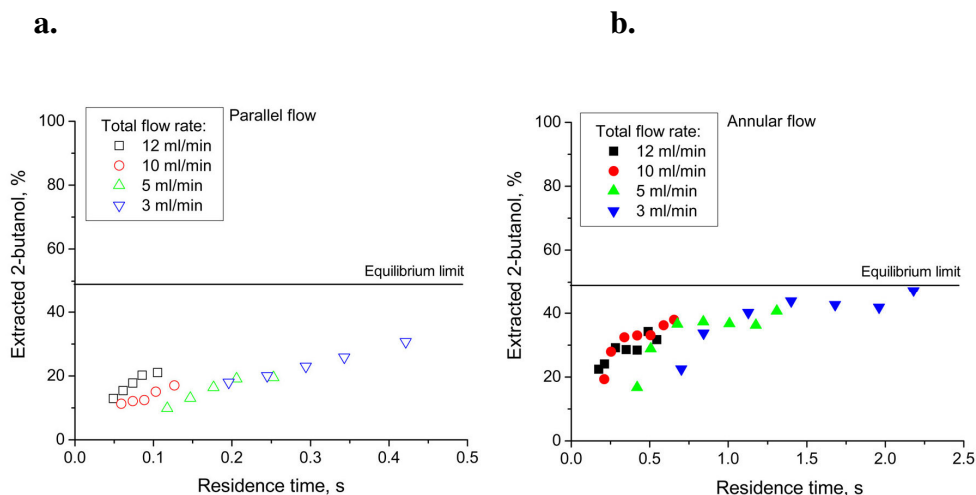
Table 3: Comparison of the extraction application of slug, bubbly, parallel and annular flow pattern

Flow pattern	S/V, m^2/m^3	Extraction efficiency, %	Maximal throughput, ml/min	Residence time, s	S/V control
Slug	5000 - 40000	100	0.6	1.95 - 12.0	*Yes*
Bubbly	50000 - 180000	100	12	0.12 - 0.24	*Yes*
Parallel	25000 - 30000	18-60	12	0.50 - 0.45	*No*
Annular	25000 - 30000	35-90	12	0.25 - 2.50	*No*

2.5 Conclusions

In this chapter, hydrodynamics and extraction application of the slug, bubbly, parallel and annular flow regimes in the Y-mixer capillary microreactor system were investigated. The influence of the capillary length on the flow patterns was studied. Therefore, flow rate and We number based flow pattern maps for 0.4 m and 2 m capillary length were composed. By changing the capillary length from 2 to 0.4 m, the flow maps changed with annular flow transforming into the wavy annular flow and finally the parallel flow. The variation of the capillary length showed little influence on the slug and bubbly flow patterns.

The parallel and annular flow patterns were stable in narrow flow and capillary length ranges, severely limiting the range of residence times to below 2.5 s. The stable parallel flow operates in an operational window which requires equal AO flow ratios, total flow rate range from 3 to 5 ml/min and a maximal capillary length of 0.4 m. Consequently, the residence times below 1 s allow for maximal extraction efficiency of approximately 60 %. Stable annular flow was observed at an AO flow ratio of 1, a total flow rate above 3 ml/min in a capillary with a length higher than 1.5 m. The thermodynamic extraction efficiency of 90 % was obtained at a residence time of 2.5 s. The narrow operating conditions of stable parallel and annular flow give limited application potential in systems where high throughput (>3 ml/min) and residence time of a few seconds is required.

By controlling the AO flow ratios 99 % 2-butanol extraction can be achieved under both the slug and bubbly flow regimes. Under the slug flow regime the residence times of 2-12 s were by a factor of 5-50 higher as compared to other flow patterns. This regime is the most suitable for the application in mass transfer limited systems and those with slow kinetics. The residence time in slug flow can be increased to above 30 min by increasing the length of the capillary. Bubbly flow has residence times below 0.25 s, while achieving 100 % thermodynamic extraction efficiency. Furthermore, in bubbly flow surface-to-volume ratios above 150 000 m^2/m^3 can be achieved, more than 3 times higher than in the slug, parallel or annular flow. Therefore, it is suitable for application in mass transfer limited and fast kinetic reaction systems, particularly in cases where short residence times are required.

By operating in bubbly flow in capillary microreactor at throughputs higher than 10 ml/min, similar performance can be achieved as in the case of the interdigital mixer

microreactor. Therefore, the low cost capillary microreactor, with four stable operating flow patterns and a throughput range from g/h to kg/h, presents a flexible alternative to chip and microstructured microreactors for lab and pilot scale applications.

Nomenclature

D	- diameter, m
C	- concentration, mol/m^3
F	- flow rate, m^3/s
k_La	- mass transfer coefficient, s^{-1}
$K_{2\text{-}BuOH}$	-partition coefficient, -
V	-volume, m^3
L	-slug length, m
γ	-fugacity coefficient, -
M	-molar mass, g/mol
ρ	-density, kg/m^3
$E\%$	-thermodynamic extraction efficiency, -
S/V	-surface-to-volume ratio, m^2/m^3

Subscripts

org	- organic phase
aq	- aqueous phase
c	- continuous phase
d	- dispersed phase
2-BuOH	-2- butanol
eq	- equilibrium

Dimensionless numbers:

$$Ca = \frac{Viscous\ force}{Surface\ tension\ force} = \frac{\mu v}{\sigma} \qquad \text{- Capillary number}$$

$$Re = \frac{Inertial\ force}{Viscous\ force} = \frac{\rho v D}{\mu} \qquad \text{- Reynolds number}$$

$$We = \frac{Inertial\ force}{Surface\ tension\ force} = \frac{\rho v^2 D}{\sigma} \qquad \text{- Weber number}$$

References

(1)   Ahmed-Omer, B.; Barrow, D.; Wirth, T. Effect of segmented fluid flow, sonication and phase transfer catalysis on biphasic reactions in capillary microreactors. *Chem. Eng. J.* 2008, *135S*, S280.

(2)   Wiles C.; Watts P. An Integrated Microreactor for the Multicomponent Synthesis of r-Aminonitriles, *Org. Process Res. Dev.* 2008, *12*, 1001.

(3)   Sahoo, H. R.; Kralj, J. G.; Jensen, K. F. Multistep Continuous-Flow Microchemical Synthesis Involving Multiple Reactions and Separations. *Angew. Chem., Int. Ed.* 2007, *46*, 5704.

(4)   Dessimoz, A. L.; Cavin, L.; Renken, A.; Kiwi-Minsker, L. Liquid-Liquid two-phase flow patterns and mass transfer characteristics in rectangular glass microreactors. *Chem. Eng. Sci.* 2008, *63*, 4035.

(5)   Cubaud, T.; Ulmanella, U.; Ho, C. M. Two-phase flow in microchannels with surface modifications, *Fluid Dyn. Res.* 2006, *38*, 772.

(6)   Dreyfus, R.; Tabeling, P.; Willaime, H. Ordered and disordered patterns in two-phase flows in microchannels. *Phys. Rev. Lett.* 2003, *90*, 144505.

(7)   Zhao, Y.; Chen, G.; Yuan, Q. Liquid-Liquid Two-Phase Flow Patterns in a Rectangular Microchannel, *AIChE J.* 2006, *52*, 4052.

(8)   Shui, L.; van den Berg, A.; Eijkel, J. C. T. Interfacial tension controlled W/O and O/W 2-phase flows in microchannel. *Lab Chip* 2009, *9*, 795.

(9)   Salim, A.; Fourar, M.; Pironon, J.; Sausse, J. Oil-water two-phase flow in microchannels: Flow patterns and pressure drop measurements. *Can. J. Chem. Eng.* 2008, *86*, 978.

(10) Cherlo, S. K.; Pushpavanam, S.; Experimental and Numerical Investigations of Two-Phase (Liquid-Liquid) Flow Behavior in Rectangular Microchannels. *Ind. Eng. Chem. Res.* 2010, *49*, 893.

(11) Guillot, P.; Colin, A. Stability of parallel flows in a microchannel after a T junction, *Phys. Rev. Lett.* 2005, *72*, 066301.

(12) Kashid, M.N.; Agar, D.W.; Hydrodynamics of liquid–liquid slug flow capillary microreactor: flow regimes, slug size and pressure drop. *Chem. Eng. J.* 2007, *131*, 1.

(13) Zhao, Y.; Chen, G.; Yuan, Q. Liquid-Liquid Two-Phase Flow Patterns in a Rectangular Microchannel, *AIChE J.* 2006, *52*, 4052.

(14) Burns, J. R.; Ramshaw, C. The intensification of rapid reactions in multiphase systems using slug flow in capillaries *Lab. Chip* 2001, 1, 10.

(15) Garstecki, P.; Fuerstman, M.; Stone, H.; Whitesides, G. Formation of droplets and bubbles in a microfluidic t-junctionscaling and mechanism of break-up. *Lab. Chip* 2006, *6*, 437.

(16) Fries, D. M.; Voitl, T.; von Rohr, P. R.; Liquid extraction of vanillin in rectangular microreactors. *Chem. Eng. Technol.* 2008, *31*, 1182.

(17) Zhao, Y.; Chen, G.; Yuan, Q; Liquid–liquid two-phase mass transfer in the T-junction microchannels. *AIChE J.* 2007, *53*, 3042.

(18) Uada, A. S.; Fernandez-Nieves, A.; Stone, H. A.; Weitz, D. A.; Dripping to Jetting Transitions in Coflowing Liquid Streams. *Phys. Rev. Lett.* 2007, *99*, 094502.

(19) Berčić, G.; Pintar, A. The role of gas bubbles and liquid slug lengths on mass transport in the Taylor flow through capillaries *Chem. Eng. Sci.* 1997, *52*, 3709.

(20) Xu, J.H.; Li, S.W.; Tan, J.; Luo, G.S. Correlation of droplet formation in T-junction microfluidic devices: from squeezing to dripping. *Microfluid. Nanofluid.* 2008*, 5,*711.

(21) de Menech, M.; Garstecki, P.; Jousse, F.; Stone, H.A. Transition from squeezing to dripping in a microfluidic T-shaped junction. *J. Fluid Mech.* 2008*, 595*, 141.

(22) Van Stein, V.; Kleijn, C. R.; Kreutzer, M. T.; Predictive model for the size of bubbles and droplets created in microfluidic T-junctions. *Lab Chip* 2010, *10*, 2513.

(23) Benz, K.; Jäckel, K.P.; Regenauer, K.J.; Schiewe, J.; Drese, K.; Ehrfeld, W.; Hessel, V.; Löwe H. Utilization of Micromixers for Extraction Processes. *Chem. Eng. Technol.* 2001, 24, 11.

(24) Taha, T.; Cui, Z. F. Hydrodynamics of slug flow in capillaries. *Chem. Eng. Sci.* 2004, *59*, 1181

(25) He, Q.; Kasagi, N. Phase-Field simulation of small capillary-number two-phase flow in a microtube, *Fluid Dyn. Res.* 2008, *40,* 497.

(26) Wang, P.; Dwarakanath, V.; Rouse, B. A.; Pope, G. A.; Sepehrnoori, K. Partition coefficients for alcohol tracers between nonaqueous-phase liquids and water from UNIFAC-solubility method. *Adv. Water Res.* 1998, *21*, 171.

(27) Renon H.; Prausnitz, J. M. Local composition in thermodynamic excess functions for liquid mixtures. *AIChE J.* 1968, *14*, 135.

(28) Gierycz, P. Descruiption of binary systems containing hydrocarbons and alcohols by a modified NRTL equation. *Thermochim. Acta* 1987, *116*, 267.

(29) Hilal, S. H.; Karickhoff, S. W.; Carreira, L. A. Prediction of the Solubility, Activity Coefficient and Liquid/Liquid Partition Coefficient of Organic Compounds. *QSAR Comb. Sci.* 2004*, 23*, 709.

Chapter 3. Liquid-liquid slug flow: hydrodynamics and pressure drop

Abstract

In this chapter, the hydrodynamics and the pressure drop of liquid-liquid slug flow in round capillary microreactor are presented. Two liquid-liquid flow systems are considered, viz. water-toluene and ethylene glycol/water-toluene. The slug lengths of the alternating continuous and dispersed phases were measured as a function of the slug velocity (0.03 – 0.5 m/s), the organic-to-aqueous flow ratio (0.1 – 4.0), and the capillary internal diameter (248 µm and 498 µm). The pressure drop is modeled as the sum of two contributions: the frictional and the interface pressure drop. Two models are presented, viz. the stagnant film model and the moving film model. Both models account for the presence of a thin liquid film between the dispersed phase slug and the capillary wall. It is found that the film velocity is of negligible influence on the pressure drop. Therefore, the stagnant film model is adequate to accurately predict the liquid-liquid slug flow pressure drop. The influence of inertia and the consequent change of the slug cap curvature are accounted for by modifying Bretherton's curvature parameter in the interface pressure drop equation. The stagnant film model is in good agreement with experimental data with a mean relative error of less than 7%.

3. 1 Introduction

3.1.1 Hydrodynamics of two-phase flow in microchannels

Capillary two-phase hydrodynamics have three considerable distinctions from two-phase flows in macrosystems: first, there is an increase in the ratio of the surface area of the phases to the volume that they occupy; second, the flow is characterized by small Capillary numbers at which surface tension forces predominate over viscous forces; and third, the microroughness and wettability of the wall of the microchannel exert a considerable influence on the flow pattern formation. In laminar multiphase microflow systems, the dominating interfacial and inertial forces result in various regularly shaped interfaces[1]. A large number of studies can be found in literature on the achievable flow patterns in gas-liquid systems[2-9] while relatively few studies are focusing on the hydrodynamics of liquid-liquid systems[10-13]. Depending on the total flow rate and the volumetric flow ratio, several liquid-liquid flow patterns are achievable in microchannels, such as: annular, parallel, bubbly or slug flow. Annular and parallel flows are observed when the inertial forces are competing with the interfacial forces (at *We* numbers > 1)[13]. The interfacial tension tends to minimize the interfacial area, while the inertial force is deforming and dragging the interface in the direction of the flow. Due to the competing nature of the inertial and interfacial forces, annular and parallel flows are easily destabilized by changing flow rates and volumetric flow ratios[10,13]. Slug[14,15] and drop flow[16,17] are extensively studied due to their easily controllable hydrodynamics and potential applications in fine chemicals synthesis and biotechnology .

Y-mixers[18] and T-mixers[19] provide a reproducible segmented slug flow, thus allowing a high degree of control over the slug size distribution and the liquid–liquid interfacial surface-to-volume ratio, which is in the range of 10 000 to 50 000 m^2/m^3 for a channel diameter in the range from tens to hundreds of micrometers[20,21]. This is one order of magnitude higher than in a stirred vessel, where the maximum surface-to-volume ratio is ca. 1000 m^2/m^3 [22,23]. The intensity of internal circulations in slugs[24,25] and therefore the overall mass transfer rate[24,26,27] depends on the slug geometry. Operation in the slug flow regime has been shown to be a useful tool for enchasing mass and heat transfer limited reactions such as nitration[28] or phase transfer catalyzed alkylations[29]. Furthermore, the ease of slug size control allows for levels of mass transfer and reaction control otherwise unachievable in stirred batch[21]. Considering industrial potential of the liquid-liquid slug flow application, in depth understanding of hydrodynamics and pressure drop is essential.

The pressure drop is an important parameter in the reactor design as it provides crucial information regarding the energy consumption, required pump capacity as well as the materials needed for the reactor construction. The investigation of pressure drop of the gas-liquid slug flow has been a subject of a large number of studies[30-35], while there are only a few studies on the liquid-liquid slug flow pressure drop. Furthermore, no pressure drop correlations have been proposed so far which include both the influence of the surface tension and the slug lengths. Last, the influence of the liquid film is not included

in the existing models. Therefore, a pressure drop model that predicts the influence of varying slug lengths, film thickness and interfacial effects on the liquid-liquid slug flow pressure drop in microchannels is needed.

The goal of this work is to develop a liquid-liquid slug flow pressure drop model describing the effect of interface surface shape, slug size and capillary diameter. Furthermore, it is important to determine the parameters with the highest impact on the pressure drop. For the model validation, experimentally measured pressure drops and slug sizes in capillaries with a diameter of 248 and 498 µm with several mixtures of immiscible liquids were used.

3.2 Previous work on slug flow pressure drop

In gas-liquid Taylor flow studies, the pressure is usually described using homogeneous[31,32,34] or Lockhart-Martinelli[35] correlations. However, in the two-phase flow the slug length has an influence on the contribution of the different terms in the total pressure drop. In the majority of studies, the interfacial effects are either neglected or included in the form of We and Bo numbers[30], therefore not accounting for the influence of the slug length on the overall pressure drop. Exceptions are the works of Kreutzer et al. (2005)[33] and Warnier et al. (2009)[35] which have included the contribution from the pressure difference over the bubble interface in the modelling. Compared to the vast number of gas-liquid studies, only two studies on liquid-liquid slug flow in microchannels are found[12,18]. Two-phase oil-water flows and pressure drop in horizontal microchannels made of quartz and glass were studied by Salim et al. (2008) [12]. The pressure drop measurements were interpreted by using the homogeneous and Lockhart-Martinelli models. The two-phase pressure drop was correlated to the single phase pressure drop of each phase over the whole length of the capillary:

$$\left(\frac{\Delta P}{L}\right)_{TP} = \left(\frac{\Delta P}{L}\right)_c + \eta \varepsilon_d \left(\frac{\Delta P}{L}\right)_d , \tag{1}$$

where $(\Delta P/L)_{TP}$ is the two phase pressure drop per unit capillary length, $(\Delta P/L)_c$ and $(\Delta P/L)_d$ are the continuous and dispersed single-phase pressure drops per unit capillary length, respectively. ε_d is the dispersed phase volume fraction and η is a fitting factor which depends on the wettability of the capillary wall. The empirical parameter η was determined from the experimental results, with values of 0.67 and 0.80 for the quartz and glass microchannels, respectively. The main drawback of this modeling approach is the absence of the surface tension and slug length influence on the pressure drop. Even an extended model[30] which includes an empirical parameter for the interfacial effects fails, because it does not distinguish between the different physics associated with different flow regimes[35].

The effect of various operating conditions on water-cyclohexane flow patterns, slug size, interfacial area and pressure drop in a PTFE Y mixer/capillary microreactor was investigated by Kashid et al. (2007) [18]. The slug flow was modeled as a series of slug unit cells, composed of a dispersed and continuous slug pair (Figure 1a). In the modeling the absence of the thin continuous phase film and a constant contact angle between the

dispersed slug and the wall were assumed. The proposed pressure drop model was interpreted in terms of two contributions: the frictional pressure drop of the individual phases (ΔP_{Fr}) and the pressure drop due to the interfacial effects (ΔP_I). For the purpose of the pressure drop modeling the slug unit length (l_U), dispersed phase length fraction (α) and the contact angle were used as input parameters (Figure 1a). The overall pressure drop was written as:

$$\Delta P_{slug\ flow} = \Delta P_{Frictional} + \Delta P_{Interfacial} = \Delta P_{Fr,c} + \Delta P_{Fr,d} + \Delta P_I \tag{2}$$

The frictional pressure drop, ΔP_{Fr}, was calculated from the Hagen-Poiseuille equation for a cylindrical tube and was expressed as a function of the slug unit length ($l_U = l_d + l_c$) and the dispersed phase length fraction ($\alpha = l_d / l_U$):

$$\Delta P_{Fr,d} = \frac{8 \mu_d v \alpha l_U}{R^2} \tag{3}$$

$$\Delta P_{Fr,c} = \frac{8 \mu_c v (1-\alpha) l_U}{R^2} \tag{4}$$

Where μ_d and μ_c are the viscosity of the dispersed and continuous phase, respectively. The superficial velocity, v, used in Eq. 3 and 4 was determined from the total flow rate:

$$v = (Q_c + Q_d) / A \tag{5}$$

The interface pressure ΔP_I was obtained from the Young-Laplace equation:

$$\Delta P_I = \frac{2\gamma}{R} \cos\theta \tag{6}$$

Combining Eqs. 2-6 yielded the model for the pressure drop across the length of the capillary:

$$\Delta P_{slug\ flow} = \frac{L}{l_U}(\Delta P_{Fr,d} + \Delta P_{Fr,c}) + \frac{2L - l_U}{l_U} \Delta P_I \tag{7}$$

The model of Kashid et al. (2007) [18] overestimated the experimental pressure drop data due to three reasons: (**I**) The interface pressure drop was calculated at a constant contact angle (Figure 1a); (**II**) the contributions of the front and rear meniscuses were summed up; (**III**) the superficial velocity of the continuous phase was used to calculate the frictional pressure loss. The proposed expression for the interface pressure would only be correct for the case of a dry wall [37,38]. If a liquid thin film is present (Figure 1b), there is no direct contact between the dispersed phase slugs and the capillary wall. Consequently, the contact angle values become substantially different from the dry wall case. Furthermore, the receding and advancing contact angles can only be assumed equal at very low velocities. The difference between them increases with the increase of the linear

velocity[38]. The front meniscus has a positive contribution to the pressure drop and the rear meniscuses has a negative contribution to the pressure drop (Figure 1a), therefore the contributions from the front and rear meniscus should be subtracted rather than summed up (Figures 1c and d). Finally, due to the presence of the liquid film, the dispersed phase slug traverses at a higher velocity than the continuous phase[35].
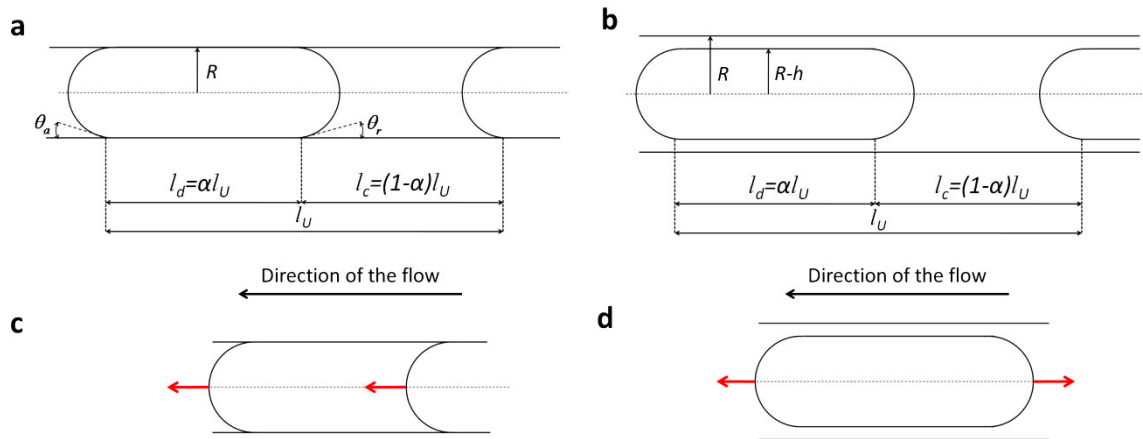

*Figure 1: **a.** Slug unit cell without film, **b.** Slug unit cell with thin film, **c.** Slug flow in the case of a dry wall. The interfaces of the slug are deformed in the direction of the flow, thus the interface pressure drop over the slug is acquired by adding the interface pressure drops, **d.** Slug flow in the case of a wetted wall. The interfaces of the slug are deformed in opposite directions, therefore the interface pressure drop over the slug is acquired by subtracting the interface pressure drops.*

3.2 Pressure drop model

Similar to the work of Kashid et al. (2007) [18] and Kreutzer et al. (2005)[33], the liquid-liquid slug flow pressure drop is considered to consist of the frictional pressure drop and interface pressure drop contributions. Two pressure drop models are developed taking into account the following assumptions:

- The flow is considered as a fully developed Hagen-Poiseuille flow, which is disturbed by the caps of the dispersed phase slug, causing an excess pressure drop.
- The frictional pressure drop is described by Eqs. 3 and 4 for the discrete and continuous phases, respectively.
- The interface pressure drop is described by the Bretherton's solution for the pressure drop over a single bubble in a capillary[39].

Computational fluid dynamics (CFD)[40] studies of velocity profiles showed that the dispersed phase slug has a parabolic profile, while the continuous phase parabolic profile is slightly disturbed near the interface. A fully developed velocity profile was observed at the centre of the continuous inter-slug. Furthermore, the influence of the liquid film surrounding the dispersed slug is included in the models. The slug flow is modeled as a

series of slug unit cells in which the dispersed phase slug is separated from the wall by a thin film of the continuous phase (Figure 1 b). In order to analyze the influence of the film velocity on the slug flow pressure drop two models were developed and evaluated: the stagnant film model and the moving film model.

3.2.1 Stagnant film model

In the stagnant film (SF) model, the thin film between the continuous phase and the dispersed phase slug is considered to be stagnant, effectively reducing the radius of the channel through which the dispersed slug, R_{slug} is traversing:

$$R_{slug} = R - h \tag{8}$$

The liquid film thickness in a circular channel was calculated as a function of the Capillary number, Ca[39]:

$$h = 1.34 R Ca^{2/3}, \tag{9}$$

which is valid in the range of h below $0.01 \cdot R$ and in the absence of significant inertial and gravitational forces. Considerable deviations from Bretherton's equation were observed at Capillary numbers higher than $5 \cdot 10^{-3}$ and for the film thickness larger than 1% of the channel radius [41-43]. Furthermore, in the systems where the continuous phase has a considerably higher viscosity than the dispersed phase the Bretherton equation needs to be corrected by a factor of $2^{2/3}$ [44]:

$$h = 1.34 R (2Ca)^{2/3} \tag{10}$$

The interface pressure drop was calculated by an analytical solution for a single bubble in two-phase flow[39], where the Laplace pressure and the change in curvature due to the presence of the liquid film surrounding the bubble were taken into account to yield:

$$\Delta P_I = C(3Ca)^{2/3} \frac{\gamma}{d} \tag{11}$$

Assuming ideally semispherical caps, the constant C, which accounts for the influence of the interface curvature, was found to be 7.16[39]. The theory of Bretherton is in a good agreement with experimental data for $Ca < 5 \cdot 10^{-3}$ and $We \ll 1$. However, for $Ca < 10^{-4}$ and $Ca > 10^{-2}$ and in cases when inertia is not negligible, the Bretherton analysis is no longer valid[33,35,45]. Several authors[46-49] have included the inertial effects in their finite element modeling of pressure drop, confirming the deviation from Eq. 11. Therefore Eq. 11 should be further extended to a wider range of operating conditions. Unfortunately, to this date, no new expression for the pressure drop over a bubble was developed, thus in the modeling of the pressure drop Eq. 11 was used.

Inserting Eqs. 3, 4, 8 and 11 into Eq. 2 results in the slug flow pressure drop equation for the stagnant film case:

$$\Delta P_{SF} = \frac{8v_{slug}\mu_d\alpha L}{(R-h)^2} + \frac{8v\mu_c(1-\alpha)L}{R^2} + \frac{L}{l_u}C(3Ca)^{2/3}\frac{\gamma}{d} \tag{12}$$

3.2.2 Moving film model

In order to analyze the influence of the film velocity on the slug flow pressure drop a second model was developed which considers a constant thickness moving film between the dispersed slug and the capillary wall. The only difference between the stagnant (SF) and moving film (MF) pressure drop models is in the term describing the frictional losses of the dispersed phase (Eq. 13). The derivation of this term is presented in the appendix. The shear stress and the velocity are assumed to be continuous through the fluid-fluid interface and a no-slip boundary condition is applied at the channel wall.

$$\Delta P_{Fr,d} = \frac{4v_{slug}L\alpha}{\dfrac{R^2-(R-h)^2}{\mu_c}+\dfrac{0.5(R-h)^2}{\mu_d}} \tag{13}$$

Combining Eqs. 2, 4, 11, and 13 yields the moving film pressure drop equation:

$$\Delta P_{MF} = \frac{4v_{slug}L\alpha}{\dfrac{R^2-(R-h)^2}{\mu_c}+\dfrac{0.5(R-h)^2}{\mu_d}} + \frac{8v\mu_c(1-\alpha)L}{R^2} + \frac{L}{l_u}7.16(3Ca)^{2/3}\frac{\gamma}{d} \tag{14}$$

Table 1 summarizes the respective contributions to the pressure drop in the two models. The difference between the models comes from the term of the dispersed phase frictional pressure drop.

Table 1. Contributions of the pressure drops for the stagnant and moving film pressure drop models.

Model	$\Delta P_{dispersed}$	$\Delta P_{continuous}$	$\Delta P_{interfacial}$
Stagnant film (SF)	$\dfrac{8v_{slug}\mu_d\alpha L}{(R-h)^2}$	$\dfrac{8v_{slug}\mu_c(1-\alpha)L}{R^2}$	$\dfrac{L}{l_U}7.16(3Ca)^{2/3}\dfrac{\gamma}{d}$
Moving film (MF)	$\dfrac{4v_{slug}L\alpha}{\dfrac{R^2-(R-h)^2}{\mu_c}+\dfrac{0.5(R-h)^2}{\mu_d}}$	$\dfrac{8v_{slug}\mu_c(1-\alpha)L}{R^2}$	$\dfrac{L}{l_U}7.16(3Ca)^{2/3}\dfrac{\gamma}{d}$

Table 2. Physical properties of the chemicals used at 20 ˚C.

Component	Density, kg/m^3	Viscosity, Pa	Surface tension, N/m
Demineralized H_2O	998.2[a]	0.00100[a]	0.0371[b]
40 wt.% ethylene glycol in H_2O	1040.3[b]	0.00246[b]	0.0231[b]
Toluene	866.7[a]	0.00059[a]	-

a-values taken from Perry et al. (1997)[22]

b-measured values

3.3 Experimental

All chemicals used in this work are commercially available GC grade and were obtained from Sigma-Aldrich. In this work two multiphase flows were studied: water-toluene (W-T) flow and ethylene glycol/water-toluene (EG-T) flow. The latter was composed of 40 wt.% of ethylene glycol in demineralized water. The interfacial surface tension was measured via a Krüss K11tensiometer. The viscosity was measured with a Brookfield LVDV-I Prime viscometer. The overview of the physical properties of the system is given in Table 2.

A schematic view of the experimental setup is shown in Figure 2. The aqueous and organic phases were mixed in a stainless steel Y-mixer with an angle between the mixer inlets of 110°. Two Y-mixers, with internal diameters of 250 or 500 µm (VICI) were used. Two HPLC pumps (Shimadzu LC-20AD) were used to feed the corresponding solutions to the Y-mixer. PEEK constrictions of 25 µm were used to reduce the pulsations caused by the pump plungers. A differential pressure sensor (26C Series, Sensortechnics) was connected at a distance of 50 cm upstream from the Y-mixer. The differential pressure sensor had a measurement range of 0-16 bars, with a 5 % relative error of measurement. The Y-mixers were connected to a 5 m long fused silica capillary with the same nominal internal diameter. The actual hydraulic diameters of the capillaries were 248 µm and 498 µm as calculated via Eq. 4 using single phase pressure drop measurements. The relative error of the single phase measurements was 5 %, which corresponds to the differential pressure sensor measurement accuracy. The Y mixer-capillary assemblies were oriented horizontally with respect to the gravity vector unless otherwise mentioned.
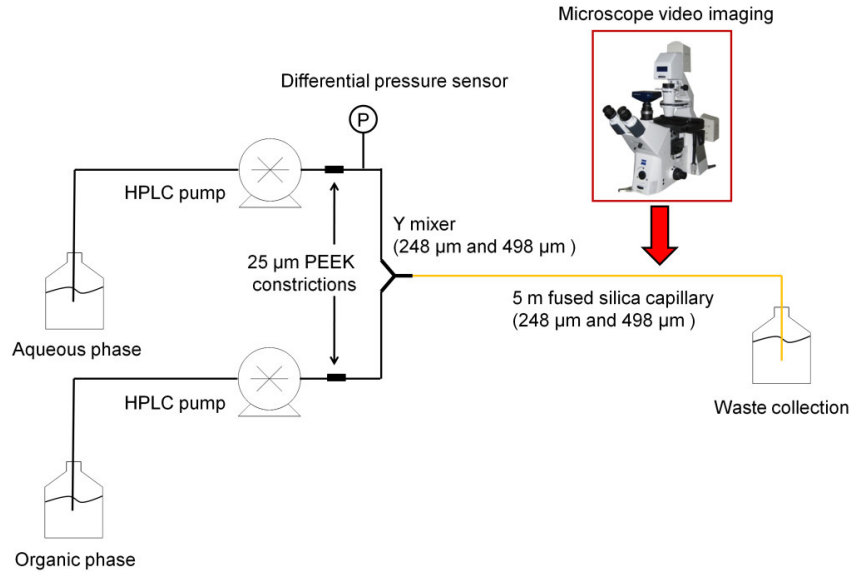
Figure 2: Experimental setup: Stainless steel Y-mixer coupled with a 248/498-µm-internal-diameter silica capillary. Supply of the organic and aqueous mixtures was provided by two HPLC pumps (Shimadzu LC-20AD).

The experiments were performed at a flow rate range of 0.05-1.5 ml/min and 0.35-6 ml/min for the 248 µm and 498 µm capillaries, respectively. The organic-to-aqueous volumetric flow ratio range was varied from 0.06 to 5. All experiments were performed by first pumping the aqueous phase, followed by the organic phase. The measured pressure drop of the Y mixer-capillary assembly consists of contributions from the single phase pressure drop over the feed line upstream from the Y-mixer (ΔP_{SP}), the pressure drop over the Y-mixer (ΔP_Y), and the two phase slug flow pressure drop over the capillary length (ΔP_{TP}):

$$\Delta P_{Measured} = \Delta P_{SP} + \Delta P_Y + \Delta P_{TP} \qquad (15)$$

The two-phase slug flow pressure drop was calculated by subtracting the ΔP_{SP} and ΔP_Y terms from the experimental value. The sum of the ΔP_{SP} and ΔP_Y values was obtained from pressure drop measurements with and without capillary.

Microscope video imaging of the slug flow was done with a Zeiss Axiovert 200 MAT microscope coupled with a high speed imaging camera (Redlake MotionPro CCD). The videos were recorded at a rate from 800 to 2500 frames per second at a resolution of 1280x480. Under each operational condition a sequence of 25 to 100 slug length units were analyzed. The slug velocity, v_{slug}, slug size, slug unit length, and dispersed phase length fraction, were obtained via video imaging analysis using Matlab R2007b Image processing. The measured lengths were averaged to obtain the mean value and the standard deviation, which are presented. The dispersed slug velocity was calculated by dividing the distance it traveled by the measurement time interval.

3.4 Results and discussion

3.4.1 Stable regime for slug flow operation

The hydrodynamics were studied in 248 µm and 498 µm internal diameter capillaries at different viscosities and interface surface tensions using the W-T and EG-T two-phase flows. The linear velocity at an equal organic-to-aqueous volumetric (OA) ratio was varied in the range of 0.03 – 0.5 m/s to identify the boundaries of a stable slug flow regime, which is characterized by a reproducibility of the slug length, with the standard deviation of slug lengths below 50 % [21]. At linear velocities higher than 0.19 m/s the slug flow became unstable, generating slugs from 200 µm to several millimeters in size. Zhao et al. (2006)[13] used the Weber number, which represents the ratio between the inertial and surface tension forces, to express a criterion for the transition between flow patterns. The transition from slug to parallel flow takes place at increasing flow rate and was observed at $We > 0.5$ and $We > 0.8$ for the W-T and EG-T flows, respectively.

3.4.2 Slug flow unit length and film thickness

The modeling of the slug flow pressure drop requires several hydrodynamic input parameters – slug unit length, dispersed phase length fraction and film thickness.
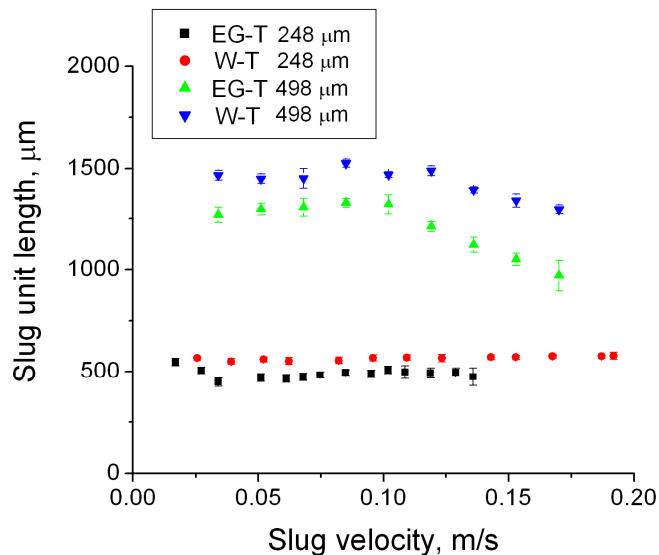

Figure 3: The slug unit length (l_U in Eqs. 12 and 14) of the water-toluene (W-T) and ethylene glycole/water-toluene (EG-T) slug flow in the 248 µm and 498 µm capillaries as a function of slug velocity at an O/A ratio of 1.

Table 3. *Re*, *Ca*, *We* and *Bo* numbers for water-toluene (W-T) and ethylene glycol/water-toluene (EG-T) flows.

Flow	Capillary	*Re*	*Ca*	*We*	*Bo*
W-T	248 μm	6.3 – 47.5	$6.9 \cdot 10^{-4} - 5.2 \cdot 10^{-3}$	$4.3 \cdot 10^{-3} - 2.5 \cdot 10^{-1}$	$1.6 \cdot 10^{-2}$
W-T	498 μm	16.7 – 84.4	$9.2 \cdot 10^{-4} - 4.6 \cdot 10^{-3}$	$1.5 \cdot 10^{-2} - 3.9 \cdot 10^{-1}$	$6.4 \cdot 10^{-2}$
EG-T	248 μm	1.9 – 16.2	$1.9 \cdot 10^{-3} - 1.6 \cdot 10^{-2}$	$2.6 \cdot 10^{-3} - 3.6 \cdot 10^{-1}$	$2.7 \cdot 10^{-2}$
EG-T	498 μm	7.2 – 37.1	$3.7 \cdot 10^{-3} - 1.9 \cdot 10^{-2}$	$2.7 \cdot 10^{-2} - 7.0 \cdot 10^{-1}$	$1.1 \cdot 10^{-1}$

The influence of the slug velocity on the organic and aqueous slug size is shown in Figure 3. In the 498 μm capillary, the slug size decreased with increasing slug velocity above 0.1 m/s, which is in agreement with data of Kashid et al. (2007) [18]. The slug unit length remained relatively constant in the 248 μm capillary for slug velocities above 0.034 m/s. In both cases, the slug length was shorter in the flow with higher viscosity of the continuous phase (EG-T), which created a higher hydrodynamic flow resistance. Consequently, the flow of the dispersed phase was pinched in the mixer by the continuous phase into smaller slugs. The Reynolds number, which represents the ratio of the inertial to viscous forces, in the W-T flow was twice as large as compared with that in the EG-T flow (Table 3). This indicates that the inertial forces are larger in the W-T flow. The lower hydrodynamic resistance and the tendency of the inertial forces to drag the surface downstream are responsible for the larger slug sizes in the W-T flow. Low values of the *Ca* number, which represents the ratio between the viscous and surface tension forces, show that the surface tension dominates the viscous forces. With increasing slug velocity the *We* number increases, indicating that the main competing forces in the system are the inertial and surface tension forces.
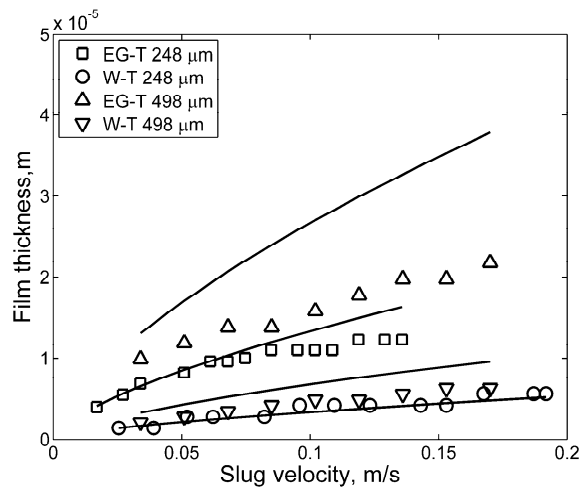

Figure 4: Measured film thickness (points) and Bretherton's equation predictions of the film thickness (solid line) for the cases of the water-toluene (W-T) and ethylene glycole/water-toluene (EG-T) slug flows in the 248 μm and 498 μm capillaries as a function of slug velocity at an OA ratio of 1.

The film thickness in the 248 µm capillary increases with increasing slug velocity in accordance with Eqs. 9 and 10 in the W-T and EG-T flows, respectively (Figure 4). However, the film thickness was overestimated in the 498 µm capillary, where an asymmetrical distribution of the film thickness was observed (Figure 5a). The continuous phase has a higher density than the dispersed phase in both two-phase flows. The slug of the continuous phase is displaced from the centerline by gravity, resulting in an uneven film thickness around the slug (Figure 5 b). To illustrate the degree of film displacement, the top film thickness was reduced down to approximately 1 µm, while the bottom film thickness increased up to 21 µm. Consequently, the average deviations from the Eqs. 9 and 10 were 21 % and 38 %, for the W-T and EG-T flows, respectively.
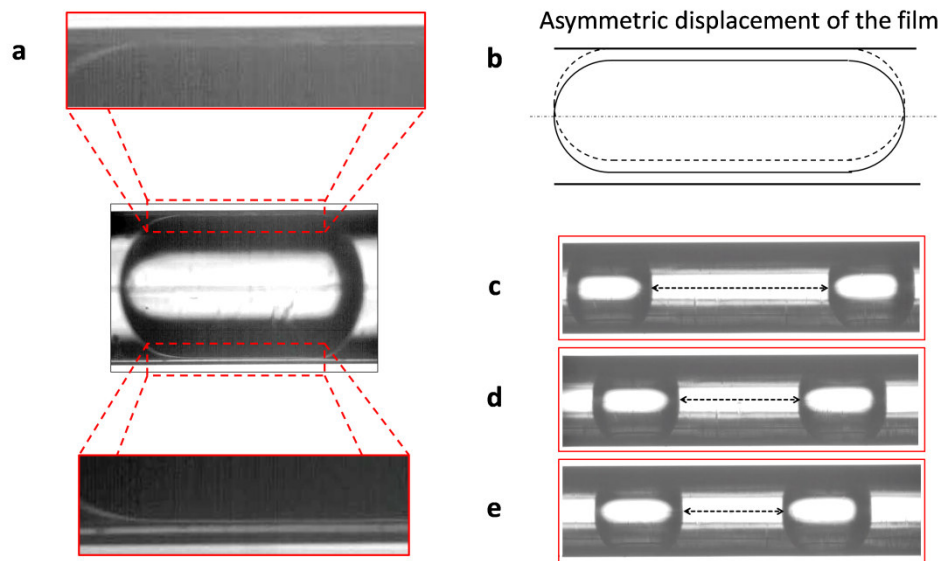
*Figure 5: Influence of gravity in the 498 µm capillary: **a.** and **b.** Asymmetric displacement of the thin film in the horizontal capillary, **c.** Stable flow in the horizontal capillary, **d.** and **e.** Draining of the film in the vertical capillary, thereby shortening the distance between two subsequent dispersed slugs.*

The influence of gravity on the slug movement was studied in the 498 µm capillary oriented horizontally and vertically. A stable slug flow was observed in the horizontally oriented capillary (Figure 5 c), while disturbances in the slug size were observed in the vertically oriented capillary (Figures 5 d, e) where the draining of the continuous phase occurred, thus pushing the less dense, dispersed phase upwards and reducing the distance between the two subsequent slugs. No disturbances were observed in the 248 µm capillary. The Bond number, the ratio of gravitational force to the surface tension force, is listed in Table 3 for both capillaries. From these results it can be concluded that gravity does not influence the hydrodynamics of slug flow at *Bo* numbers below 0.03.

With increasing *We* number the interfacial forces, which stabilize the slug cap curvature, become insufficient to maintain the semispherical shape of the caps. As a result, the nose of the slug becomes elongated and the rear of the slug flattened. The advancing and the receding contact angle of the slug caps measured for the 248 µm capillary were measured in order to investigate the effect of the cap curvature. It is important to note that the slug cap contact angle is not the equivalent to the one used to characterize wetting, as the dispersed phase is separated from the capillary wall by a thin film. In this study, the slug cap contact angles are used only as a measurement of the slug cap deformation. The measured contact angles as a function of slug velocity are shown in Figure 6. The decrease in the advancing angle shows the stretching of the front cap, while the increase in the receding angle indicates the flattening of the back cap. Kreutzer et al. (2005)[50] numerically modeled this effect for a gas bubble.
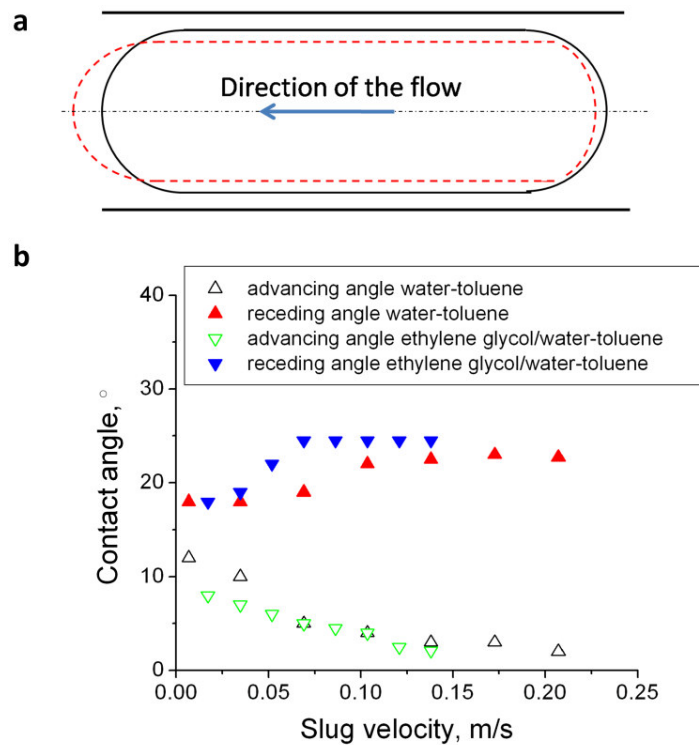
*Figure 6: Deformation of the water-toluene (W-T) slug shape with increasing inertia in the 248 µm capillary: **a.** Schematic view of the slug at different We numbers. Solid line: We = 5·10^{-3}, dashed line: We= 2·10^{-1}, **b.** Change of the advancing and receding slug cap contact angles as a function of slug velocity.*
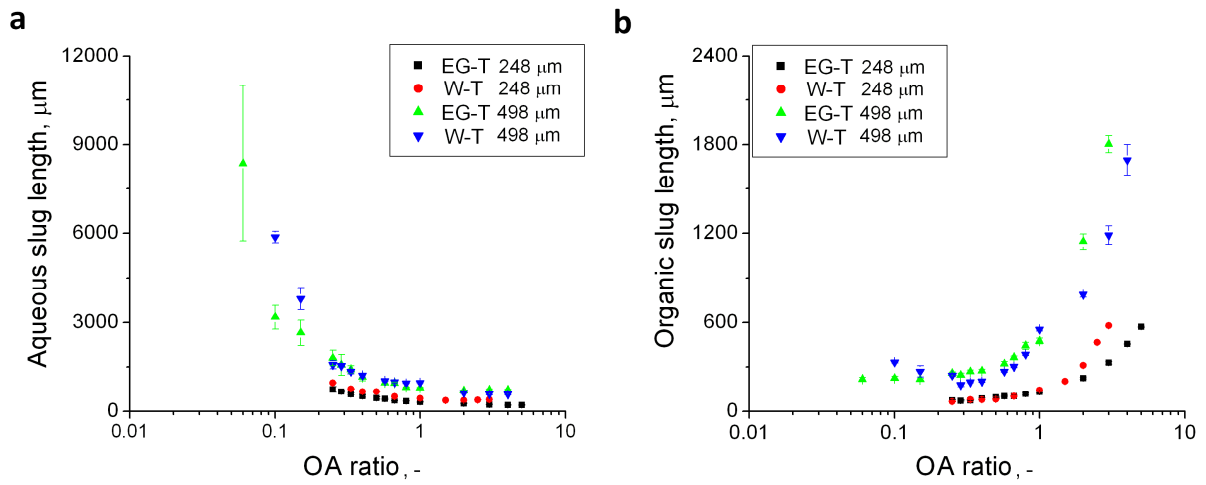
*Figure 7: The slug length of the (**a.**) the continuous, aqueous and (**b.**) the dispersed, organic phase of the water-toluene (W-T) and ethylene glycole/water-toluene (EG-T) slug flow in the 248 µm and 498 µm capillaries as a function of the OA ratio at a total flow rate of 0.1 ml/min.*
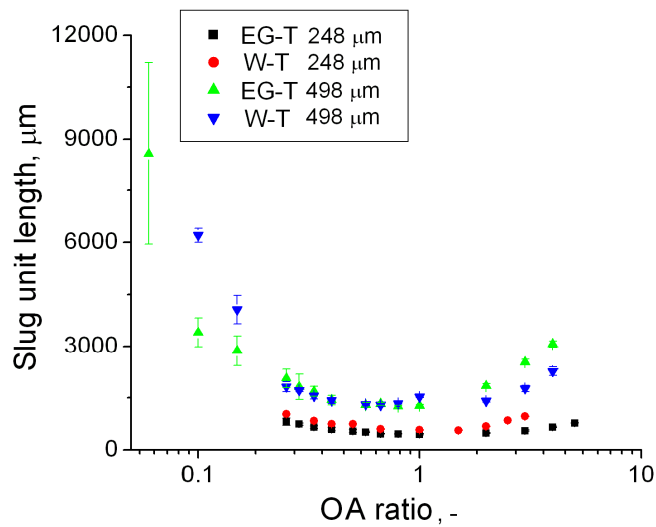
Figure 8: The slug unit length (l_U in Eqs. 12 and 14) of the water-toluene (W-T) and ethylene glycole/water-toluene (EG-T) slug flow in the 248 µm and 498 µm capillaries as a function of the OA ratio at a total flow rate of 0.1 ml/min.
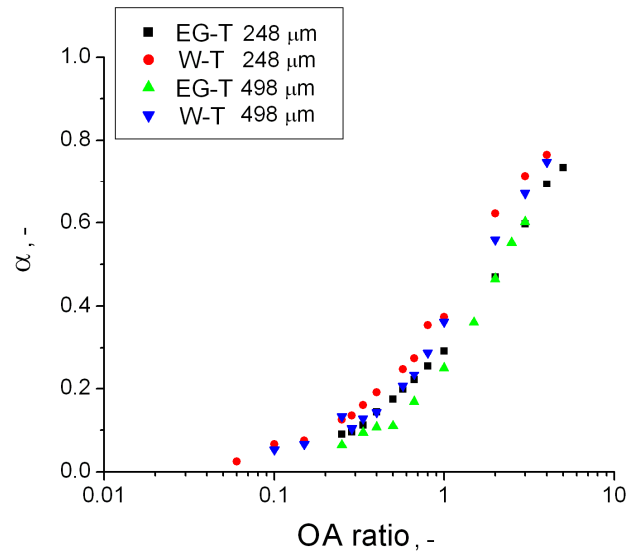
Figure 9: The dispersed phase length fraction of the water-toluene (W-T) and ethylene glycole/water-toluene (EG-T) slug flow in the 248 µm and 498 µm capillaries as a function of the OA ratio at a total flow rate of 0.1 ml/min.

The variation of the organic-to-aqueous flow rate (OA) ratio was found to be an effective method to control the slug size[18,21]. By increasing the OA ratio the aqueous slug size decreases while the organic slug size increases (Figures 7 a, b). The slug unit length decreases with increasing OA ratio and reaches a minimum at an OA ratio of approximately 1 and 0.8 in the 248 µm and 498 µm capillaries, respectively (Figure 8). The minimal slug unit length corresponds to the conditions of approximately equal organic and aqueous volumetric flow rates. By operating at the conditions of unequal flow rates will result in the increase of slug size, consequently increasing the slug unit length. The influence of the OA ratio on the dispersed phase length fraction, α, is shown in Figure 9.

3.4.3 Pressure drop model comparison

The stagnant film (SF) and moving film (MF) models were compared with the Kashid et al. (2007)[18] and Salim et al. (2008)[12] models for the case of W-T flow in the 248 µm capillary (Figure 10). The model of Kashid et al. (2007)[18] overestimates the experimental data as a result of summation of the interface pressure contributions from the front and rear meniscuses. The model of Salim et al. (2008)[12] underestimates the experimental data because it does not contain the term accounting for the contribution of the interface pressure drop.
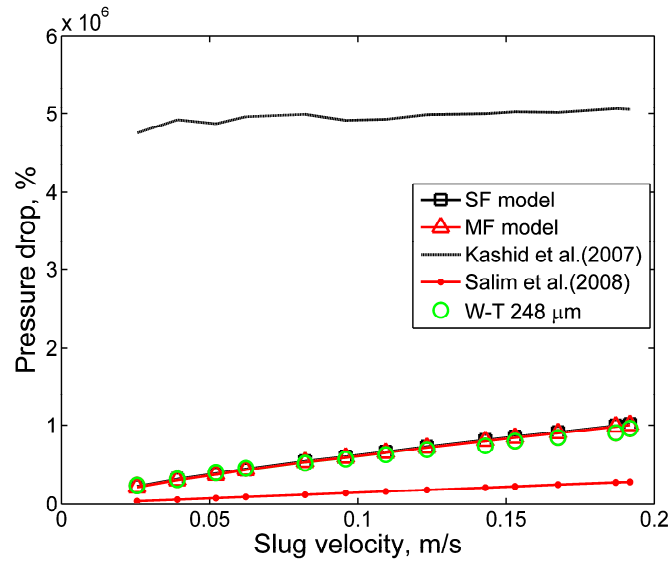
Figure 10: Comparison of the stagnant film (SF) and moving film (MF) models with the models of Kashid et al. (2007) [18] and Salim et al. (2008) [12] on the case of the water-toluene (W-T) flow in the 248 μm capillary. The SF and MF model results were different by less than 1.4 %.

The model accuracy was evaluated via the mean relative error (MRE) method:

$$MRE = \frac{\displaystyle\sum_{n=1}^{N} \frac{\left|\Delta P_{model} - \Delta P_{experimental}\right|}{\Delta P_{experimental}} \cdot 100}{N} \%$$

The SF and MF models were found to be in good agreement with the experimental data, with a mean relative error less than 5 %. The relative difference in the prediction of the pressure drop between the SF and MF models was lower than 1.4%, which indicates that the film velocity has very little influence on the overall pressure drop. The sensitivity of the influence of the standard deviation of the model parameter values on the pressure drop model results was evaluated (Table 4). The highest relative standard deviations taken for the slug and film velocities, dispersed phase length fraction and film thickness gave relative differences in the pressure drop below 2.2 %. The slug length unit, and therefore the total number of slug interfaces in the capillary, has the largest influence on the pressure drop. The highest relative standard deviation of 8% resulted in a difference in the model pressure drop values of 5 %. The film velocity is an order of magnitude lower than the slug velocity, therefore the standard deviation of the film velocity resulted in model result differences below 1 %. Compared to the SF model, the MF model requires additional assumptions concerning the shear stress and the velocity throughout the interface. Therefore, the SF was chosen for the interpretation of the experimental data.

Table 4. The effect of deviations of input parameters on the calculated pressure drop

Parameter	The largest standard deviation of measurement, %	Difference in pressure drop, %
Slug velocity	2	<2
Dispersed phase fraction	10	<1
Film thickness	100	<2.2
Slug length unit	8	<5

3.4.4 Interface pressure drop and the curvature parameter

The individual contributions of the dispersed and continuous frictional pressure drop and the interface pressure drop to the overall pressure drop for the W-T flow in the 248 µm capillary are shown in Figure 11. The interface pressure drop was found to have the highest contribution to the overall pressure drop, with a contribution above 60 %. Therefore, the correct prediction of the interface pressure drop is important to provide a high accuracy of the pressure drop estimation by the SF model.
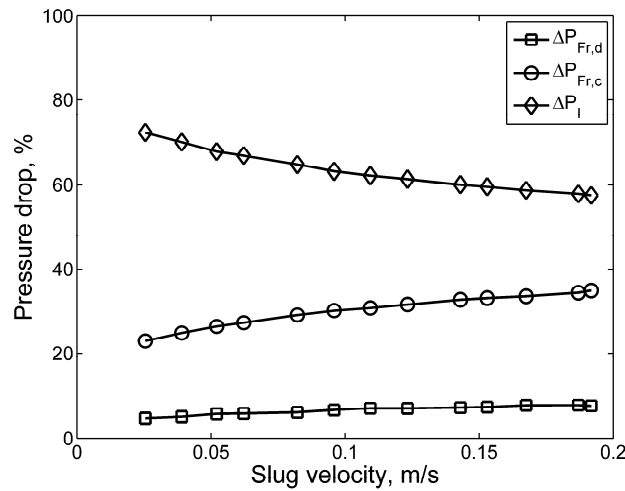
Figure 11: Contributions of the dispersed and continuous phase frictional pressure drop and the interface pressure drop to the total slug flow pressure drop at an OA ratio of 1 in the case of the water-toluene (W-T) flow in the 248 µm capillary.

The interface pressure drop was calculated by Eq. 11 derived under conditions when inertial, viscous and gravitational forces are negligible as compared to the interfacial forces, resulting in the semispherical shape of the meniscus in circular capillaries[39]. In this case, the curvature parameter C is equal to 7.16. Wong et al. (1995)[51] studied the two-phase pressure drop in various capillary cross sections, viz. polygonal, square, slot and circular, yielding an equation similar to the correlation of Bretherton:

$$\Delta P_I = \frac{C_d}{A} \cdot (Ca)^{2/3}, \qquad\qquad (16)$$

where the mathematically equivalent curvature parameter, represented by the C_d/A ratio, depended on the curvature of the bubble. The C_d/A parameter was in the range from 3.15 to 10.02 depending on the cross sectional geometry. Van Stein et al. (2008) [52] used the curvature parameter of 2.39 for slug flow pressure drop modeling in a square capillary with a 800 µm hydraulic diameter. Therefore, it is clear that the curvature parameter is highly dependent on the shape of the bubble curvature. The computation of the interface pressure drop becomes even more complicated due to the Marangoni effect[50] caused by the traces of impurities which can change the results of the Bretherton theory up to a factor of $4^{2/3}$ [53].

The influence of the slug velocity on the W-T and EG-T flow pressure drops in the 248 µm and 498 µm capillaries is shown in Figure 12. The pressure drop calculated by the SF model was in a good agreement with experimental results, with a mean relative error less than 10 %. The value of the curvature parameter of 7.16 provides a good agreement with the experimental results in the 248 µm capillary, while in the 498 µm capillary a value of 3.48 should be used to fit the experimental data due to the asymmetrical distribution of the film. The SF model underestimates the experimental data by approximately 5.5 % at slug velocities below 0.06 m/s, while at higher velocities it overestimates the measured pressure drop. With increasing slug velocity, the shape of the meniscus changes, the front end being elongated and the rear end of the slug being flattened (Figure 6), resulting in the change of the curvature parameter and with it the interface pressure drop. The asymmetric distribution of the film affects the curvature parameter in the 498 µm capillary as well.

In the present study, the contribution from the gravity and inertia forces should be taken into account (Figures 5 and 6), in the cases where a non-spherical shape of the slug cap was observed. The effect of flow velocity on the curvature parameter was determined by Eq. 12 by using the pressure drop measurements (Figure 13). The shape of the slug cap curvature represents the balance of the dominant forces present in the system, most notably the inertial and surface tension forces. With increasing velocity two effects occur, namely increase in the film thickness and deformation of the front and back meniscuses. The increase in the film thickness squeezes the slug cap, thus deforming the curvature. It can be seen in Figure 13 b, that the curvature parameter decreases at higher We number. Therefore, in order to accurately model the pressure drop, the change of the slug cap curvature must be accounted for by modifying the curvature parameter values as a function of the slug velocity.

Figure 12: Modeling of the water-toluene (W-T) and ethylene glycole/water-toluene (EG-T) slug flow pressure drop in the 248 µm and 498 µm capillaries as a function of slug velocity at an OA ratio of 1 with the stagnant film model (solid line).

a.   **b.**
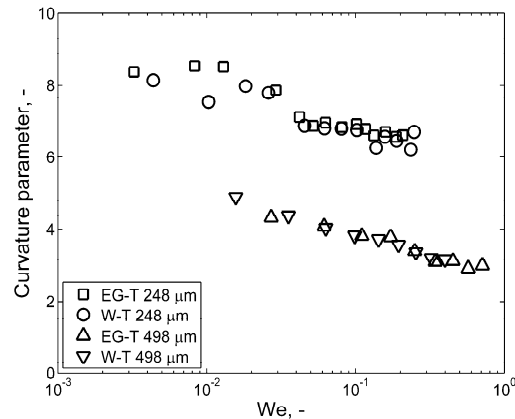
*Figure 13: The curvature parameter of the water-toluene (W-T) and ethylene glycole/water-toluene (EG-T) slug flow in the 248 µm and 498 µm capillaries as a function of: **a.** slug velocity, **b.** We number.*

3.4.5 Effect of slug size, viscosity and capillary diameter on the pressure drop

The comparison of the experimental pressure drop with the predicted values for different OA ratios for the W-T and EG-T flows in the 248 µm and 498 µm capillaries is shown in Figure 14. Since the experiments with the OA ratios were performed at a slug velocity of 0.034 m/s, the curvature parameter values of 8.14 and 4.21 were applied for the 248 µm and 498 µm capillaries, respectively (Figure 13 a). The SF model predicts the experimental values with a mean relative error lower than 7 %. With increasing OA ratio the total pressure drop increased, reaching a maximum after which it decreased with

further increase in the OA ratio. Contrary to the SF model, the previously discussed[12,18] liquid-liquid pressure drop models could not predict the influences of the OA ratio and the changing slug size on the overall pressure drop.

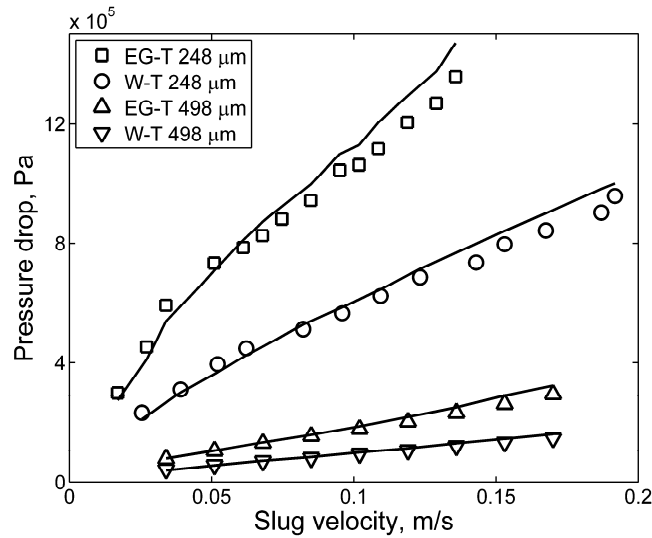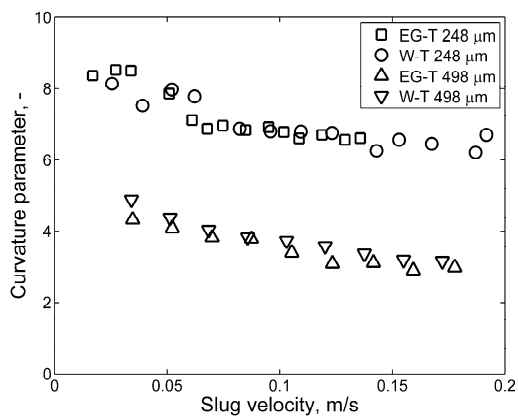*Figure 14: Modeling of the water-toluene (W-T) and ethylene glycole/water-toluene (EG-T) slug flow pressure drop in the 248 µm and 498 µm capillaries as a function of the OA ratio at a total flow rate of 0.1 ml/min with the stagnant film model (solid line).*
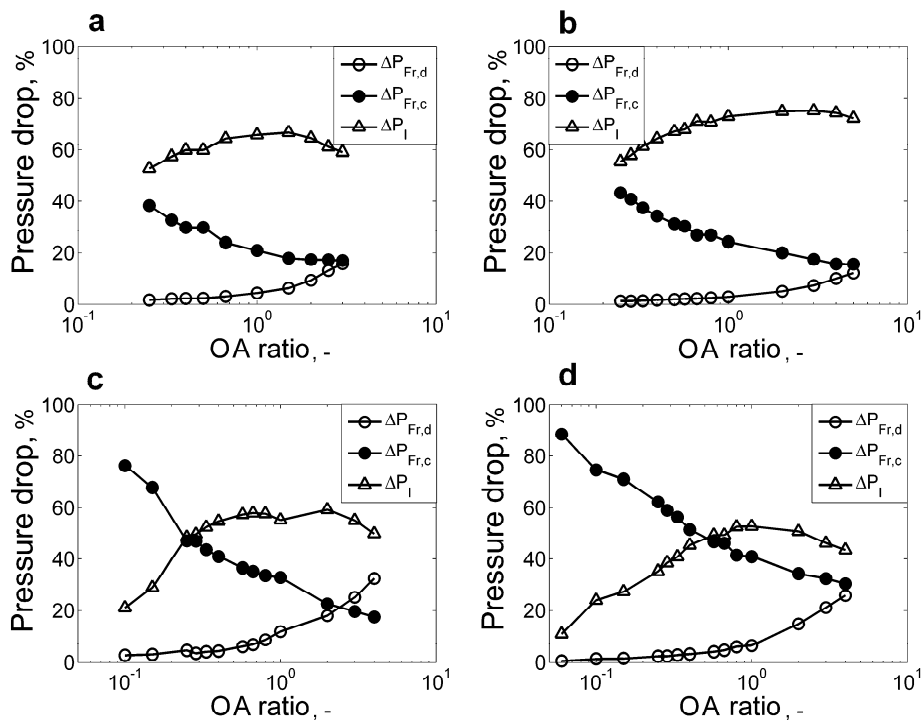
*Figure 15: Stagnant film (SF) model results for the individual contributions of the dispersed and continuous phase frictional pressure drops and the interface pressure drop to the total pressure drops at different OA ratios, viscosities and capillary diameters at a total flow rate of 0.1 ml/min: **a.** W-T 248 µm, **b.** EG-T 248 µm, **c.** W-T 498 µm, **d.** EG-T 498 µm.*

In order to understand the influence of the viscosity, capillary diameter and OA ratio on the slug flow pressure drop, individual dispersed and continuous frictional and interface pressure drop contributions were analyzed (Figure 15). In the 248 µm capillary the interface pressure drop accounts for more than 60 % of the total pressure drop for both W-T and EG-T flows. With increasing OA ratios the aqueous slugs become smaller while the organic slugs increase in size (Figure 7). Consequently, the continuous phase pressure drop decreases, while the dispersed phase pressure drop increases. The interface pressure drop is proportional to the total number of slug interfaces in the system. Therefore, it reaches a maximum when there is maximal number of interfaces in the system. The maximal number of interfaces is present in the system when the slug unit length is minimal (Figure 8). By increasing the capillary diameter the interface pressure decreases, consequently lowering the interface pressure contribution below 50 %. In both systems the pressure drop reaches the maximum value at the OA ratio in the range of 0.8-1.5. In this range the maximal number of slugs and interfaces is present in the capillary, and thus the highest frictional and interface pressures are achieved. The viscosity has a twofold influence. First, the slug size decreases as viscosity increases (Figure 3), consequently increasing the overall number of slugs and interfaces in the system, and therefore the frictional and interface pressure drops (Figure 15). Furthermore, with increasing viscosity the continuous phase frictional pressure drop increases, due to the higher hydrodynamic flow resistance.

In order to determine the accuracy of the models, the measured pressure drop was compared with the predicted values (Figure 16). For the W-T and EG-T flows in the 248 µm capillary the mean relative error was 4.84 % and 3.95 %, respectively. In the 498 µm capillary the mean relative error was 4.38 % and 6.78 %, for W-T and EG-T flows, respectively.
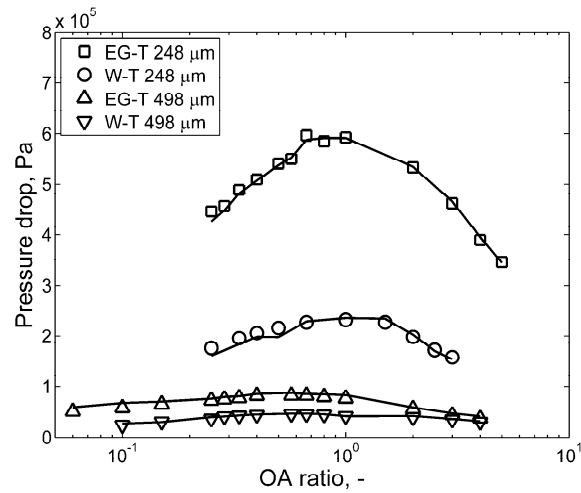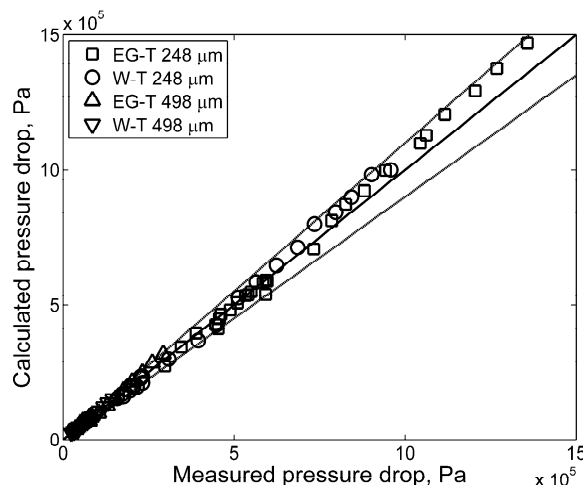

Figure 16: Comparison of the water-toluene (W-T) and ethylene glycole/water-toluene (EG-T) slug flow pressure drop in the 248 µm and 498 µm capillaries calculated via the stagnant film (SF) model and the measured slug flow pressure drop show good agreement within ± 7% relative error range.

3.5 Conclusions

In this work the hydrodynamics and pressure drop of liquid-liquid slug flow in round capillary microreactor were investigated. The continuous and dispersed phase slug sizes were found to be dependent on the slug velocity, organic to aqueous flow ratio, viscosity and capillary diameter. The film thickness in the 248 µm capillary was found to be in good agreement with the film thickness model developed by Bretherton[39]. In the 498 µm capillary the influence of gravity was observed, resulting in an asymmetrical film distribution. The gravity effects were found to be absent at Bo numbers below 0.03. Under the studied conditions, surface tension and inertia were found to be the dominant forces influencing the slug flow.

The stagnant and moving film models have been developed and compared to the liquid-liquid pressure drop studies found in literature. The developed models accounted for two sources of pressure drop: (**I**) frictional pressure drop, and (**II**) interface pressure drop. The film velocity was found to be of negligible influence on the pressure drop. Therefore, the mathematically simple stagnant film model was found to be appropriate for the slug flow pressure drop modeling. The pressure drop was found to be highly dependent on the slug size. The correct modeling of the interface pressure drop, often referred to as the "Bretherton's problem", was found to be crucial for the accurate modeling of the slug flow pressure drop. The existing solution to the pressure drop over a bubble or slug is valid for conditions where inertia is absent. With increasing inertia, the deformation of the ideally semispherical slug cap curvature was observed. Consequently, the curvature parameter of Bretherton's interface pressure drop equation was found to decrease. It was concluded that for the accurate modeling of the pressure drop, the change of the slug cap curvature must be accounted for by modifying the curvature parameter.

By changing the flow ratios, the slug sizes of the continuous and dispersed phases changed, thus varying the total number of interfaces in the system, and consequently the frictional and interface pressure drop terms.

To the best of the author's knowledge the developed model is the first to account for the influence of varying flow ratio and slug size on the liquid-liquid slug flow pressure drop. Last, the developed model was found to be in good agreement with experimental data with a mean relative error lower than 7 %.

Nomenclature

A	cross-sectional area of the capillary, m^2
Bo	Bond number, -
Ca	Capillary number, -
d	diameter of the capillary, m
g	gravity, m/s)
h	film thickness, m
l	slug length, m
L	length of the capillary, m
N	number of experimental measurements, -
Q	volumetric flow rate, m^3/s
R	internal radius of capillary, m
Re	Reynolds number, -
v	velocity, m/s
V	volume, m^3
We	Weber number, -
ΔP	pressure drop, Pa

Greek letters

α	dispersed phase fraction, -
ε	volume fraction, -
γ	interfacial surface tension, N/m
μ	viscosity, Pa s
η	empirical parameter dependent on the capillary wall properties, -
ρ	density, kg/m^3
θ	contact angle, °

Subscripts

c	continuous phase
d	dispersed phase
Fr	frictional
I	Interface
L	length
MF	moving film
SF	stagnant film
SP	single phase
TP	two-phase
U	slug unit cell
Y	Y-mixer

Abbreviations

EG-T	ethylene glycol/water-toluene
MF	moving film
SF	stagnant film

OA   organic-to-aqueous flow ratio
W-T   water-toluene

Appendix. The moving film (MF) model

The model considers a moving film with a constant thickness. A no-slip boundary between the capillary wall and the moving film is assumed. Furthermore, the shear stresses and the velocity are assumed to be continuous throughout the fluid-fluid interface. The steady state, laminar flow of two immiscible fluids is considered. The two fluids have constant density and viscosity.

The momentum balance is given with the following equation:

$$(2\pi r L \phi_{rz})\big|_r - (2\pi r L \phi_{rz})\big|_{r+\Delta r} + (2\pi r \Delta r)(\phi_{zz})\big|_{z=o} - (2\pi r \Delta r(\phi_{zz})\big|_{z=L} = 0 \qquad (A.1)$$

Dividing Eq. A.1 by $2\pi L \Delta r$ and taking the limit as $\Delta r \rightarrow 0$, gives:

$$\frac{\partial}{\partial r}(r\phi_{rz}) = \left(\frac{\phi_{zz}\big|_{z=o} - \phi_{zz}\big|_{z=L}}{L}\right) r \qquad (A.2)$$

The evaluation of the components ϕ_{rz} and ϕ_{zz}, gives:

$$\phi_{rz} = \tau_{rz} + \rho v_r v_z = -\mu \frac{\partial v_z}{\partial r} + \rho v_r v_z \qquad (A.3)$$

$$\phi_{zz} = p + \tau_{zz} + \rho v_z v_z = p - 2\mu \frac{\partial v_z}{\partial z} + \rho v_z v_z \qquad (A.4)$$

Assuming $v_z = v_z(r)$, $v_r = 0$ and p = p(z), Eq. A.2 yields:

$$\frac{\partial}{\partial r}(r\tau_{rz}) = \left(\frac{p_0 - p_L}{L}\right) r \qquad (A.5)$$

Integration of Eq. A.5 gives:

$$\tau_{rz} = \left(\frac{p_0 - p_L}{2L}\right) r + \frac{C_1}{r} \qquad (A.6)$$

The Eq. A.6 can be rewritten for the continuous phase (film) as:

$$\tau_{rz}^{I} = \left(\frac{(p_0 - p_L)}{2L}\right) r + \frac{C_1^{I}}{r} \qquad (A.7)$$

and for the dispersed phase (slug) as:

$$\tau_{rz}^{II} = \left(\frac{(p_0 - p_L)}{2L}\right) r + \frac{C_1^{II}}{r} \qquad (A.8)$$

The shear stress, τ_{rz}, is assumed to be continuous throughout the fluid-fluid interface. The following boundary conditions are taken:

B. C. 1 at r= (R-h) $\tau_{rz}^{I} = \tau_{rz}^{II}$

B. C. 2 at r = 0 τ_{rz}^{II} = finite

From B. C. 1 it is clear that $C_1^{I} = C_1^{II} = C_1$ while B. C. 2 yields C_1 =0.

Substituting Newton's law of viscosity and integration gives

$$v_z^I = -\left(\frac{p_0 - p_L}{4\mu_c L}\right)r^2 + C_2^I \tag{A.9}$$

for the continuous phase (film) and:

$$v_z^{II} = -\left(\frac{p_0 - p_L}{4\mu_d L}\right)r^2 + C_2^{II} \tag{A.10}$$

for the dispersed phase (slug).

By applying the following boundary conditions:

B. C. 3 at r=R $v_z^I = 0$

B. C. 4 at r=0 $v_z^{II} = v_{max}^{II}$

B. C. 5 at r=(R-h) $v_z^{II} = v_z^I$

Eqs. A.9 and A.10 yield the following relations:

$$v_z^I = \left(\frac{p_0 - p_L}{4\mu_c L}\right)R^2\left(1 - \frac{r^2}{R^2}\right) \tag{A.11}$$

$$C_2^{II} = v_{max}^{II} \tag{A.12}$$

$$C_2^{II} = \left(\frac{p_0 - p_L}{4L}\right)\left(\frac{R^2 - (R-h)^2}{\mu_c} + \frac{(R-h)^2}{\mu_d}\right) \tag{A.13}$$

$$v_z^{II} = \left(\frac{p_0 - p_L}{4L}\right)\left(\frac{R^2 - (R-h)^2}{\mu_c} + \frac{(R-h)^2 - r^2}{\mu_d}\right) \tag{A.14}$$

Average velocities of the slug and film can be determined by:

$$\overline{v}_{slug} = \frac{\int_0^{2\pi}\int_0^{(R-h)} v_z^{II} r\,dr\,d\theta}{\int_0^{2\pi}\int_0^{(R-h)} r\,dr\,d\theta} \tag{A.15}$$

$$\overline{v}_{film} = \frac{\int_0^{2\pi}\int_{R-h}^R v_z^I r\,dr\,d\theta}{\int_0^{2\pi}\int_{R-h}^R r\,dr\,d\theta} \tag{A.16}$$

Combining Eqs. A.11, A.14, A.15 and A.16 gives the average film velocity and the slug velocity, respectively.

$$\overline{v}_{film} = \frac{\frac{(p_0 - p_L)R^2}{4\mu_d L}\left(0.25R^2 - 0.5(R-h)^2 + \frac{0.25(R-h)^4}{R^2}\right)}{0.5R^2 - 0.5(R-h)^2} \tag{A.17}$$

$$\overline{v}_{slug} = \left(\frac{p_0 - p_L}{4L}\right)\left(\frac{R^2 - (R-h)^2}{\mu_c} + \frac{0.5(R-h)^2}{\mu_d}\right) \tag{A.18}$$

Finally, the pressure drop equation with moving film becomes:

$$\Delta P = \Delta P_{Fr} + \Delta P_I = \Delta P_{Fr,d} + \Delta P_{Fr,c} + \Delta P_I \tag{A.19}$$

$$\Delta P = \frac{4\overline{v}_{slug}L\alpha}{\dfrac{R^2-(R-h)^2}{\mu_c}+\dfrac{0.5(R-h)^2}{\mu_d}} + \frac{8v\mu_c(1-\alpha)L}{R^2} + \frac{L}{l_u}7.16(3Ca)^{2/3}\frac{\gamma}{d} \qquad (A.20)$$

References

(1)   Hessel, V.; Renken, A.; Schouten, J.C.; Yoshida J.L.;. Micro Process Engineering, Vol.1: Fundamentals, Operations and Catalysts. WILEY-VC Verlag GmbH & Co. KGaA, Weinheim, 2009.

(2)   Cubaud, T.; Ulmanella, U.; Ho, C.M. Two-phase flow in microchannels with surface modifications. *Fluid Dyn. Res.* 2006, *38*, 772.

(3)   Haverkamp, V.; Hessel, V.; Löwe, H.; Menges, G.; Warnier, M.J.F.; Rebrov, E.V.; de Croon, M.H.J.M.; Schouten, J.C.; Liauw, M.A. Hydrodynamics and mixer- induced bubble formation in microbubble columns with single and multiple channels. *Chem. Eng. Technol.* 2006, *29*, 1015.

(4)   Hassan, I.; Vaillancourt, M.; Pehlivan, K. Two-phase flow regime transitions in microchannels: a comparative experimental study. *Microscale Therm. Eng.* 2005, *9*, 165.

(5)   Lee, C.Y.; Lee, S.Y. Influence of surface wettability on transition of two-phase flow pattern in round mini-channels. *Int. J. Multiphas. Flow* 2008, *34*, 706.

(6)   Serizawa, A.; Feng, Z.; Kawara, Z. Two-phase flow in microchannels. *Exp. Therm. Fluid Sci.* 2002, *26*, 703.

(7)   Waelchli, S.; von Rohr, P.R. Two-phase flow characteristics in gas–liquid microreactors. *Int. J. Multiphas. Flow* 2006, *32*, 791.

(8)   Yue, J.; Luo, L.; Gonthier, Y.; Chen, G.; Yuan, Q. An experimental investigation of gas–liquid two-phase flow in single microchannel contactors. *Chem. Eng. Sci.* 2008, *63*, 4189.

(9)   Zhao, T.S.; Bi, Q.C. Co-current air–water two-phase flow patterns in vertical triangular microchannels. *Int. J. Multiphas. Flow* 2001, *27*, 765.

(10) Dessimoz, A. L.; Cavin, L.; Renken, A.; Kiwi-Minsker, L. Liquid-Liquid two-phase flow patterns and mass transfer characteristics in rectangular glass microreactors. *Chem. Eng. Sci.* 2008, *63*, 4035.

(11) Dreyfus, R.; Tabeling, P.; Willaime, H. Ordered and disordered patterns in two-phase flows in microchannels. *Phys. Rev. Lett.* 2003, *90*, 144505-1.

(12) Salim, A.; Fourar, M.; Pironon, J.; Sausse, J. Oil-water two-phase flow in microchannels: Flow patterns and pressure drop measurements. *Can. J. Chem. Eng.* 2008, *86*, 978.

(13) Zhao, Y.; Chen, G.; Yuan, Q.; Liquid-Liquid Two-Phase Flow Patterns in a Rectangular Microchannel, *AIChE J.* 2006, *52*, 4052.

(14) Cherlo, S. K.; Pushpavanam, S. Experimental and Numerical Investigations of Two-Phase (Liquid-Liquid) Flow Behavior in Rectangular Microchannels. *Ind. Eng. Chem. Res.* 2010, *49,* 893.

(15) Kashid, M.N.; Harshe, Y.M.; Agar, D.W. Liquid–liquid slug flow in a capillary: an alternative to suspended drop or film contactors. *Ind. Eng. Chem. Res.* 2007, *46*, 8420.

(16) Nisisako, T.; Torii, T.; Higuchi, T. Droplet formation in a microchannel network. *Lab. Chip* 2002, *2*, 24.

(17) Uada A. S.; Lorenceau, E.; Link, D. R.; Kaplan, P. D.; Stone, H. A.; Weitz, D. A. Monodisperse double emulsions generated froma microcapllary device. *Science* 2005, *308*, 537.

(18) Kashid, M.N.; Agar; D.W. Hydrodynamics of liquid–liquid slug flow capillary microreactor: flow regimes, slug size and pressure drop. *Chem. Eng. J.* 2007, *131*, 1.

(19) Garstecki, P.; Fuerstman, M. J.; Stonec, H. A.; Whitesides, G. M. Formation of droplets and bubbles in a microfluidic T-junction-scaling and mechanism of break-up. *Lab. Chip* 2006, *6*, 437.

(20) Ehrfeld, W.; Hessel, V.; Loewe, H. Microreactors: New Technology for Modern Chemistry, Wiley-VCH, Weinheim, 2000.

(21) Jovanović, J.; Rebrov, E.V.; Nijhuis, T.A.; Hessel V.; Schouten, J.C. Phase transfer catalysis in segmented flow in a microchannel: fluidic control of selectivity and productivity, *Ind. Eng. Chem. Res.* 2010, *49, 2681.*

(22) Perry, R. H.; Green, D. W. Perry's Chemical Engineers Handbook, 7th ed.; McGraw-Hill, New York, 1997.

(23) Ruiz, M. C.; Lermanda, P.; Padilla, R. Drop size distribution in a batch mixer under breakage conditions. *Hydrometallurgy* 2002, *63*, 65.

(24) Kashid, M.N.; Garlach, I.; Franzke, J.; Acker, J.F.; Platte, F.; Agar, D.W.; Turek, S. Internal circulation within the liquid slugs of liquid-liquid slug flow capillary microreactor. *Ind. Eng. Chem. Res.* 2005, *44*, 5003.

(25) Taha, T.; Cui, Z.F. Hydrodynamics of slug flow in capillaries. *Chem. Eng. Sci.* 2004, *59*, 1181.

(26) Burns, J.R.; Ramshaw, C. The intensification of rapid reactions in multi-phase systems using slug flow in capillaries. *Lab. Chip* 2001, 1, 10.

(27) Dummann, G.; Quittmann, L.; Groschel, W.; Agar, D.W.; Worz, O.; Morgenschweis, K. The capillary-microreactor: a new reactor concept for the intensification of heat and mass transfer in liquid-liquid reactions. *Catal. Today* 2003, *79*, 433.

(28) Ducry, L.; Roberge, D. M. Controlled autocatalytic nitration of phenol in a microreactor. *Angew. Chem.* 2005, *117*, 8186.

(29) Hisamoto, H.; Saito, T.; Tokeshi, M.; Hibara, A.; Kitamori, T. Fast and high conversion phase-transfer synthesis exploiting the liquid–liquid interface formed in a microchannel chip. *Chem. Commun.* 2001, *24*, 2662.

(30) Chen, I.Y.; Yang, K.S.; Wang, C.C. An empirical correlation for two-phase frictional performance in small diameter tubes. *Int. J. Heat Mass Transf.* 2002, *45*, 3667.

(31) Chung, P.M.Y.; Kawaji, M. The effect of channel diameter on adiabatic two-phase flow characteristics in microchannels. *Int. J. Multiphas. Flow* 2004, *30*, 735.

(32) Kawahara, A.; Chung P.M.Y.; Kawaji, M. Investigation of two phase flow pattern, void fraction and pressure drop in a microchannel. *Int. J. Multiphas. Flow* 2002, *28*, 1411.

(33) Kreutzer, M.T.; Kapteijn, F.; Moulijn, J.A.; Heiszwolf, J.J. Multiphase monolith reactors: chemical reaction engineering of segmented flow in microchannels. *Chem. Eng. Sci.* 2005, *60*, 5895.

(34) Triplett, K.A.; Ghiaasiaan, S.M.; Abdel-Khalik, S.I.; LeMouel, A.; McCord, B. N. Gas–liquid two-phase flow in microchannels Part II: Void fraction and pressure drop. *Int. J. Multiphas. Flow* 1999, *25*, 395.

(35) Warnier, M.J.F.; de Croon, H.J.M.; Rebrov, E.V.; Schouten, J.C. Pressure drop of gas-liquid Taylor flow in round microcapillaries for low to intermediate Reynolds numbers. *Microfluid. Nanofluid.* 2009, *8*, 33.

(36) Lockhart, R.W.; Martinelli, R. C. Proposed correction of data for isothermal two-phase component flow in pipes. *Chem. Eng. Prog.* 1949, *45*, 39.

(37) Horvolgyi, Z.; Kiss, E.; Janos, P. Experimental studies on the control of slug flow by interfacial forces in silylated capillaries. *Colloids Surf.* 1991, *55*, 257.

(38) Lee, C.Y.; Lee, S.Y. Pressure drop of two-phase dry-plug flow in round mini-channels: Influence of surface wettability. *Exp. Therm. Fluid Sci.* 2009, *32*, 1716.

(39) Bretherton, F.P. The motion of long bubbles in tubes. *J. Fluid Mech.* 1961, *10*, 166.

(40) Kashid, M.N.; Rivas, D.F.; Agar, D.W.; Turek, S. On the hydrodynamics of liquid-liquid slug flow capillary microreactors. *Asia-Pac. J. Chem. Eng.* 2008, *3*, 151.

(41) Aussillous, P.; Quere, D. Quick deposition of a fluid on the wall of a tube *Phys. Fluids* 2000, *12*, 2367.

(42) Irandoust, S.; Andersson, B. Liquid film in Taylor flow through a capillary. *Ind. Eng. Chem. Res.* 1989, *28*, 1684.

(43) Marchessault, R.N.; Mason, S.G. Flow of entrapped bubbles through a capillary. *Ind. Eng. Chem.* 1960, *52*, 79.

(44) Bico, J.; Quere, D. Liquid trains in a tube. *Europhys. Lett.* 2000, *51*, 546.

(45) Walsh, E.; Mazychka, Y.; Walsh, P.; Egan, V.; Punch, J. Pressure drop in two phase slug/bubble flows in mini scale capillaries. *Int. J. Multiphas. Flow* 2009, *35*, 979.

(46) Heil, M. Finite Reynolds number effects in the Bretherton problem. *Phys. Fluids* 2001, *13*, 2517.

(47) Fujioka, H.; Grotberg, J. B. The steady propagation of a surfactant-laden liquid plug in a two-dimensional channel. *Phys Fluids* 2005, *17*, 1.

(48) Ratulowski, J.; Chang, H. Transport of gas bubbles in capillaries. *Phys. Fluids A* 1989, *10*, 1642.

(49) Westborg, H.; Hassager, O. Creeping motion of long bubbles and drops in capillary tubes. *J. Colloid Interf. Sci.* 1989, *133*, 135.

(50) Kreutzer, M.T.; Kapteijn, F.; Moulijn, J.A.; Kleijn, C.R.; Heiszwolf, J.J. Intertial and interfacial effects on pressure drop of Taylor flow in capillaries. *AIChE J.* 2005, *51*, 2428.

(51) Wong, H.; Radke, C. J.; Morris, S. The motion of long bubbles in polygonal capillaries. Part 2. Drag, fluid pressure and fluid flow. *J. Fluid Mech.* 1995, *292*, 95.

(52) van Stein, V.; Kreutzer, M. T.; Kleijn, C. R. Velocity fluctuations of segmented flow in microchannels. *Chem. Eng. J.* 2008, *135S*, S159.

(53) Ratulowski, J.; Chang, H. Marangoni effects of trace impurities on the motion of long gas bubbles in capillaries. *J. Fluid Mech.* 1990, *210*, 303.

Chapter 4. Slug flow microreactor for phase transfer catalysis: control of selectivity and productivity

Abstract

Precise control over the interfacial area of aqueous and organic slugs in segmented flow in a microchannel reactor provides an attractive means to optimize yield and productivity of a phase transfer catalyzed reaction. In this chapter the selective alkylation of phenyl-acetonitrile to the monoalkylated product in a microchannel of 250 μm internal diameter operated continuously and solvent free in the slug flow regime is studied. The conversion of phenylacetonitrile increases from 40 % to 99 % as a result of 97 % larger slug surface-to-volume ratio when the volumetric aqueous-to-organic phase flow ratio is raised from 1.0 to 6.1 at the same residence time. The larger surface-to-volume ratio significantly promotes catalyst phase transfer but decreases selectivity due to the simultaneous increase of the rate of the consecutive reaction to the dialkylated product. There exists an optimum flow ratio with a maximal productivity. Conversion and selectivity in the microchannel reactor are both significantly larger than in a stirred reactor.

4.1 Introduction

The key factor in phase transfer catalysis (PTC) is the ability of the catalyst to penetrate the interface between two immiscible (liquid) phases to be transferred into the phase where the reaction takes place[1,2]. Conversion and selectivity of phase transfer catalyzed reactions in stirred reactors depend, among other things, on the rate of catalyst transfer across the interface between the liquid drops of both phases in the mixed suspension in the reactor. These liquid drops usually have a wide size distribution as the result of an inhomogeneous energy dissipation induced by the mechanical stirring of the suspension. A microchannel reactor provides an attractive alternative to the stirred reactor because it can be operated in the so-called segmented or slug flow regime where liquid slugs move along the channel with a narrow slug size distribution and a well-defined slug surface-to-volume ratio. Microchannel reactors are well-known as continuous flow devices that offer many advantages in achieving controllable, safer, more atom efficient and chemically selective syntheses[3,4,5]. Furthermore, the small size of the microreactors allows for integration of reaction with separation and analysis[6,7].

In a PTC system, like in any other catalytic system, the overall rate of reaction is determined by a combination of the intrinsic reaction kinetics and the rate of transport of the catalyst and reacting species to the location where the reaction takes place (Figure 1a). The intrinsic reaction kinetics can be manipulated by the reaction temperature, the type and concentration of the catalyst, and the reactant concentration. Most often, the overall rate of a catalytic reaction is largely limited by the transport of the reactants to the reaction site. Similarly, the rate of a PTC reaction is most often limited by the rate of catalyst phase transfer, usually from an aqueous to an organic phase, which leads to long times needed to complete the reaction[8]. The stirring of the phases in conventional liquid-liquid reactors generates a wide range of drop sizes with diameters varying from tens of micrometers up to millimeters (Figure 1b). Therefore, the liquid-liquid interfacial surface area varies considerably from one drop to another[9-16]. Since the rate of catalyst phase transfer is proportional to the interfacial surface area, each drop acts like a single reactor, each with its own rate of catalyst transfer, and thus, different rates of reaction for different drops are obtained. This means that the reaction time also varies from drop to drop, which may lead to a variation in selectivity.

It should be noted that a high interfacial surface area also increases the rates of the consecutive or parallel reactions, some of which may be unwanted. For example, the rate of the hydrolysis side reaction increases with a larger interfacial surface area in the PTC phenol acylation, thus decreasing selectivity[17]. In the PTC alkylation of 2-phenyl-propionitrile, the side product formed by deprotonation acts as a catalyst poison, effectively lowering both conversion and selectivity. Therefore, the challenge in phase transfer catalysis is to control the drop size distribution of both phases, and consequently, the size of the interfacial surface area (i.e. surface-to-volume ratio), the rate of catalyst transfer, and finally the selectivity. The aim of this chapter is to demonstrate that microchannel

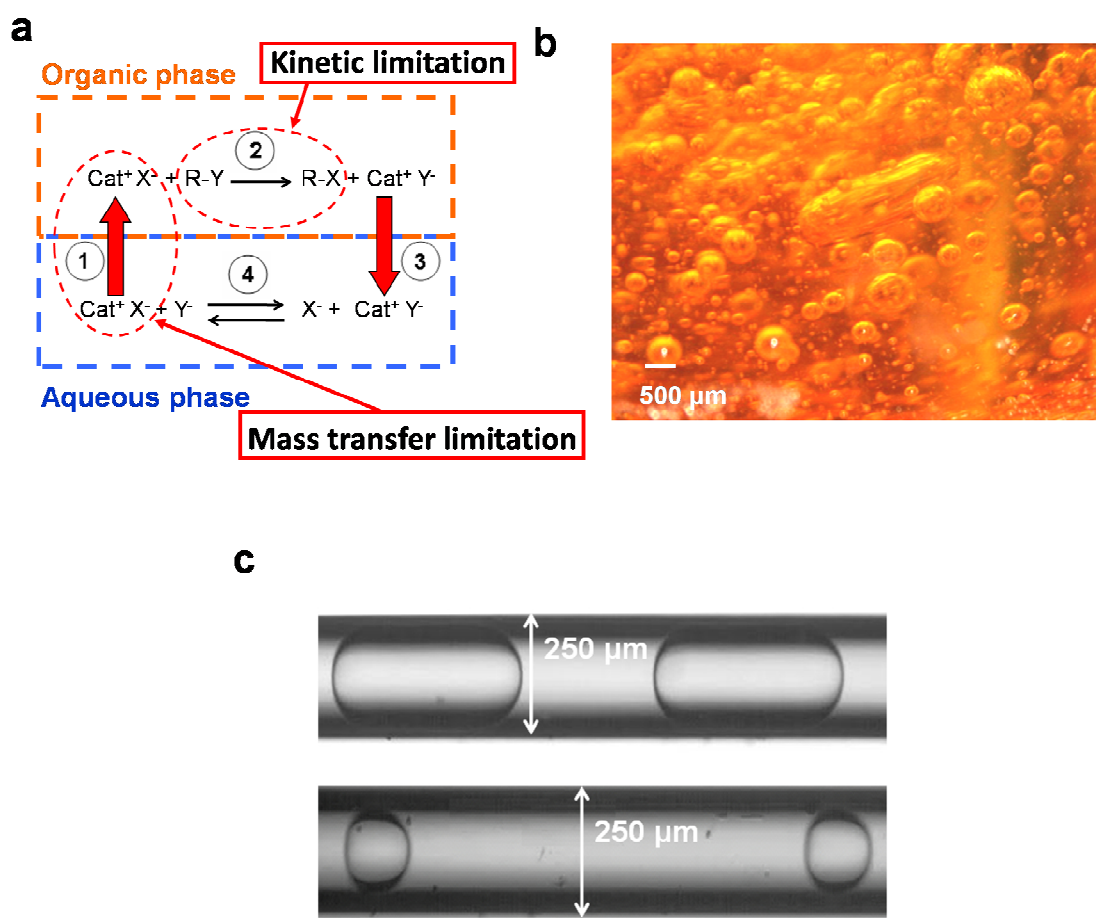reactors are suitable devices for microfluidic control of conversion and selectivity in a PTC reaction.

*Figure 1. **a,** Mass transfer and kinetic rate limitations in phase transfer catalysis. **b,** A wide range of drop sizes generated by conventional stirring in a stirred reactor containing a mixture of the aqueous and organic phases. The reactants are transferred from the continuous phase to the dispersed phase where the reaction takes place, therefore different drop sizes will yield different rates of reaction. **c,** Uniform liquid-liquid slug flow (top) and drop flow (bottom) generated in the 250 μm internal diameter capillary.*

4.1.1 Hydrodynamics of the slug flow system

In liquid-liquid microchannel flow, different flow patterns are found as a function of the volumetric flow ratio of two immiscible liquids, i.e., annular flow, parallel flow, drop flow, or slug flow[18,19]. A simple Y-mixer already provides reproducible segmented slug flow[20], which allows a high degree of control over the slug size distribution and the liquid-liquid interfacial surface-to-volume ratio (Figure 1c). This surface-to-volume ratio is in the

range of 10000 to 50000 square meters per cubic meter of slug volume[21] in the case of microchannels with a typical diameter of the order of tens to hundreds of micrometers. This is one order of magnitude higher than in a stirred vessel where the maximum surface to volume ratio is ca. 1000 m^2/m^3 .[22]

In a fluid dynamic study on segmented flow in microchannels, Kashid and Agar[23] showed that the flow rates of both phases influence the lengths of the slugs, and thus the size of their interfacial surface area. This implies that by increasing the volumetric aqueous-to-organic phase ratio, the slugs containing the continuous organic phase become shorter, while the slugs of the segmented aqueous phase become longer. Consequently, the rate of catalyst transfer across the aqueous slug cap interface increases, due to increasing surface-to-volume ratio of the organic inter-slug. Furthermore, at shorter lengths of the organic inter-slugs, the degree of internal circulation of the organic liquid in these slugs increases[24], therefore decreasing mass transfer contact times and increasing the rate of removal of the catalyst and reactant species from the interface, thus further increasing the rate of transport across this interface (Figure 2). These increased rates of interfacial transfer will not only boost the reaction rate but will also influence the reaction's yield and productivity.

4.1.2 PTC in microchannels

The first study of a PTC reaction in a microchannel was performed by Hisamoto et al. (2001)on a diazo coupling reaction[25]. They showed that the specific interfacial surface area in the microchannel during parallel flow of the phases was twice as high as compared to a stirred batch reactor. This relatively small increase in the interfacial surface area already enabled efficient transfer of 5-methyl resoncinol from the organic phase to the aqueous phase where the diazo coupling reaction was completed with almost 100 % conversion. The first example of PTC alkylation in a microreactor was given by Ueno et al. (2003) [26]. By employing segmented flow in 200 µm internal diameter microchannels, the conversion was 54 % higher than that obtained in a batch reactor. Okamoto et al. (2006) reported on PTC alkylation of malonic acid dimethylester in slug flow. The conversion was 21 % higher in a 500 µm internal diameter microchannel as compared to that in a batch reactor[27]. Ahmed-Omer et al. (2008) investigated a number of process intensification techniques in a two-phase slug flow reaction system in a microreactor[28]. The combination of sonification and phase transfer catalysis proved superior to any other combination of process intensification techniques. Phase transfer catalysis in microchannel reactors has been the subject of a number of patents as well. Monzyk and Brophy (2004) developed a multichannel device for performing reactions and separations[29]. The Merck Company patented a microdevice that integrates mixing, heating, and sonification units for the o-alkylation of 5-bromosalicylaldehyde, achieving 60 % conversion[30]. In summary, the literature shows that performing phase transfer catalysis in a microchannel generally yields higher conversions than in a stirred reactor.
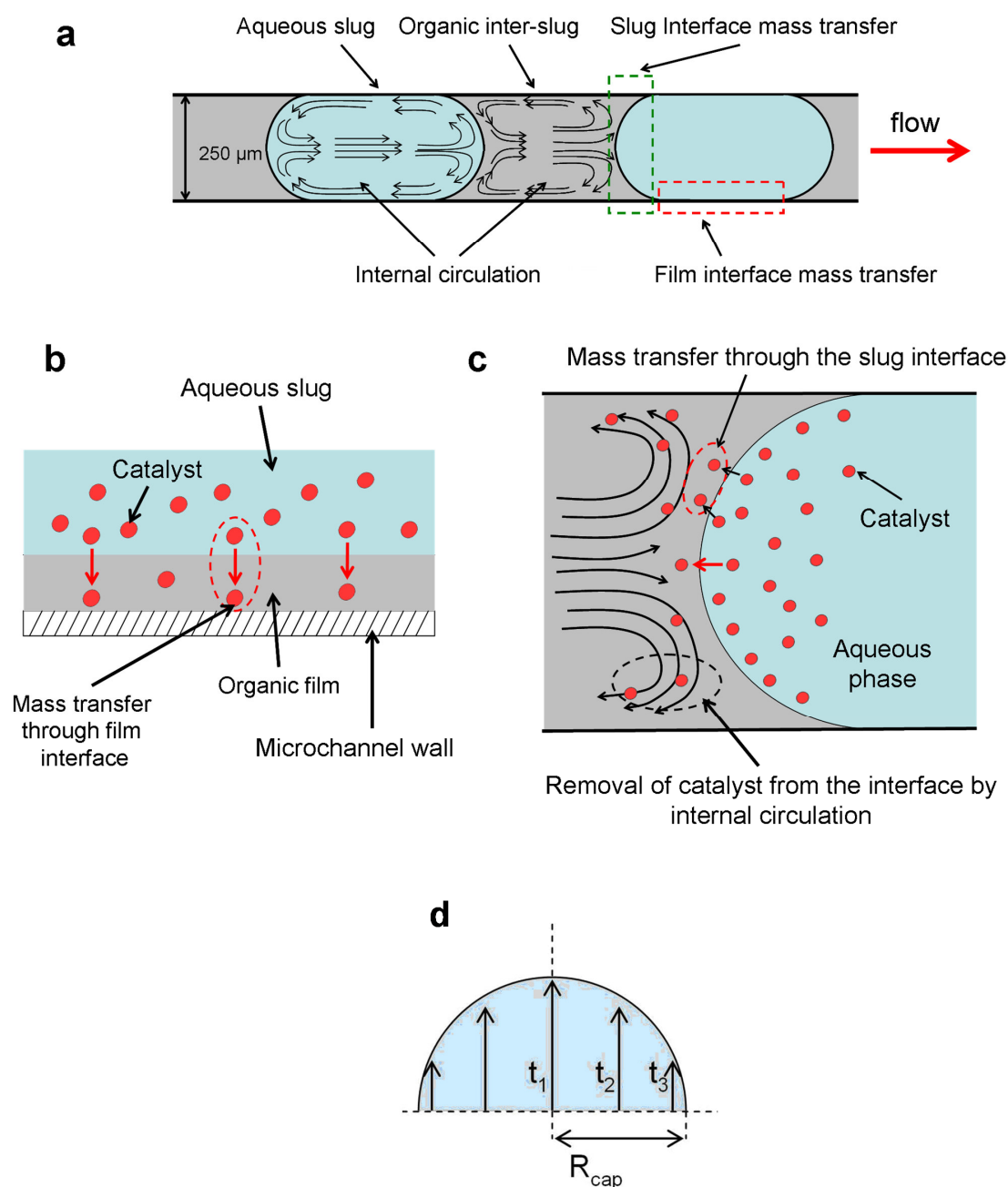
Figure 2. a, Two types of mass transfer in segmented slug flow in a microchannel: (i) mass transfer through the interface separating the organic film from the aqueous slug, and (ii) mass transfer through the aqueous-organic slug interfaces. b, Mass transfer through the interface between the aqueous slug and the organic film. c, Mass transfer through the interface between the aqueous slug and the organic slug. Internal circulation removes the species from the interface, thus accelerating the rate of interface mass transfer. d, Different contact times for mass transfer depending on the position along the slug cap.

In this chapter it will be shown how conversion and selectivity can be manipulated by choosing the proper liquid-liquid flow conditions. In order to achieve fluidic control, the control over slug sizes must be ensured. First, the flow rate range for a stable slug flow must be determined. The variation of the ratio of the aqueous and organic phase flow rates (i.e. the aqueous-to-organic flow ratio), allows slug size manipulation and consequently slug surface-to-volume ratio control. Finally, the optimum aqueous-to-organic flow ratio for the maximal productivity must be determined.

4.2 Experimental section

Physical Properties. The viscosity of the organic mixture for the mass transfer calculations was measured with a Brookfield LVDV-I Prime viscosimeter at the reaction temperature (80˚C). The surface tension between the aqueous and organic mixture was measured via the Du Noüy Ring method at the reaction temperature. The organic mixture viscosity was measured to be 4.01 mPas and the organic-aqueous surface tension was 22.17 mN/m.

Chemicals and catalyst. All chemicals used in this work are commercially available and were obtained from Sigma-Aldrich. The organic phase consisted of a mixture of phenyl-acetonitrile (**1**) and n-butyl bromide (**2**) at a molar ratio of 1 to 4. The organic phase contained decahydronaphthalene at a concentration of 1.15 mol/L as the internal standard in the GC analysis. The aqueous phase was composed of a mixture of 45 wt % KOH and 0.12 wt % of the phase transfer catalyst triethylbenzylammonium chloride (TEBA) in de-mineralized water.

Experimental microchanel reactor setup. The microchannel reactor assembly is shown in Figure 3. The mixing of the phases was done in a Y-mixer with an angle between the mixer inlets of 110$^\text{o}$. The internal diameter of the Y-mixer inlets and outlet was 250 μm. Two HPLC pumps (Shimadzu LC-20AD) were used to feed the aqueous and organic phase flows to the Y-mixer. The residence time for the reaction was provided with a 10 m long PEEK capillary with an internal diameter of 250 μm connected to the Y-mixer. PEEK has excellent chemical resistivity to hydroxides and haloalkanes and it is also attractive from the point of view of microreactor system assembly due to the fact that PEEK capillaries and other units (mixers, valves) are readily available from HPLC suppliers. The temperature of the lines from the pumps, the Y-mixer, and the capillary was maintained at 80˚C with a thermostatic bath (Lauda E 300). The outlet of the capillary was connected to a vessel with an aqueous solution of NH$_4$Cl maintained at 10˚C to quench the reaction.

Conventional batch reactor setup. Batch experiments were carried out in a 250 mL round bottom flask coupled with a reflux condenser. Heating was provided via a water bath. Stirring was performed with a mechanical Teflon blade stirrer. All batch reactor

experiments were performed with 40 mL of the organic mixture and 40 mL of the aqueous mixture at a temperature of 80˚C and a stirring rate of 800 rpm.

Post reaction workup. The organic phase was separated from the aqueous phase via syringe and was analyzed by GC analysis. No further purification of the organic phase was performed in order to detect all side products. In order to detect phenylacetic acid and n-butanol, which are soluble in water, the aqueous phase was extracted with toluene and analyzed via GC.

Analysis. The reactants and reaction products were quantitatively analyzed using a Varian CP-3800 gas chromatograph equipped with a 30 m x 0.25 mm CP-Sil column and an FID detector. The products were qualitatively identified via GC-MS.

Microscopic video imaging of the segmented slug flow was done with a Zeiss Axio Observer D1m microscope coupled with a high speed imaging camera (MotionPro10000). The magnification used was 50x. The videos were recorded at a rate of 2000 frames per second at a resolution of 1280x480. In order to visualize the slug flow, a 20 cm long PTFE capillary with an internal diameter of 250 μm was connected downstream to the PEEK capillary. The estimation of the slug lengths and the interfacial surface areas was performed via image analysis using Matlab^{TM} software.
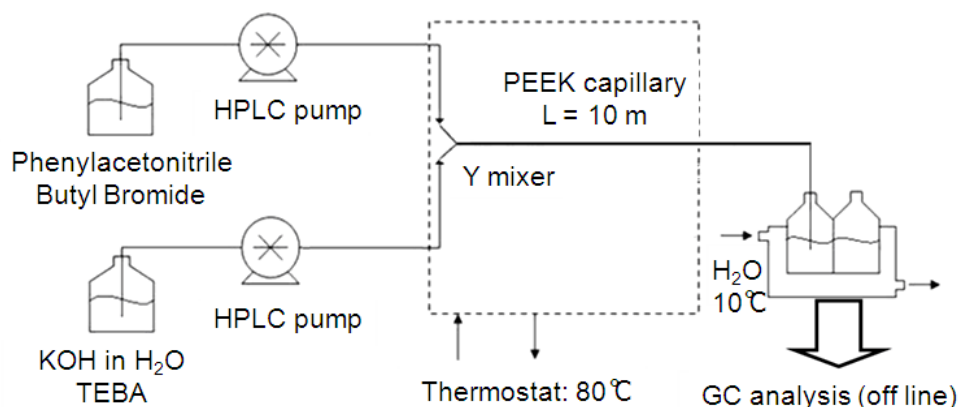
*Figure 3. Experimental setup: a PEEK Y-mixer coupled with a 250 μm internal diameter PEEK capillary, heated by a thermostatic bath. Supply of the reactants (**1, 2**) and the phase transfer catalyst (TEBA) is provided via two HPLC pumps (Shimadzu LC-20AD).*

4.3 Results and Discussion

Since the stability and reproducibility of the slug flow is crucial for the microreactor study, the stable flow operating regimes were identified. An unstable flow regime is characterized by very low slug length reproducibility, i.e. the mean percentage deviation of slug lengths is above 50 % (Figure 4). In the unstable regime the slug lengths can range from 100 μm up to 15 mm, without any observable reproducible flow regime. Furthermore, in the unstable flow different regimes such as bubbly and slug flow are occurring simultaneously. The stable regime is characterized by a reproducible slug flow.

In order to determine the stability of the flow regime, total flow rates were varied from 50 to 250 µL/min, at aqueous-to-organic volumetric flow ratio (AO ratio) of 1.0. These flow rates correspond to slug residence times from 2.0 to 9.8 minutes.
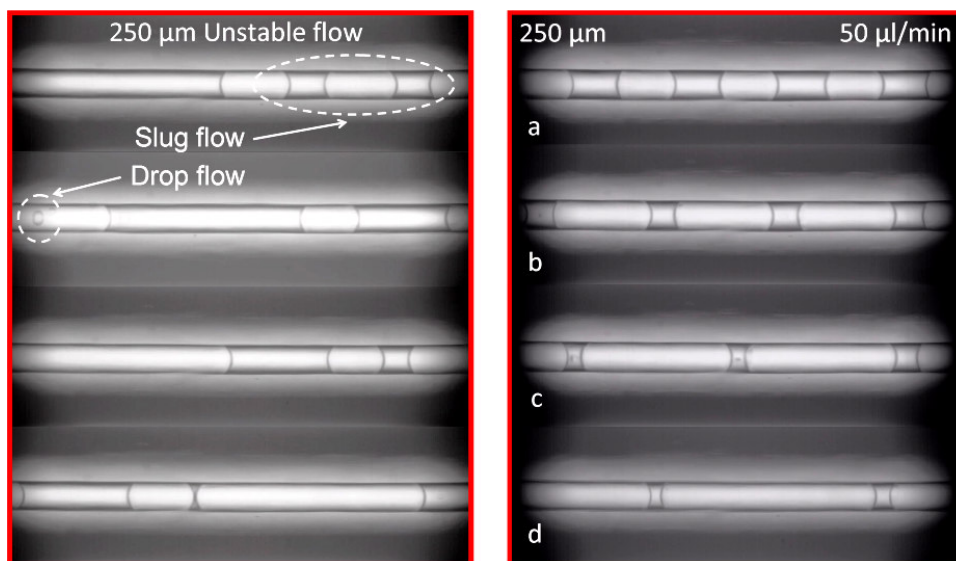

*Figure 4. **a.** Unstable (left) and stable flow (right) in 250 m capillary. Slug sizes (dark slugs-organic phase, white slugs-aqueous phase) in the stable flow as a function of AO ratio: a) AO of 1 b) AO of 2.3 c) AO of 4 d) AO of 6.1*

The influence of the total flow rates on the slug length and flow stability is shown in Figure 5a. In the stable flow regime, a slight decreasing trend of slug lengths is observed with increasing flow rates. The lengths of aqueous slugs show higher degree of reproducibility than the organic slugs. At a flow rate of 250 µL/min the slug flow becomes unstable with generated organic slug sizes ranging from 200 to 630 µm.

The Weber number, representing the ratio between the inertial and surface tension forces, was used by Zhao et al. (2006)[18] to express a criterion for the transition between the flow patterns:

$$We = \frac{\rho v^2 D}{\gamma} \tag{1}$$

In this work the unstable flow was observed at a Weber number above $9.9 \cdot 10^{-3}$ for the organic phase and above $1.13 \cdot 10^{-2}$ for the aqueous phase. When compared with data of Zhao et al. (2006) [18], these Weber numbers correspond to the transition region between the slug flow and parallel flow.

The study of the influence of the changing AO ratios on the slug lengths was performed at total flow rate of 50 µL/min, with AO ratios from 1.0 to 9.0. First, the ratio of the aqueous and organic slug volumes acquired by microscope measurements was compared to the AO ratios set by the pumps (Figure 5 b). At AO ratios from 1.0 to 4.0 there is a good agreement of measured and set AO ratios. At flow ratios above 6.0, a higher deviation of

measured AO ratios from the set values is observed. The slug lengths as a function of AO ratios are shown in Figure 5 c.
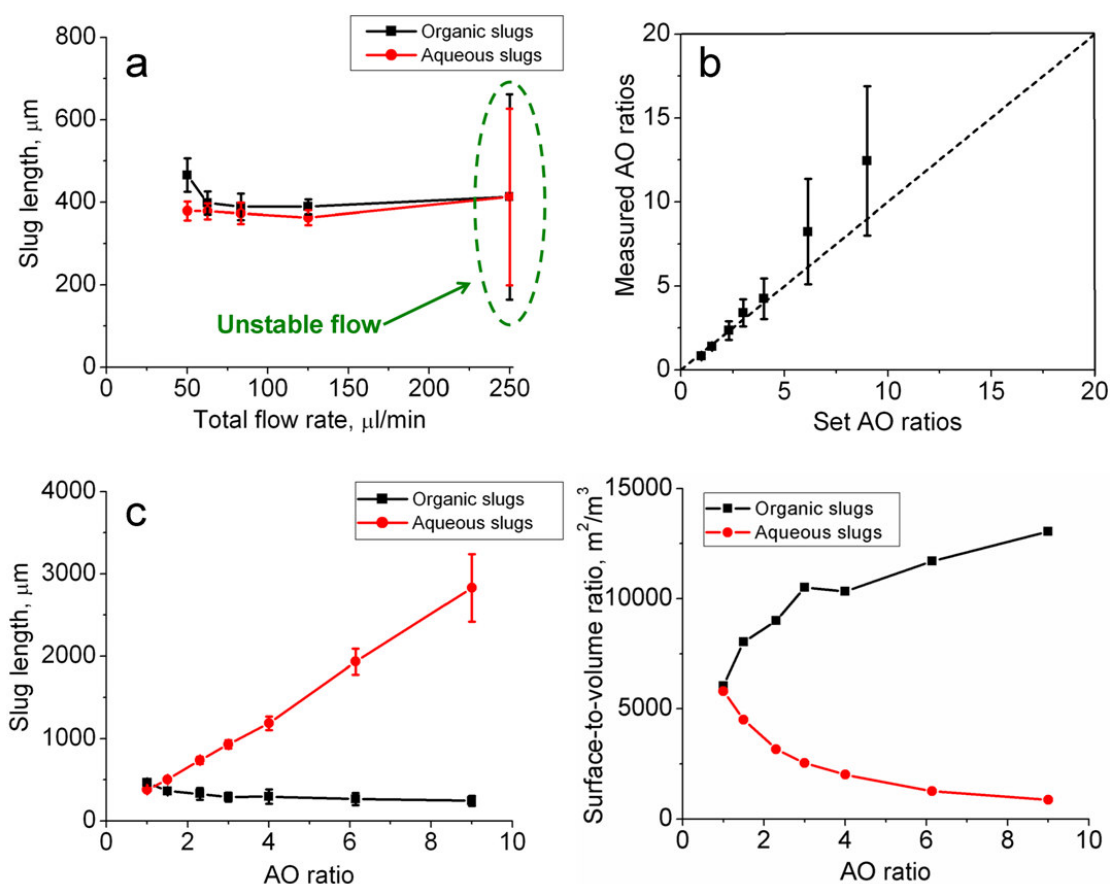

*Figure 5. **a.** Slug sizes and flow stability as a function of total flow rate at equal AO ratio. **b.** Measured AO ratios vs. the set AO ratios. **c.** Length of organic and aqueous slugs for different AO ratios. **d.** Surface-to-volume ratio of organic and aqueous slugs for different AO ratios.*

With increasing AO ratios the aqueous slugs become longer while the organic slugs decrease in size (Figure 4). Furthermore, the reproducibility of the aqueous slug length measurements decreases at AO ratios higher than 6.0. It is important to note that the reproducibility of organic slug measurements remains relatively constant throughout all of the experiments. Since the total flow is constant, in order to change the AO ratio, one must decrease the organic flow rate and increase the aqueous flow rate. Therefore, the organic slugs are "chopped off" by the higher flow of aqueous phase, yielding reproducible organic slug sizes. Since at higher AO ratios the organic flow rates are more than 6 times lower than the aqueous flow, the force exerted by the organic phase on the aqueous phase in the Y junction is lower than the force of the aqueous phase exerted on the organic phase. Consequently, the aqueous slugs are "chopped off" by the organic phase in an

irregular fashion, which accounts for the decreased reproducibility of aqueous slugs at higher AO ratios.

Substantial research has been performed on mass transfer mechanisms in gas-liquid segmented flow (Taylor (1961)[31], Berčić and Pintar (1997)[32], Irandoust and Andersson (1988)[33], Kreutzer et al. (2001)[34]), however little data is found about the mass transfer mechanism in liquid-liquid segmented flow. In a gas-liquid segmented slug flow, there are two mechanisms of mass transfer (Figure 2 a): (i) via the interface separating the slug from the thin film that is present between the slug and the microchannel wall (Figure 2 b), or (ii) via the interfaces at the front and back sides of the slug (Figure 2 c). These transfer rates may differ in magnitude as they are both proportional to the respective interfacial surface areas, while contributing both to the overall rate of reaction. The degree of influence of mass transfer via the film on the overall mass transfer is not clear in the case of liquid-liquid slug flow. The film thickness can be estimated by applying the Bretherton law[35]:

$$\delta = 0.66D\left(\frac{\mu_{org}v_{slug}}{\gamma}\right)^{\frac{2}{3}} \tag{2}$$

For the calculation of the film thickness, the values of viscosity and surface tension were taken at the temperature of 80°C, and superficial slug velocity of 0.017 m/s, which are the conditions at which the study of the slug size on the conversion and selectivity was performed. The film thickness was calculated to be 3.5 µm thick. The experimental observations with a microscope at a resolution of 3.0 µm/pixel, however, do not confirm an existence of a film. Berčić and Pintar[32] observed that the mass transfer through the film is negligible compared to the mass transfer through the slug caps. The work of Kreutzer et al. (2001)[34] indicates that the film mass transfer is important only when there is a catalyst deposited on the wall, otherwise the film gets quickly saturated and most of the mass transfer occurs through the slug caps. Harries et al. (2003)[36] and Burns and Ramshaw (2001)[37] made similar observation in their work on liquid-liquid slug flow in capillary, in which they concluded that mass transfer occurs only through the slug cap interfaces, since no liquid film was observed. Therefore, it was assumed that there is no film present or that the mass transfer via the film can be neglected and the transfer occurs only through the slug caps. Because the liquid-liquid segmented flow system is laminar, the movement of the aqueous slug is analogue to the movement of a single bubble through the stagnant liquid. Assuming that all resistance to mass transfer is located in the organic phase, this case can be modeled via the penetration theory[38]. Since the caps are parabolic, and the internal circulation streamline system is three dimensional, the mass transfer contact times are not identical (Figure 2 d). Consequently, for each position along the cap there is a local mass transfer coefficient. In order to acquire the overall mass transfer coefficient over the cap, one must average out the local mass transfer coefficients over the cap as shown in the work of Wenmackers et al. (2009)[39], which yields the overall slug cap mass transfer coefficient:

$$k_{cap,avg} = \frac{\int_0^{R_{cap}} \pi r k_l \, dr}{\int_0^{R_{cap}} \pi r \, dr} \tag{3}$$

Assuming a semi-spherical shape of the slug cap, Eq. 3 yields:

$$k_{cap,avg} = \frac{8}{3} \sqrt{\frac{v_{slug} D_{Cat^+OH^-}}{\pi R_{cap}}} \tag{4}$$

Eq. 4 shows that the mass transfer coefficient through the caps is independent of the aqueous or organic slug size. However, the $k_l a$ value of the mass transfer through the caps depends on the organic slug size, since the decrease of organic slug size increases the surface-to-volume ratio, and thus $k_l a$. Figure 5 d shows that with increasing AO ratios, the surface-to-volume ratio of organic slugs increases, as a consequence of decreasing organic slug lengths. Consequently, the $k_l a$ is expected to increase with increasing AO ratios, resulting in higher reaction rates.

4.3.1 Phase transfer alkylation of Phenylacetonitrile

The PTC alkylation of phenylacetonitrile was selected as a model reaction (Figure 6). The reaction system is composed of two phases: an organic phase containing the alkylating agent (n-butyl bromide (**2**)) and phenylacetonitrile (**1**) and an aqueous phase containing potassium hydroxide and the phase transfer catalyst (triethylbenzylammonium chloride, TEBA). The reaction was performed under solvent free conditions. The phases are mixed in a Y-mixer that is connected to a PEEK capillary of 250 μm internal diameter. The catalyst-hydroxy complex penetrates the interface between the aqueous and the organic slugs in the capillary and is transferred into the organic phase in which the reaction takes place (Figure 3 a)[2,40,41,42]. Then, the catalyst-bromide complex transfers back to the aqueous phase. In the batch reactor, the reaction takes place in the organic phase, which is dispersed in the continuous aqueous phase, therefore generating a wide range of drop sizes and surface areas and thus yielding varying mass transfer and reaction rates. The reaction yields two major products, mono- (**3**) and dialkylated (**4**) phenylacetonitrile, and also phenylacetic acid (**5**) as a side product (Figure 5 b). The alkyl halide to alcohol hydrolysis does not occur when alkylation is performed with alkyl halides via phase transfer catalysis[43, 44]. No hydrolysis of n-butyl bromide was observed after 24 h at 100°C, when a quaternary salt and lipophilic catalysts were employed[45]. Kinetic studies in batch reactors have shown that the reaction rate increases with increasing interfacial surface area[46], even at high stirring speeds[47].

hydrodynamics of the slug flow was observed when the catalyst concentration was varied at a total flow rate of 50 μL/min. The maximal catalyst concentration was 15.7 mmol %

and it is limited by the catalyst solubility. No significant increase of the conversion was found at catalyst concentrations larger than 13.0 mmol % (Figure 7 a). In this case, the reaction rate only can be further increased by enlarging the interfacial surface area via increasing AO ratios. Therefore, all other experiments were carried out at the catalyst concentration of 13.0 mmol %.
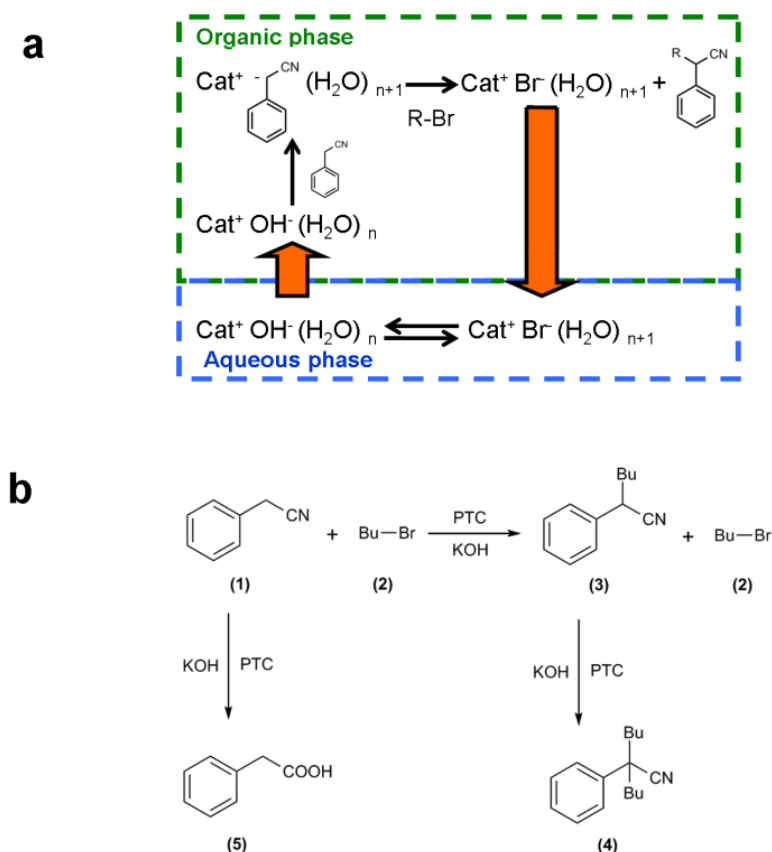

*Figure 6. **a.** Mass transfer and kinetic steps in the phase transfer alkylation of phenyl-acetonitrile: mass transfer of the catalyst-hydroxide complex to the organic phase, followed by deprotonation of the phenylacetonitrile and subsequent alkylation to the monoalkylated product. The catalyst-bromide complex transfers back to the aqueous phase where it transforms into the catalyst-hydroxide complex, ready for an another cycle of phase transfer. **b.** Reaction scheme of the phase transfer alkylation of phenylacetonitrile (**1**) with n-butyl bromide (**2**) yielding the monoalkylated (**3**) and dialkylated (**4**) reaction products. The hydrolysis side reaction yields phenylacetic acid (**5**). The Phase Transfer Catalyst (PTC) is triethylbenzylammonium chloride (TEBA).*

The aqueous and organic slug lengths and the related surface-to-volume ratios were varied by changing the AO ratio. The residence time of the catalyst and reactants was the same for all AO ratios by keeping the total volumetric flow rate constant. Microscopic flow imaging showed that the average length of the organic slugs decreased by approximately 48 % from 465 to 240 μm when the AO ratio was increased from 1.0 to 6.1. As a result, the average surface-to-volume ratio increased more than 97 % from 6000 to 13000 m^2/m^3. The calculations of the mass transfer coefficient through the slug caps showed that it is

independent from the slug sizes. However, since the surface-to-volume ratio increases with decreasing organic inter-slug size, the overall mass transfer coefficient, $k_l a$ increases (Table 1). The conversion of phenylacetonitrile increased from 40 % to 99 % when the AO ratio increased from 1.0 to 6.1 (i.e. by increasing the surface-to-volume ratio from 6000 to 13000 m^2/m^3) at a constant total flow rate of 50 μL/min (Figure 6 b).

Table 1. Organic slug lengths and specific interfacial surface areas at different volumetric aqueous-to-organic phase flow (AO) ratios.

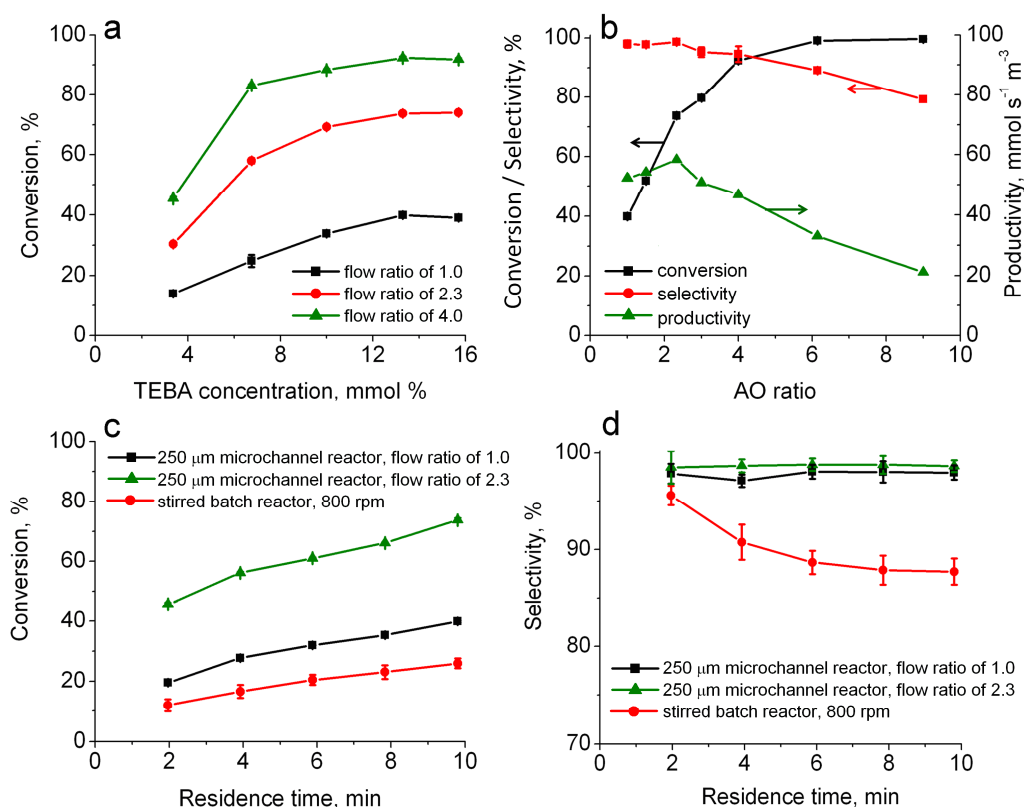| AO ratio, -	Organic slug length, μm	Surface-to-volume ratio, m^2/m^3	Cap mass transfer coefficient, k_l, m/s	$k_l a$, $m^3_l/m^3_r s$	Conversion*, %
1.0	467	6000	$8 \cdot 10^{-5}$	0.48	40
2.3	330	9000	$8 \cdot 10^{-5}$	0.72	74
4.0	295	10300	$8 \cdot 10^{-5}$	0.82	92
6.1	265	13000	$8 \cdot 10^{-5}$	0.94	99

* at 80˚C and residence time of 9.8 min.

Figure 7. **a,** Conversion as a function of catalyst concentration at different aqueous-to-organic phase volumetric flow ratios (temperature: 80˚C; residence time: 9.8 min). **b,** Conversion, selectivity, and productivity as a function of flow ratio (temperature: 80˚C; catalyst concentration: 13 mmol %; residence time: 9.8 min). **c. and d.** Conversion and selectivity as a function of residence time (temperature: 80˚C; catalyst concentration: 13 mmol %).

The phase transfer catalysis system is a complex system in which the catalyst constantly switches phases, thus making the measurement of the mass transfer difficult. Therefore, the presence of mass transfer limitation can only be observed indirectly. The strong dependence of conversion on the increasing surface-to-volume ratio under conditions where catalyst concentration does not influence the conversion is one of such indirect observations of mass transfer limitations. Unfortunately, due to the difficulties in decoupling the mass transfer rate from the kinetic rate, one cannot conclude that the system is mass transfer limited. The absence of the first order dependence of the mass transfer and conversion (Table 1) indicates that the system is still kinetically limited. Furthermore, the work of Makosza et al. (1977)[41] claims that the kinetic mechanism is dependent on the surface area and that there are no mass transfer limitations, which was disputed by Starks, Halpern and Liotta (1994)[2]. Due to the complexity of the system, to this date, the discussion on the mass transfer and reaction mechanism remains open. A detailed study of the reaction mechanism is presented in chapter 5.

The selectivity to the monoalkylated reaction product decreased at flow ratios larger than 2.3 (Figure 6 c) due to an increased rate of the consecutive reaction yielding the dialkylated product. There is a large excess of the aqueous phase at these higher flow ratios. For example, the aqueous flow rate was 25 μL/min at a flow ratio of 1.0, while it was 45 μL/min at a flow ratio of 9.0. In the latter case, the organic phase throughput was only 5 μL/min since the total flow rate was kept constant at 50 μL/min to maintain a constant residence time. Therefore, there exists an optimum AO ratio of 2.3, which allows for a maximum productivity of the monoalkylated product (Figure 6 b). Although the conversion continued to increase at flow ratios larger than 2.3, the productivity decreased. (Here the productivity was defined as the total number of moles of the monoalkylated product that were produced per unit of time per unit of microchannel volume.) No formation of the hydrolysis by-product **(5)** was observed. Furthermore, no formation of n-butanol, which is a product of n-butyl bromide hydrolysis, was observed, confirming the phase transfer catalyzed inhibition of alkyl halide hydrolysis.

Experiments at different residence times were performed at AO ratios of 1.0 and 2.3 in the microchannel reactor and at a volume ratio of 1.0 in a stirred batch reactor. At a residence time of 9.8 minutes, phenylacetonitrile conversions of 40 % and 74 % were achieved in the microchannel reactor at flow ratios of 1.0 and 2.3, respectively, compared to only 26 % in the batch reactor (Figure 4 c). Although at the flow rate of 250 μL/min, which corresponds to the residence time of 2.0 min, the organic slug sizes vary from 200 to 630 μm the there is a good reproducibility of conversion data (microchannel reactor mean percentage deviation of 5 % vs. 17 % in the batch reactor). This indicates that the 250 μL/min conversion data is averaged out over the time of sampling, since each sample was taken at 2 min intervals. Furthermore, it shows that the narrow slug size distribution obtained in the microchannel reactor, even at unstable flow conditions, yields better reproducibility than the batch reactor.

The selectivity in the stirred batch reactor decreased with conversion, achieving a value of 88 % at a residence time of 9.8 minutes. The decreasing selectivity with residence time in the batch reactor can be explained by slower rate of droplet breakup and coalescence compared to the reaction rate, resulting in different reaction rates for each droplet. Unlike the batch reactor, the microchannel reactor showed an almost constant selectivity of approximately 98 % at all conversions (Figure 4 d).

In phase transfer catalysis, emulsion formation is a common problem in liquid-liquid reaction systems. It is usually avoided by using solvents such as toluene or dichloromethane. The disadvantage is the longer residence time needed to complete the reaction since the solvents dilute the reactants. In segmented microchannel flow, electrostatic colloidal stabilization[48] cannot occur and emulsion formation is eliminated because the slugs of one phase are always separated in space from the slugs of the other phase. This allows for solvent free operation and significantly simplifies post reaction workup, which is an important advantage of continuous flow operation in microchannel reactors[49]. According to our best knowledge, we present herein the first demonstration of a PTC reaction in a microchannel reactor operated without a solvent.

4.4 Conclusion

The calculations of mass transfer via penetration theory indicated that the mass transfer is dependent only on the organic slug lengths. At catalyst concentrations above 13 mmol % no further increase in conversion was observed. The absence of linear dependence of mass transfer coefficient and conversion indicates that the kinetic limitation is present. Under these conditions, by increasing the organic slug length, the reaction rate increases due to increase of the slug surface-to-volume ratios, which was confirmed with the conversion results. At the same time, the rate of the byproduct formation in a consecutive reaction increased. The decrease in selectivity was observed when aqueous-to-organic flow ratio was increased. Thus, an optimum aqueous-to-organic volumetric ratio of 2.3 was found that gave a conversion of 74 % with a product selectivity of 99 %. Previous works on phase transfer catalyzed alkylations in microchannels by Ueno et al. (2003)[26] and Okamoto (2006) [27] reported approximately 1.5 and 1.2 times higher conversions, respectively, compared to the batch reactor. The application of the fluidic control methodology by varying the aqueous-to-organic flow ratio from 1 to 6.1, yields a 1.5 to 3.8 times increase in conversion compared to the batch reactor. At the optimum flow ratio of 2.3, a 1.8 times increase in conversion and a 12 % increase in selectivity were achieved compared to the batch reactor.

It is important to note that the aqueous and organic flow rates, the volumetric flow ratio, the slug length, and the residence time in the microchannel reactor are all interconnected and influence each other. For example, one cannot change the total flow rate without changing the residence time, nor can one change the volumetric flow ratio without affecting the slug length. This requires careful selection of the flow conditions in the

microchannel reactor where the productivity of the reaction is maximal. This maximum productivity is obviously a function of the conversion, selectivity, and the flow rate of the main reactant (phenylacetonitrile) at the optimum aqueous-to-organic volumetric ratio.

In conclusion, we have demonstrated the potential of using a continuous microchannel reactor in solvent-free and selective phase transfer alkylation where the interface between the segmented liquid phases can be precisely tuned to optimize the productivity. This provides a clear advantage over traditional stirred (batch) vessels. Scale-up to the required production capacity (viz., moles of reaction product per unit of time) may be relatively easily done by selecting the proper number of parallel microchannels (numbering up).

Nomenclature

$D_{Cat^+OH^-}$ - *diffusion coefficient of catalyst-hydroxide complex, m^2/s*

D - *Diameter of the microchannel capillary, m*

k_la - *Liquid side mass transfer coefficient multiplied by the surface to volme ratio, $m^3_l/m^3_r s$* $k_{cap,avg}$ - *Average liquid side mass transfer coefficient through the slug cap, m/s*

R_{cap} - *Radius of the half spherical slug cap, m*

r - *Radial position along the inside the half spherical slug cap, m*

μ_{org} - *Viscosity, Pas*

v_{slug} - *Superficial velocity of the slug, m/s*

ρ - *density, kg/m^3*

γ - *Interfacial surface tension between the organic and aqueous phase, N/m*

References

(1) Dehmlow, E.V. Phase-Transfer Catalyzed Two-Phase Reactions in Preparative Organic Chemistry. *Angew. Chem.* 1974, *86*, 187.

(2) Starks, C.; Liotta, C.; Halpern, M. *Phase-Transfer Catalysis: Fundamentals, Applications and Industrial Perspectives*, Chapman & Hall, London, 1994.

(3) Hogan, J. Lab on a chip: A little goes a long way. *Nature* 2006, *442*, 351.

(4) Jensen, K.F. Microreaction engineering—is small better? *Chem. Eng. Sci.* 2001, *56,* 293.

(5) Ducry, L.; Roberge, D.M. Controlled autocatalytic nitration of phenol in a microreactor. *Angew. Chem. Int. Ed.* 2005, *44*, 7972.

(6) Haswell, S.J. Chemical technology: All together now. *Nature* 2006, *441*, 705.

(7) Sahoo, H.R.; Kralj, J.G.; Jensen, K.F. Multistep Continuous-Flow Microchemical Synthesis Involving Multiple Reactions and Separations. *Angew. Chem. Int. Ed.* 2007, *46*, 5704.

(8) Yadav, G.D.; Jadhav, Y.B. Kinetics and modeling of liquid-liquid phase transfer catalysed synthesis of *p*-chlorophenyl acetonitrile: role of co-catalyst in intensification of rates and selectivity. *J. Mol. Catal.* 2003, *192*, 41.

(9) Vermeulen, T.; Williams, G.M.; Langlois, G.E. Interfacial area in liquid-liquid and gas-liquid agitation. *Chem. Eng. Prog.* 1955, *51*, 85F.

(10) Rodger, W.A.; Trice, V.G.; Rushton, J.H. Effect of fluid motion on interfacial area of dispersions. *Chem. Eng. Prog.* 1956, *52*, 515.

(11) Weinstein, B.; Treybal, R.E. Liquid-liquid contacting in unbaffled, agitated vessels. *AIChE J.* 1973, *19*, 304.

(12) Mlynek, Y.; Resnick W. Drop sizes in an agitated liquid-liquid system. *AIChE J.* 1972, *18*, 122.

(13) Laso, M.; Steiner, L.; Hartland, S. Dynamic simulation of agitated liquid-liquid dispersions - II. experimental determination of breakage and coalescence rates in a stirred tank. *Chem. Eng. Sci.* 1987, *42*, 2437.

(14) Zhou, G.; Kresta, S.M. Evolution of drop size distribution in liquid-liquid dispersions for various impellers. *Chem. Eng. Sci.* 1998, *53*, 2099.

(15) Pacek, A.W.; Chasart, S.; Nienow, A.W.; Bakker, A. The influence of impeller type on mean drop size and drop size distribution in an agitated vessel. *Chem. Eng. Sci.* 1999, *54*, 4211.

(16) Ruiz, M.C.; Lermanda, P.; Padilla, R. Drop size distribution in a batch mixer under breakage conditions. *Hydrometallurgy* 2002, *63*, 65.

(17) Lee, Y.; Yeh, M.; Shih, Y. Phase-Transfer Catalytic Kinetics of the Synthesis of Phenyl Benzoate. *Ind. Eng. Chem. Res.* 1995, 34, 1572.

(18) Zhao, Y.; Chen, G.; Yuan, Q. Liquid-liquid two-phase flow patterns in a rectangular microchannel. *AIChE J.* 2006, *52*, 4052.

(19) Baroud, C.N.; Willaime, H. Multiphase flows in microfluidics. *C. R. Physique* 2004, *5*, 547.

(20)   Kashid, M.N. Experimental and Modelling Studies on Liquid-Liquid Slug Flow Capillary Microreactors. *Ph.D. Thesis*, Technical University of Dortmund, 2007.

(21)   Ehrfeld, W.; Hessel, V.; Loewe, H., *Microreactors: New Technology for Modern Chemistry*, Wiley-VCH, Weinheim, 2000.

(22)   Perry, R.H.; Green, D.W. *Perry's Chemical Engineers Handbook*, 7th Edition, McGraw-Hill, New York, 1997.

(23)   Kashid, M.N.; Agar, D.W. Hydrodynamics of liquid-liquid slug flow capillary microreactor: Flow regimes, slug size and pressure drop. *Chem. Eng. J.* 2007, *131*, 1.

(24)   Taha, T.; Cui, Z.F. Hydrodynamics of slug flow inside capillaries. *Chem. Eng. Sci.* 2004, 59, 1181.

(25)   Hisamoto, H.; Saito, T.; Tokeshi, M.; Hibara, A.; Kitamori, T. Fast and high conversion phase-transfer synthesis exploiting the liquid–liquid interface formed in a microchannel chip. *Chem. Commun.* 2001, *24*, 2662.

(26)   Ueno, M.; Hisamoto, H.; Kitamori, T.; Kobayashi, S. Phase-transfer alkylation reactions using microreactors. *Chem. Commun.* 2003, *8,* 936.

(27)   Okamoto, H. Effect of Alternating Pumping of Two Reactants into a Microchannel on a Phase Transfer Reaction. *Chem. Eng. Technol.* 2006, *29*, 504.

(28)   Ahmed-Omer, B.; Barrow, D.; Wirth, T. Effect of segmented fluid flow, sonication and phase transfer catalysis on biphasic reactions in capillary microreactors. *Chem. Eng. J.* 2008, *135S*, S280.

(29)   Monzyk, B.; Brophy, J.H. *Patent WO2004037399A2*, 2004.

(30)   Wurziger, H.; Pieper, G.; Schmelz, M.; Schwesinger, N. *Patent WO0249737A1*, 2002.

(31)   Taylor, G.I.; Deposition of a viscous fluid on the wall of a tube. *J.Fluid.Mech.* 1961, *10*, 161.

(32)   Bercic, G.; Pintar, A. The role of gas bubbles and liquid slug lengths on mass transport in the Taylor flow through capillaries. *Chem. Eng. Sci.* 1997, *52*, 3709.

(33)   Irandoust, S.; Andersson, B. Mass transfer and liquid-phase reactions in a segmented two-phase flow monolithic catalyst reactor. *Chem. Eng. Sci.* 1988, *43*, 1983.

(34)   Kreutzer, M. T.; Du, P.; Heiszwolf, J. J.; Kapteijn, F.; Moulijn, J. A. Mass transfer characteristics of three-phase monolith reactors. *Chem. Eng. Sci.* 2001, *56*, 6015.

(35)   Bretherton, F. P. The motion of long bubbles in tubes. *J. Fluid Mech.* 1961, 10, 166.

(36)   Harries, N.; Burns, J.R.; Barrow, D.A.; Ramshaw, C. A numerical model for segmented flow in a microreactor. *Int. J. Heat Mass Tran.* 2003, *46*, 3313.

(37)   Burns, J. R.; Ramshaw C. The intensification of rapid reactions in multiphase systems using slug flow in capillaries. *Lab on a Chip* 2001, *1*, 10.

(38)   Higbie, R.; Rate of Absorption of a Gas into a Still Liquid. *Trans. AIChE* 1935, *31*, 365.

(39)   Wenmakers, P. W. A. M.; Meeuwse, M.; de Croon, M. H. J. M.; van der Schaaf, J.; Shouten, J. C. Transient gas-liquid mass transfer model for thin liquid films on structured solid packings, *Chem. Eng. Res. Des.* 2010, *80*, 270.

(40)   Sasson, Y.; Neumann, R.; *Handbook of Phase Transfer Catalysis*, Chapman & Hall, London, 1997.

(41)   Makosza, M.; Bialecka, E. Reactions of organic anions. LXXIII Alkylation of phenylacetonitrile at the interface with aqueous sodium hydroxide. *Tetrahedron Lett.* 1977, *2*, 183.

(42)   Rabinovitz, M.; Cohen, Y.; Halpern, M. Hydroxide Ion Initiated Reactions Under Phase Transfer Catalysis Conditions: Mechanism and Implications. New Synthetic Methods. *Angew. Chem. Int. Ed.* 1986, *25,* 960.

(43)   Silhanek, J.; Bartl, J.; Mateju, R.; Zbirovsky, M. Inhibition by phase transfer catalysts. *React. Kinet. Catal. Lett.* 1982, *19*, 115.

(44)   Durst, H. D.; Liebeskind, L. Phase Transfer Catalysis. The Acetoacetic Ester Condensation. *J. Org. Chem.* 1974, *39*, 3271.

(45)   Zahalka, H. A.; Sasson, Y. The effect of acetate ion on the phase transfer catalyzed alkaline hydrolysis of alkyl halides. *J. Mol. Catal.*, 1983, *18*, 57.

(46)   Sawarkar, C.S.; Juvekar, V.A. Kinetics of an Interfacial Reaction. Hydroxide Ion Catalyzed C-Alkylation of Phenylacetonitrile. *Ind. Eng. Chem. Res.* 1996, *35*, 2581.

(47)   Halpern, M. *PTC Commun.* 2005, *13*.

(48)   Lyklema, J. *Fundamentals of Interface and Colloid Science*, Vol. 2, Academic Press, London, 1995.

(49)   Hessel, V.; Kralisch, D.; Krtschil, U. Sustainability through green processing - novel process windows intensify micro and milli process technologies. *Energy Environ. Sci.* 2008, *1*, 467.

Chapter 5. Microreactor as a powerful tool for reaction mechanistic studies: control of liquid-liquid interface of a phase transfer catalysed alkylation

Abstract

Microreactors allow a degree of control over a chemical reaction unattainable in conventional stirred reactors, making them powerful yet rarely used tools for kinetics studies. In this chapter the precise control over the slug lengths in a microreactor was employed to study a complex system of liquid-liquid phase transfer catalyzed alkylation of phenylacetonitrile in a basic medium. The influence of the surface-to-volume ratio, the reactant molar ratios, hydroxide and phase transfer catalyst concentrations on the reaction were investigated in order to observe the reaction on the liquid-liquid interface. The interfacial reaction was interpreted with two proposed mechanisms existing in the literature: the Starks extraction and Makosza interfacial mechanisms. The results showed a strong indication that the reaction proceeds via the interfacial mechanism which was further modified in order to observe the interfacial reaction, allowing for the measurement of the observed interfacial reaction rate constant.

## 5.1 Introduction

The sub-millimeter inner diameter channels allow for surface-to-volume ratios in the higher than 10000 m^2/m^3 [1], thus allowing for a significant intensification of the mass and heat transfer[2]. Depending on the total flow rate and the volumetric flow ratio, several liquid-liquid flow patterns are achievable in microchannels, such as: annular, parallel, bubbly or slug flow[3]. In literature most attention has been given to the hydrodynamics of liquid-liquid slug flow[4-6], due the high degree of control that can be achieved over the slug length. By varying the flow ratio, the surface-to-volume ratio can be controlled with a high degree of accuracy[7]. The ability to control the surface-to-volume ratio allows the study of surface dependent reactions (i.e. mass transfer limited and interfacial reactions) thus making them powerful tools for kinetic screening[8].

In conventional liquid-liquid stirred tank reactors wide droplet size distributions[9] are found, resulting in considerable variations of the liquid–liquid interfacial surface area from one drop to another. In phase transfer catalysis (PTC) reactions, drop size control presents a challenge as the size of the interfacial surface area (i.e., surface-to-volume ratio) determines the rate of the reaction. Consequently, microreactors, providing a level of reaction control unachievable in the conventional reactors, have been successfully employed in phase transfer catalyzed diazo coupling[10] and alkylation reactions[7,11,12].

5.1.1 PTC/OH alkylation

Alkylation of weakly acidic organic substrates (pKa ~ 15-24) usually requires the presence of strong, co-solvents and hazardous bases such as sodium methoxide[13]. The employment of a phase transfer catalyst allows aggressive bases to be replaced by mild bases (e.g. sodium hydroxide) while simultaneously alleviating the need for a co-solvent[14]. PTC is both economically and environmentally favorable over traditional chemical methods, which resulted in a wide application in fine chemical industry, particularly in the case of alkylation, condensation and carbene addition reactions[15].
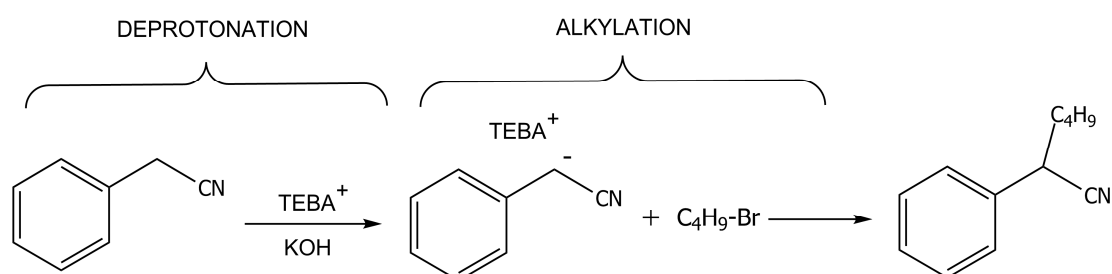
Scheme 1: PTC alkylation of phenylacetonitrile (PAN) with butyl bromide consisting of the deprotonation and alkylation steps.

As a model reaction, the base mediated phase transfer catalyzed (PTC/OH) alkylation of phenylacetonitrile (PAN), was used employing benzyltriethylammonium chloride (TEBA) as the phase transfer catalyst. The selective alkylation of PAN is an important step in fine chemical syntheses, since the arylacetic acid moiety is often encountered in anti-inflammatory drugs[16]. The alkylation of PAN is regarded as a two-step reaction. First PAN is deprotonated at the α-C site, after which the deprotonated PAN catalyst complex is alkylated to yield the α-butyl penylacetonitrile (Scheme 1).

The mechanism of the phase transfer catalyzed alkylation under basic conditions is subject of discussion, as two models exist: the Starks extraction mechanism[17] and the Makosza interfacial mechanism[18]. These mechanisms differ by the role which the phase interface plays in the reaction. The Starks extraction mechanism is schematically depicted in Figure 1 a. In the aqueous phase the quaternary ammonium cation (TEBA$^+$) forms a complex with the hydroxide anion, which transfers to the organic phase where it deprotonates PAN. The deprotonated TEBA$^+$PAN$^-$ species is alkylated by butyl bromide yielding the alkylated product and the catalyst which transfers back to the aqueous phase.

The interfacial mechanism is schematically depicted in Figure 1 b. The same two reaction steps as in the extraction mechanism can be distinguished: the deprotonation and the subsequent alkylation step. According to the mechanism, the reaction is catalyzed by a phase transfer catalyst; however it is not a "true" phase transfer catalysis reaction, as the rate of the catalyst transfer does not determine the reaction rate. In the interfacial mechanism the deprotonation is regarded as an interfacial reaction: PAN is deprotonated by the hydroxide at the liquid-liquid interface, where it forms an ion pair with the hydroxide counter-ion. The ion pair is insoluble in both phases and is anchored at the interface[17,19] until it associates with the quaternary ammonium cation and is drawn into the organic phase. Consequently, in the organic phase the deprotonated PAN is alkylated, resulting in the alkylated product and the regenerated catalyst (TEBA$^+$Br$^-$). Simultaneously, the counter-anion of the catalyst and the water molecule formed in the deprotonation reaction transfer into the aqueous phase.

The difference between the Starks extraction mechanism (Figure 1 a) and the Makosza interfacial mechanism (Figure 1 b) lies at the role of the phase interface. Both of the mechanisms describe the reaction as a two step reaction: 1) deprotonation to form TEBA$^+$PAN$^-$ complex followed by the 2) alkylation to produce the mono alkylated product (Scheme 1). The deprotonation step in the Starks extraction mechanism is described as mass transfer of the catalyst hydroxide species followed by the reaction with the organic substrate (Figure 1 c). The interfacial mechanism describes the deprotonation as an equilibrium reaction between the organic reactant and the base at the interface, followed by the reaction with the catalyst (Figure 1 d). Therefore, in the extraction mechanism the interfacial area influences the mass transfer rate of the catalyst-hydroxide pair, whereas in the interfacial mechanism the actual deprotonation of the organic reactant takes place at the interface.
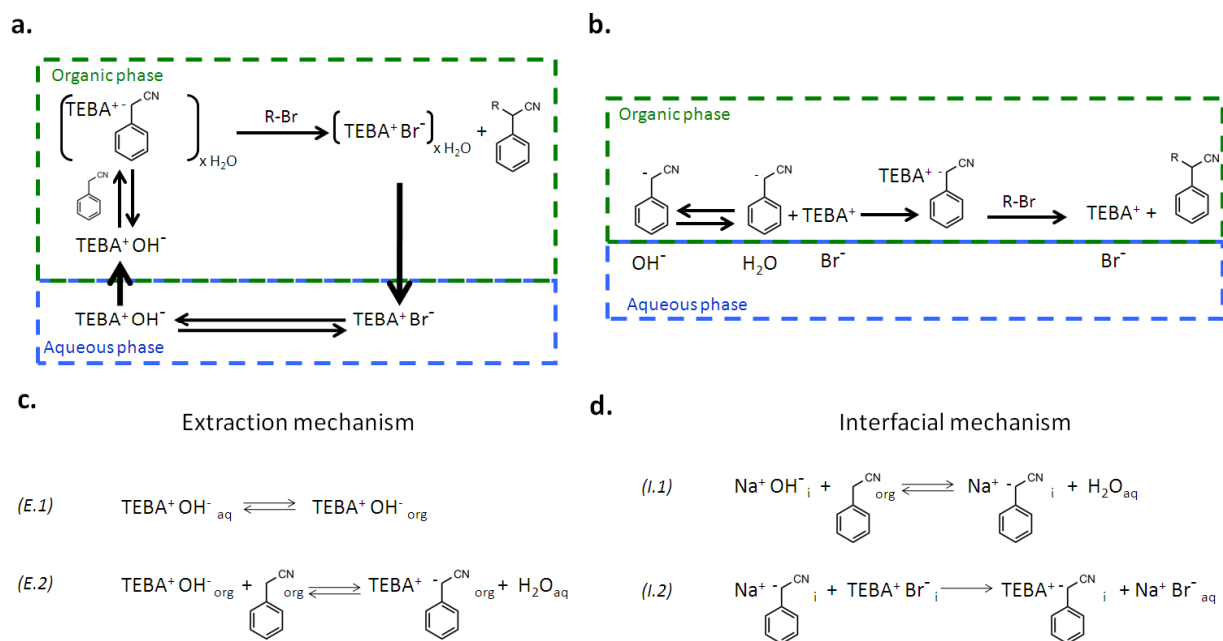
Figure 1: The Starks extraction [17] (**a.**) and the Makosza interfacial mechanism[18] (**b.**) for phase transfer catalyzed alkylation of phenylacetonitrile. Deprotonation step **c.** via the extraction mechanism consisting from the catalyst complex mass transfer (E.1) and subsequent deprotonation (E.2). **d.** via the interfacial mechanism consisting from interfacial deprotonation (I.1) and subsequent formation of the catalyst-phenylacetonitrile complex (I.2).
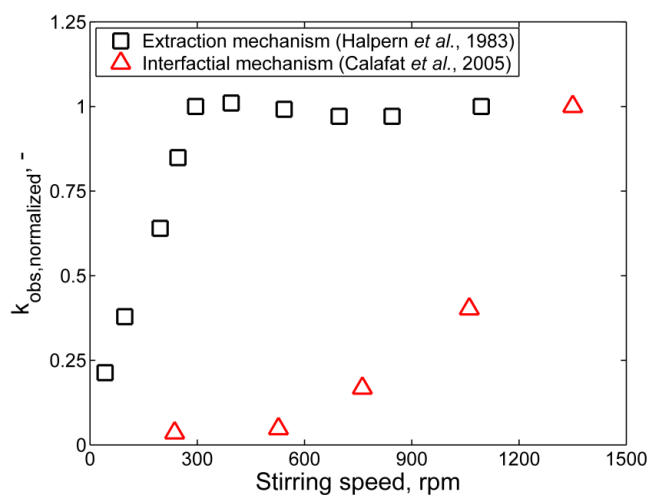

Figure 2: Pseudo-first order reaction rate constant as a function of the stirring speed (i.e. surface-to-volume ratio), for the case of the PTC reaction proceeding via the extraction and interfacial mechanism.

In stirred tank reactors, the distinction between the extraction and interfacial mechanism can be made by observing the two typical trends of the reaction as a function of stirring speed, which is correlated to the interfacial surface-to-volume ratio[19]. Figure 2 shows the typical trends of the observed reaction rate in isomerisation of allylbenzene (extraction mechanism) [20] and the alkylation of 2-phenylpropionitrile (interfacial mechanism) [21]. The mass transfer of the catalyst-hydroxide species is the rate limiting step in the reactions proceeding via the extraction mechanism at stirring rates below the threshold value (approx. 300 rpm in Figure 2).In the case of the interfacial mechanism, the reaction rate monotonously increases up to stirring speeds of 1400 rpm, due to an increase in liquid-liquid interfacial area. The interfacial mechanism was disputed by Starks[22] claiming that the two regimes shown in Figure 2 are a consequence of the inefficient stirring configuration, where the dispersion droplet size, and with it the surface-to-volume ratio does not increase with increasing stirring speed after a threshold value[23]. Therefore, in order to gain insight on the reaction mechanism, a precise control of the surface-to-volume ratios is essential.

The goal of the study is to gain insight on the influence of the interface area on the PTC/OH alkylation reaction. Previously we have shown that a high degree of control over the interface surface-to-volume ratio allows the improvement of both the conversion and selectivity in microfluidic systems[7]. Therefore, the microfluidic control of the phase interface allows for a detailed study of the effect of the interface area on the reaction kinetics, while eliminating the negative effects induced by inhomogeneous stirring in a batch reactor.

5.2 Experimental

Chemicals

All reagents used in this work are commercially available and obtained from Sigma-Aldrich. The aqueous phase consisted of potassium hydroxide (0-11 kmol/m^3) and benzyltriethylammonium chloride TEBA (0-7.4 mol/m^3) in demineralised water. The organic phase consisted of a mixture of n-butyl bromide and phenylacetonitrile at molar ratios ranging from 1 to 10. Furthermore, the organic phase contained 1.6 wt % of decahydronaphthalene used as the internal standard in the gas chromatography (GC) analysis.

Experimental microchannel reactor setup

The capillary microreactor assembly used in the experiments allowed for microscope slug flow observations, extraction and reaction experiments and is described in our previous study of the PTC/OH alkylation[7]. Mixing of the phases was done in a 250 μm inner diameter Y-mixer with an angle between the mixer inlets of 110º. The aqueous and organic phases were fed to the Y-mixer via two high performance liquid chromatography (HPLC) pumps (Shimadzu LC20-AD). Residence time for the reaction was provided by a transparent polytetrafluorethylene (PTFE) capillary with an internal diameter of 250 μm.

The feed lines, Y-mixer and PTFE capillary were kept at 80 °C via a thermostatic bath (Lauda E300).

All experiments were performed at a total flow of 100 µl/min, as it was the optimal flow rate in terms of slug length reproducibility, thus allowing estimations of surface-to-volume ratios with a standard deviation lower than 7 %. The residence time was adjusted by varying the PTFE capillary length from 0.5 to 4.4 m. The extraction experiments employed a PTFE tape coated funnel, which allowed for fast separation of the aqueous and organic phases after the PTFE capillary outlet. The organic phase was absorbed by the PTFE tape, while the aqueous phase was analyzed via UV-Vis.

Slug flow visualization

Video imaging analysis of the slug flow was performed with a Zeiss Axio Observer D1m microscope at 50x magnification coupled with a high-speed imaging camera (MotionPro10000). The videos were recorded at a rate of 2000 frames per second at a resolution of 1280 × 480. The estimation of the slug lengths and the interfacial surface areas was performed by image analysis using Matlab^{TM} software.

Analysis

The reactants and products were analyzed using a Varian CP-3800 gas chromatograph equipped with a 30 m × 0.25 mm CP-Sil column and a flame ionization detector (FID). The products were qualitatively identified by GC-mass spectrometry (MS). The aqueous phase catalyst compositions were analyzed via off-line UV-Vis spectroscopy (Shimadzu UV-2501PC) using the absorption band of phenyl group the TEBA at 262.5 nm.

5.3 Results

In order to gain insight on the reaction occurring on the phase interface, a high degree of control over the surface-to-volume ratio must be achieved. The study of the reaction occurring at the interface of the aqueous and organic phases consisted of four separate parts:

- Study of slug flow hydrodynamics in order to determine the surface-to-volume ratios.
- Study of the TEBA extraction and determination of the partition coefficients for the reaction modeling.
- Parametric study in order to determine reaction conditions when the reaction rate dependents solely on the interface area.
- Kinetic modeling of the reaction where the two proposed models, the Starks extraction and Makosza interfacial model are evaluated.

5.3.1 Hydrodynamics

Unlike in the case of capillaries with polar walls such as fused silica[22], in non-polar PTFE capillaries, no thin film of the continuous phase between the dispersed slug and the capillary wall is observed (Chapter 4). Consequently, the interfacial area is determined solely by the slug cap. A total flow rate of 100 µl/min was found to yield highly reproducible slugs, thus allowing accurate measurements of surface-to-volume areas according to the procedure described in Appendix A. Operation at lower flow rates, resulted in the decreased reproducibility with formation of slugs up to 1 mm long, consequently decreasing the surface-to-volume ratio. By increasing the aqueous-to-organic flow (AO) ratio from 1 to 9, the organic slug length decreased from approximately 500 µm to below 250 µm, while the aqueous slug length increased from 500 µm to approximately 2300 µm (Figure 3). The dispersed, aqueous slug size was estimated using the scaling law as shown in chapter 2:

$$\frac{L_{aq}}{D} = A + B\frac{F_{aq}}{F_{org}} = A + B(AO) \tag{1}$$

where L_{aq} is the aqueous slug length; D is the diameter of the capillary; F_{aq} is the aqueous (dispersed) phase flow rate and F_{org} the organic (continuous) flow rate; while A and B are the fitting parameters which are determined by the geometry of the system. In the work of Garstecki et al. (2006) the parameter A was found to be independent from the physical properties of the fluids and equal to 1. Therefore, Eq.1 was simplified to yield:

$$\frac{L_{aq}}{D} = 1 + B\frac{F_{aq}}{F_{org}} = 1 + B(AO) \tag{2}$$

The continuous, organic phase slug length was found to be inversely proportional to the AO ratio:

$$\frac{L_{org}}{D} = 1 + B\frac{F_{org}}{F_{aq}} = 1 + \frac{B}{(AO)} \tag{3}$$

Eqs. 2 and 3 were found to be in good agreement with the experimental data (Figure 3 a). The values of the parameter B, for Eqs. 2 and 3 are approximately the same (Table 1), giving an indication that the slug sizes are determined by the geometry of the reactor.

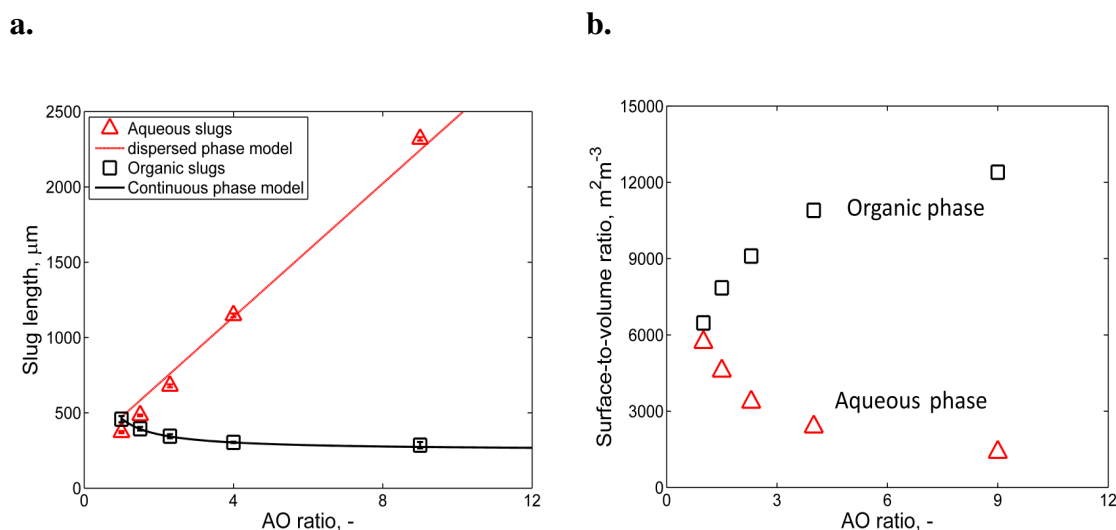**a.**   **b.**

*Figure 3: **a.** Experimental values and scaling law modeling of aqueous and organic slug sizes as a function of the aqueous-to-organic flow ratio. **b.** Organic and aqueous phase surface-to-volume ratios as a function of the aqueous-to-organic flow (AO) ratios*

Table 1: Fitting parameter B for the prediction of the continuous (organic) and disperse (aqueous) phase slug lengths in Eqs. 2 and 3.

Slug	B	R^2
Continuous	0.86	99 %
Dispersed	0.88	99 %

The surface-to-volume ratio of the organic phase was estimated by assuming semispherical slug caps as described in Appendix A. By increasing the AO ratio from 1 to 9, the organic slug size decreased resulting in the increase of the surface-to-volume ratio from 6500 to 12500 m^2/m^3 (Figure 3 b). Simultaneously, the aqueous slug size increased resulting in the decrease of the aqueous surface-to-volume ratio from 6000 to approximately 1500 m^2/m^3.

5.3.2 Extraction of TEBA

The extraction of quaternary ammonium salts is known to be difficult to measure due to the low solubility, impurities (e.g. $NR_3H^+X^-$) and decompositions of the ammonium salts in the aqueous phase to form free amines[23]. A particular problem is the the measurement of partition coefficients in reaction systems that employ concentrated bases such as the PTC alkylation of phenylacetonitrile, due to the catalyst decomposition via the Hoffman degradation[24,25]. The extraction experiments were performed in the capillary microreactor under the slug flow to avoid catalyst decomposition.

Previously we have shown that slug flow extraction in the 250 µm capillary allows equilibrium to be reached at residence times as short as 2 s [3], therefore allowing to measure the extraction of TEBA at conditions of low catalyst decomposition. In order to confirm the equilibrium operation the extraction was performed at residence times of 1 and 2 min. By increasing the AO ratio the organic slug size decreases (Figure 3 a), resulting in lower quantities of TEBA extracted into the organic phase. Consequently, the amount of extracted TEBA from the aqueous phase into the organic phase decreases from 6 to approximately 2 % (Figure 4 a). The results are consistent with previous studies where TEBA was found to have very low solubility in the organic phase[17], where up to 99 % of TEBA is in the aqueous phase[24]. Partition coefficients (Figure 4 b) used in the modeling of the reaction were calculated via the aqueous and organic phase TEBA concentrations:

$$K_{partition} = \frac{C_{TEBA,org}}{C_{TEBA,aq}} \tag{4}$$

By increasing the AO ratio from 1 to 9 the calculated partition coefficient was found to increase by approximately 50 %. The partition coefficients depend strongly on the activity coefficients and on the bulk concentrations of TEBA in both phases. With increasing AO ratios the TEBA concentrations change, and with them the activity coefficients resulting in the increase of the partition coefficient[3]. At AO ratios higher than 6 the experimental error of the partition coefficients increased, therefore for modeling purposes the partition coefficient was fixed at a constant value of 0.15 in this range.
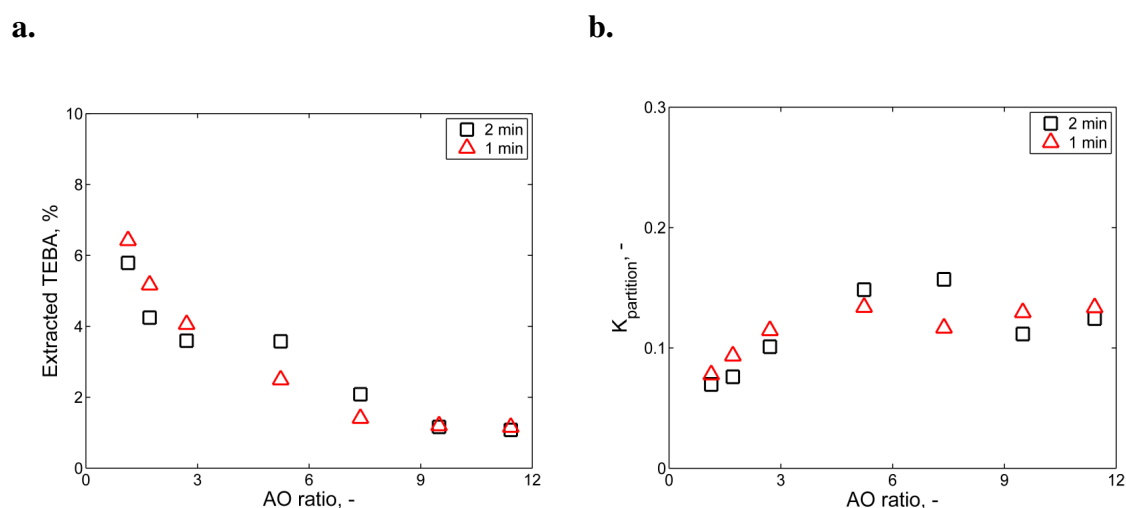
a.   **b.**

Figure 4: ***a.*** *Slug flow extraction experiments: extracted amount of TEBA from the aqueous phase as a function of the AO ratio at residence times of 1 and 2 min.* ***b.*** *TEBA partition coefficient as a function of the AO ratio at residence times of 1 and 2 min.*

5.3.4. Butyl bromide to phenylacetonitrile molar ratio

The molar ratio of butyl bromide to phenylacetonitrile (BuBr/PAN) was varied from 1 to 10, at a fixed residence time of 1 min to determine the range of reaction conditions where the zero order in butyl bromide concentration was observed. At BuBr/PAN ratios higher than 6, the concentration of butyl bromide no longer influenced the reaction (Figure 5). The large excess of butyl bromide makes the alkylation step fast compared to the deprotonation step, thus the latter becomes the rate-limiting step. Therefore, all further experiments were performed at a BuBr/PAN molar ratio of 10.
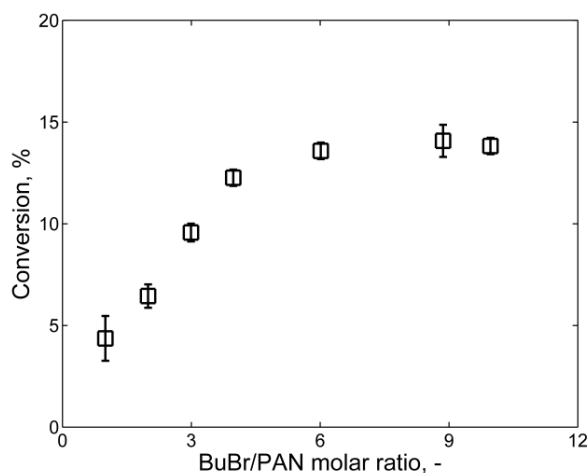
Figure 5: Conversion of phenylacetonitrile as a function of butyl bromide to phenylacetonitrile molar ratio at a residence time of 1 min and an organic surface-to-volume ratio of 6500 m^2/m^3.

5.3.5 Catalyst concentration

The influence of the TEBA concentration was investigated at a residence time of 1 min and AO ratios of 1 and 4, corresponding to organic surface-to-volume ratios of 6500 and 11000 m^2/m^3, respectively. A conversion of 5 % was observed in the blank experiments (without catalyst) at the both surface-to-volume ratios. The concentration of the TEBA was found to be of no influence on the slug size (i.e. surface-to-volume ration). By increasing the TEBA concentration the conversion increased until the TEBA concentration of 6 mol/m^3, after which the reaction was found to be independent of the concentration (Figure 6) for both of the studied surface-to-volume ratios. All reaction modeling experiments were performed at TEBA concentration of 7.4 mol/m^3 in order to eliminate the influence of catalyst concentration on the reaction rate. In this range, the conversion increased by 3.8 times when the surface-to-volume ratio was increased from 6500 to 11000 m^2/m^3.
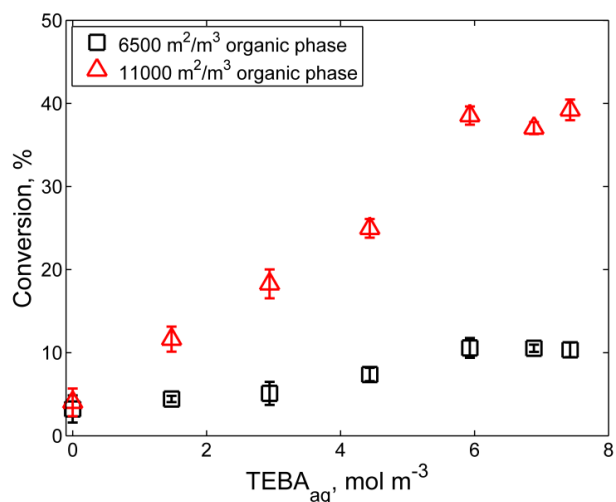
Figure 6: Conversion of phenylacetonitrile at different TEBA concentrations at a residence time of 1 min and an organic surface-to-volume ratios of 6500 and 11000 m^2/m^3.

The organic phase surface-to-volume ratio was varied from 6500 to 12500 m^2/m^3 by controlling the AO ratio from 1 to 9 at different catalyst concentrations, allowing the conversion to be increased up to 60 % at a constant residence time of 1 min (Figure 7).
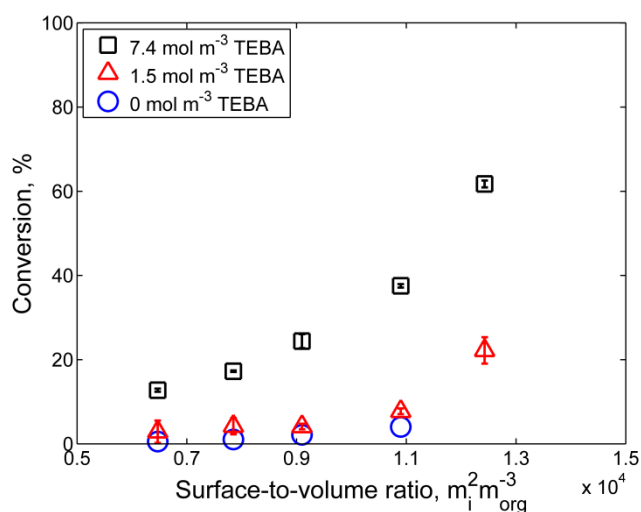

Figure 7: The conversion as a function of the organic surface-to-volume ratio at two catalyst concentrations of 1.5 and 7.4 mol/m^3, at a residence time of 1 min. The conversion in the blank experiments is given for comparison.

5.3.6 Hydroxide concentration

The influence of the aqueous hydroxide concentration was investigated at a residence time of 1 min and organic surface-to-volume ratios of 6500 and 11000 m^2/m^3. By increasing the KOH concentration from 5.9 to 11 kmol/m^3, a significant increase of conversion from

2 % to 40 % was observed (Figure 8). In literature similar trends were observed in the cases of PAN alkylation with[26] and without the PTC catalyst[27].

The exponential increase of conversion with increasing base concentration cannot be explained with the salting out of the catalyst as it is often done in the literature[24], as the extraction experiments show that more than 94 % of the TEBA species remain in the aqueous phase. Instead the increase in conversion can be explained by increasing dehydrating effect with increasing base concentrations as discussed by Albanese et al. (2001) [28]. The increase of the base concentrations decreases the negative effect of anion reactivity with the water produced in the dehydration step. Consequently, in systems with concentrated bases, the hydration of the formed anion is decreased, thus allowing for increased reactivity of the anion produced by the deprotonation step[19,29,30]. Therefore, all reaction modeling experiments were performed at a maximal base concentration of 11 kmol/m^3.
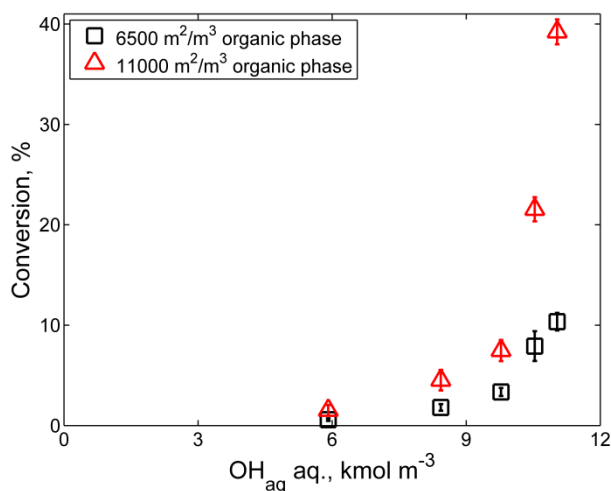

Figure 8: Conversion of phenylacetonitrile at different OH$^-$ concentrations at a residence time of 1 min and an organic surface-to-volume ratios of 6500 and 11000 m^2/m^3.

5.4 Reaction modeling

In order to observe the reaction on the phase interface, the influence from all other reaction steps on the reaction must be eliminated. By operating at conditions independent of the butyl bromide concentration (BuBr/PAN molar ratio of 10, Figure 8), the reaction becomes limited by the deprotonation step. The experiments for the modeling of the two discussed mechanisms were performed at TEBA concentrations of 7.4 mol/m^3, at which the reaction is independent of the TEBA concentration, thus allowing for the observation of the reaction step connected to the interface: the mass transfer (Figure 1 c, E.1) or the interfacial reaction (Figure 1 d, I.1).

First, the influence of the surface-to-volume ratio on the pseudo-first order reaction rate was studied. Values for the pseudo-first order reaction rate constant k_{obs} were obtained by nonlinear least squares regression, with an average standard deviation lower than 2 % (Figure 9):

$$\frac{dC_{PAN}}{dt} = -k_{obs}C_{PAN} \tag{5}$$

where C_{PAN} is the concentration of phenylacetonitrile in the organic slugs, t is the residence time in the microchannel and k_{obs} is the observed pseudo-first order reaction rate constant.

By increasing the surface-to-volume ratio from 6500 to 12500 m^2/m^3, k_{obs} increased from $2\cdot10^{-2}$ to $15\cdot10^{-2}$ s^{-1}. The strong dependence of the observed rate constant on the surface-to-volume ratio (Figure 9) is in agreement with the interface mechanism (Figure 2).
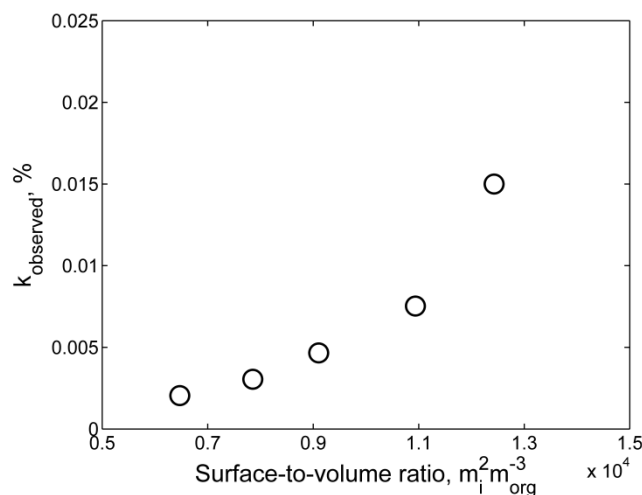

Figure 9: Pseudo-first order reaction rate constant of the PTC alkylation of phenylacetonitrile as a function of the measured organic surface-to-volume ratio.

5.4.1 Extraction mechanism model

The ion exchange reactions resulting in the formation of the TEBA$^+$OH$^-$ and TEBA$^+$ Br$^-$ species in the aqueous phase (Figure 1 a) are considered to be very fast reactions[31,32], compared to the mass transfer and alkylation. Therefore, the rate of the TEBA$^+$OH$^-$ consumption was assumed to be dominated by the mass transfer of the catalyst species. Furthermore, in the slug flow without the film, the mass transfer coefficient consists of two contributions: the aqueous and organic slug cap mass transfer coefficients. The two mass transfer contributions can be combined into an overall mass transfer coefficient for the slug cap as shown in Appendix C:

$$(k_L a)_{cap} = \frac{(ka)_{cap,aq}(ka)_{cap,org}}{\alpha(ka)_{cap,aq} + K_{partition}(ka)_{cap,org}} \qquad (6)$$

The rate equations describing the deprotonation step (Figure 1 d) of the extraction model are   as   follows:

$$\frac{dC_{TEBA^+OH^-,org}}{dt} = (k_L a)_{cap}\left(K_{partition}C_{TEBA^+OH^-,aq} - C_{TEBA^+OH^-,org}\right) - k_1 C_{TEBA^+OH^-,org}C_{PAN} + k_2 C_{TEBA^+PAN^-} \quad (7)$$

$$\frac{dC_{PAN}}{dt} = -k_1 C_{TEBA^+OH^-,org}C_{PAN} + k_2 C_{TEBA^+PAN^-} \qquad (8)$$

$$\frac{dC_{TEBA^+PAN^-}}{dt} = k_1 C_{TEBA^+OH^-,org}C_{PAN} - k_2 C_{TEBA^+PAN^-} \qquad (9)$$

The concentration profiles are shown in Figure 10 a and the corresponding kinetic parameters are listed in Table 2. It can be seen that a satisfactory agreement is achieved between the experimental and predicted profiles at all AO ratios except 9 where an exponential decay cannot be adequately predicted by the model. The mass transfer coefficient values $(k_L a)_{cap}$ are increasing with increasing AO ratio (i.e. increasing surface-to-volume ratio), which is consistent with the previous findings in the slug flow[7]. The rate constants for the deprotonation step, however do not follow any observable trend, indicating the proposed extraction mechanism model is not correct.

Table 2: Modeled values of the cap mass transfer coefficient ($(k_L a)_{cap}$), the deprotonation rate constants (k_1, k_2) for the extraction mechanism at different AO ratios (average standard deviation of 5.1 %).

AO ratio, -	$(k_L a)_{cap}$, s^{-1}	k_1, $m^3 s^{-1} mol^{-1}$	k_2, s^{-1}
1.0	3.02 ± 0.03	10.10 ± 0.11	1.37 ± 0.02
1.5	3.56 ± 0.02	0.34 ± 0.002	1.81 ± 0.01
2.3	4.25 ± 0.01	0.45 ± 0.001	0.05 ± 0.0001
4.0	5.28 ± 0.05	8.33 ± 0.08	5.00 ± 0.05
9.0	9.13 ± 0.28	5.42 ± 0.16	11.68 ± 0.35

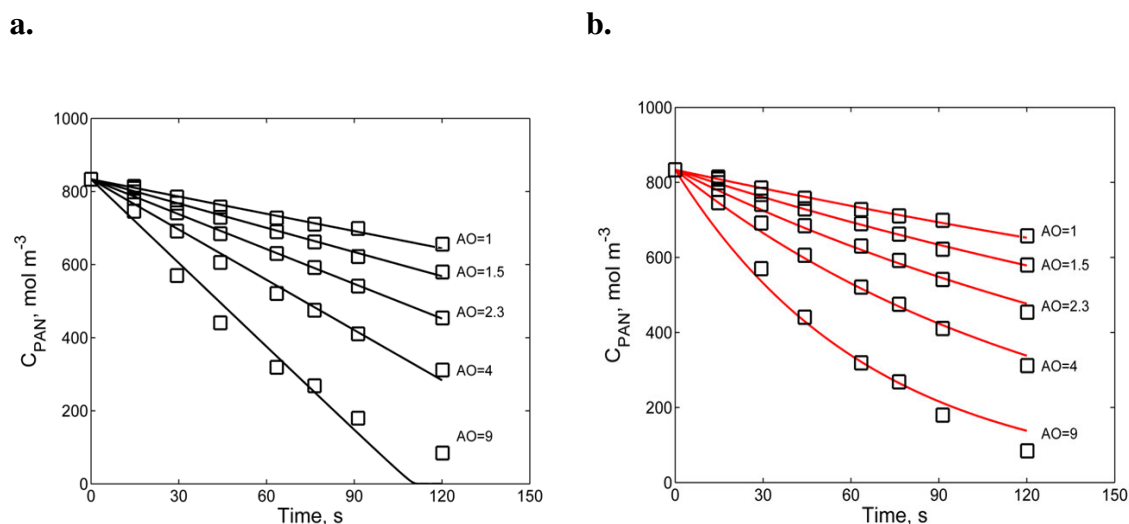**a.**   **b.**

*Figure 10: Experimental (points) and modeling results (line) via the extraction mechanism (**a.**) and the interfacial mechanism (**b.**) for the concentration of phenylacetonitrile at different AO ratios.*

There are several arguments against the extraction mechanism for the PTC/OH alkylation of phenylacetonitrile:

- The operation in a microchannel under slug flow regime excludes the mass transfer limitation[3]. Furthermore, extraction experiments performed at different residence times indicated that the TEBA concentrations are at equilibrium (Appendix B).
- TEBA has low solubility in the organic phase with majority of the species residing in the aqueous phase[23]. The extraction experiments showed that by increasing the AO ratio, and with it the surface-to-volume ratio, the amount of extracted TEBA in the organic phase reduces from 6 % to 2 % (Figure 4 a). Simultaneously, by increasing the surface-to-volume ratio the conversion increases by two orders of magnitude (Figure 8). The decreasing amount of extracted catalyst and the simultaneous increase of the conversion are in contradiction with the extraction model.
- The formation of water in the step E.2 (Figure 1 c), can only occur near the interface as water is insoluble in the organic phase.
- With increasing surface-to-volume ratio the pseudo-first order reaction rate does not reach a threshold value indicating the elimination of mass transfer limitations (Figure 9). The observed rate pseudo-first order constant exhibits strong dependence on the surface-to-volume ratio, which is consistent with the previous reports of the interfacial mechanism (Figure 2).

The values of the reaction rate constants of the deprotonation step acquired from the extraction model have no functional dependence and are random (Table 2), indicating that the modeling results have no physical meaning. Last, the extraction model provided a poor fit at higher AO ratios (Figure 10 a).

5.4.2 Interface mechanism model

The deprotonation of the organic substrate at the interface without a phase transfer catalyst was found to be an equilibrium reaction[28,33]. The role of the catalyst in the interface mechanism is to shift the equilibrium at the interface towards the deprotonated reactant by removing it from the surface[19]. It is important to note the conceptual difference of the catalyst role in both mechanisms. In the extraction mechanism the catalyst transfers the hydroxide anions into the organic phase, and thus facilitates deprotonation, whereas in the interface mechanism it shifts the interfacial equilibrium towards deprotonation.

Operation at conditions where the reaction is independent of the alkylating agent (Figure 5) allows for the observation of the deprotonation reaction shown in Figure 1 d. The rate equations describing the deprotonation step of the interfacial model are as follows:

$$\frac{dC_{PAN}}{dt} = -k_1 C_{PAN} C_{OH}{}^i + k_2 C_{PAN^-}{}^i C_{H_2O} \tag{10}$$

$$\frac{dC_{PAN^-}}{dt} = k_1 C_{PAN} C_{OH} + k_2 C_{PAN^-} C_{H_2O} - k_3 C_{PAN^-} C_{TEBA} \tag{11}$$

With the addition of the phase transfer catalyst, the equilibrium of the interface deprotonation is shifted towards the deprotonated PAN. Furthermore, by operating at TEBA concentrations where no influence on the reaction is observed (Figure 6), allows for measuring of the interface deprotonation (Figure 1 d, I.1). Consequently, Eq. 10 can be rewritten as:

$$\frac{dC_{PAN}}{dt} = -k_{\text{interface}} C_{PAN} C_{OH}{}^i \tag{12}$$

The interface hydroxide concentration, $C_{OH}{}^i$, is determined by the coverage of the interface surface with the OH$^-$ ions available for the deprotonation. The interface surface coverage with OH$^-$ ions can be expressed as:

$$N_{OH}{}^i = \frac{\beta C_{OH,bulk}}{a_{aq}} \tag{13}$$

where N_{OH} is the OH$^-$ surface coverage in mol/m^2, $C_{OH,bulk}$ is the aqueous bulk OH$^-$ concentration, a_{aq} is the aqueous surface-to-volume ratio and β is the fraction of the bulk OH$^-$ ions covering the interface. It is important to note that β cannot be determined directly as the number of OH$^-$ ions covering the interface depends on many factors including the OH$^-$ concentration, water activity, surface tension and temperature. When operating at concentrated OH$^-$ solutions the surface coverage is assumed constant. Finally, the interface OH$^-$ concentration is defined as:

$$C_{OH}{}^i = N_{OH}{}^i a_{org} = \beta C_{OH,bulk} \frac{a_{org}}{a_{aq}} \tag{14}$$

Therefore Eq. 12 can be rewritten as:

$$\frac{dC_{PAN}}{dt} = -k_{interface} \beta \frac{a_{org}}{a_{aq}} C_{OH,bulk} C_{PAN} \tag{15}$$

Since the experiments were performed at conditions where β and $C_{OH,bulk}$ are constant, Eq. 15 becomes:

$$\frac{dC_{PAN}}{dt} = -k_{interface,obs} \frac{a_{org}}{a_{aq}} C_{PAN} \tag{16}$$

where $k_{interface,obs} = k_{interface} \beta C_{OH,bulk}$ is the observed rate constant of the interfacial deprotonation.

The derived model predicts the experimental results with high accuracy with an average standard deviation of 1.6 % (Figure 10 b). In order to interpret the accuracy of the model, the observed interfacial deprotonation reaction rate must be studied. According to the developed model, with the increase of the surface-to-volume ratio, the amount of OH$^-$ ions available for the deprotonation will increase, while the rate constant of the deprotonation should remain unchanged. The increase of the surface-to-volume ratio from 6500 to 12500 m^2/m^3, had little influence on the observed deprotonation rate constant $k_{interface,obs} = k_{interface} \beta C_{OH,bulk}$ (Figure 11), indicating that the reaction proceeds via the interfacial deprotonation mechanism. The observed interface deprotonation rate constant was determined to be $1.72 \pm 0.02 \cdot 10^{-3}$ s^{-1}.
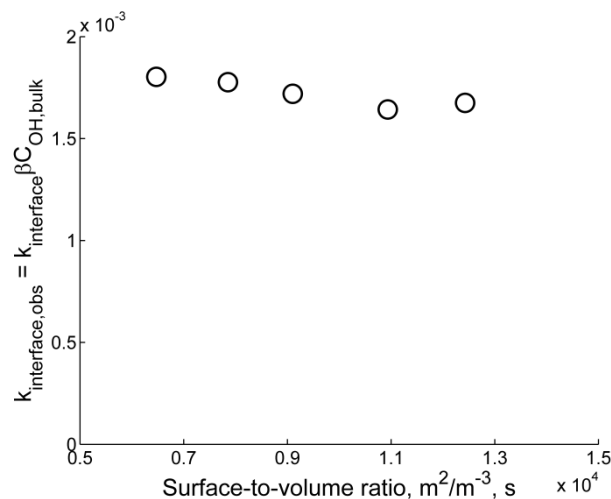

Figure 11: Observed rate constant of the interfacial deprotonation as a function of the organic surface-to-volume ratio.

5.5 Conclusions

The kinetic study of phase transfer catalyzed alkylation of phenylacetonitrile in a microreactor has been performed to distinguish between two possible reaction mechanisms: (i) the extraction mechanism where the deprotonation reaction is limited by mass transfer and (ii) the interfacial mechanism, where the rate limiting step occurs at the interface. Slug flow in a capillary microreactor allowed for precise control of the interface surface-to-volume ratio by varying the aqueous-to-organic flow ratio. Correlations for the slug size prediction and geometrical analysis of the slug cap, allowed for accurate measurements of the slug surface-to-volume ratio estimation.

In the absence reactants, the equilibrium concentrations of the phase transfer catalyst are rapidly achieved between the aqueous and organic phases. Strong dependence of the deprotonation reaction on the interfacial surface-to-volume ratio at conditions when the reaction is independent of the catalyst concentration gave strong indication that the reaction proceeds via the interfacial mechanism. Furthermore, the interfacial mechanism model was found to accurately predict the reaction in the whole range of aqueous-to-organic flow ratios studied. The interfacial model was modified in order to describe the interface deptrotonation reaction as a function of the hydroxide interface concentration, consequently accounting for the influence of the surface-to-volume ratio on the reaction. Finally, the observed rate constant of the interface deprotonation step was studied at surface-to-volume ratios from 6500 to 12500 m^2/m^3. The interface deprotonation rate constant was independent of the surface-to-volume ratio, indicating that the intrinsic rate of deprotonation was measured.

Appendix A: Estimation of the slug surface-to-volume ratios

The lengths of organic and aqueous slugs and the dimensions of the slug caps were defined according to Figure A.1, allowing for the estimation of the surface and volume ratios.
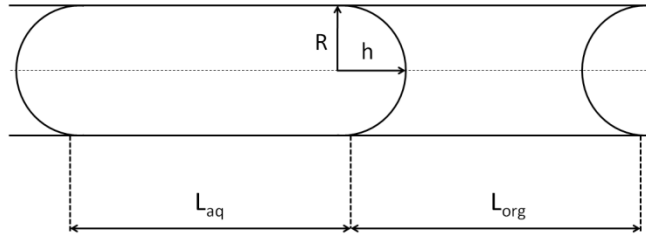

Figure A.1: The characteristic dimensions of the slug cap and the lengths of the aqueous and organic slugs used in the surface-to-volume estimation.

The volume and the surface of the hemispherical caps can be calculated using Eqs. A.1 and A.2:

$$V_{cap} = \frac{1}{6}\pi h\left(3R^2 + h^2\right) \tag{A.1}$$

$$S_{cap} = \pi\left(R^2 + h^2\right) \tag{A.2}$$

The volume of the cylindrical slug section was calculated using Eq. A.3:

$$V_{cylinder} = \pi R^2 L_{slug} \tag{A.3}$$

Combination of Eqs. A.2 and A.3 yields for the total volume of the aqueous and organic slugs:

$$V_{aq} = \pi R^2 L_{aq} + \frac{2}{6}\pi h\left(3R^2 + h^2\right) \tag{A.4}$$

$$V_{org} = \pi R^2 L_{org} - \frac{2}{6}\pi h\left(3R^2 + h^2\right) \tag{A.5}$$

In the microscope analysis no organic film was observed (at a resolution of 3.7 μm/pixel). Therefore it can be concluded that the liquid-liquid interface occurs only at the caps, with no interface at the cylindrical part of the slugs. Furthermore, in all measurements the parameter h was constant, with an average value of 65 ± 10 μm. Therefore, the total liquid-liquid interfacial area per slug is as follows:

$$S_{L-L} = 2\pi\left(R^2 + h^2\right) \tag{A.6}$$

The experimentally obtained surface-to-volume (SV) ratio is calculated by combining A.4, A.5 and A.6:

$$SV = \frac{S_{L-L}}{V} \tag{A.7}$$

Appendix B: Decomposition of the phase transfer catalyst and slug flow extraction

Extraction experiments of TEBA from the KOH aqueous solution (11 kmol/m^3) with pure butyl bromide performed in 2 ml vials at 80 °C showed decreasing aqueous TEBA concentrations in time due to the decomposition. The decomposition of TEBA under aforementioned conditions was found to be a first order reaction with a reaction rate constant of $5.9 \cdot 10^{-6}$ s^{-1} (Figure B.1 a). In order to confirm the equilibrium operation the extraction was performed at residence times of 1 and 2 min (Figure B.1 b)
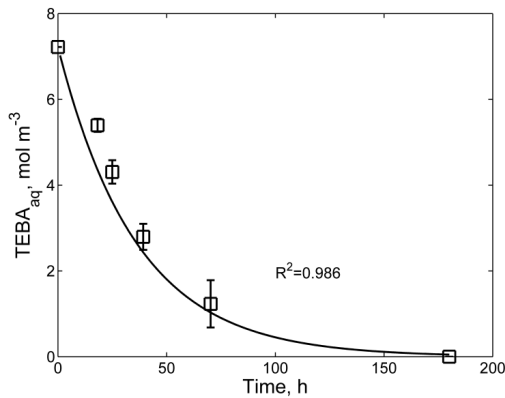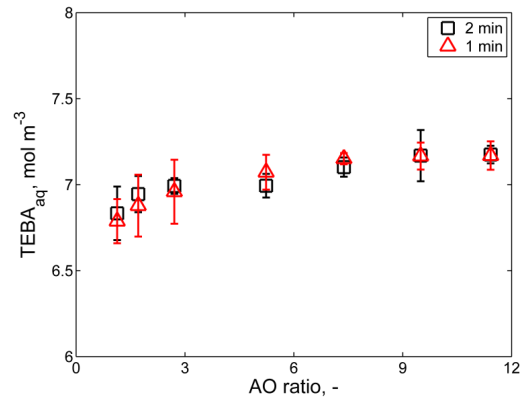
a.   **b.**

Figure B.1: **a.** Decomposition of the TEBA$^+$Br$^-$ via the Hoffman degradation in the multiphase system composed of butyl bromide (organic phase) and a hydroxide solution of 11 kmol/m^3 (aqueous phase). **b.** Slug flow extraction experiments: aqueous concentration of TEBA as a function of the different AO ratios at residence times of 1 and 2 min.

Appendix C: Slug cap mass transfer model

Since the molar flux is the same for the slug and continuous phase it can be written:

$$-J_{cap} = (ka)_{cap,aq} V_{aq} (C_{bulk,aq} - C_{i,aq}) \tag{B.1}$$

$$-J_{cap} = (ka)_{cap,org} V_{org} (K_{partition} C_{i,aq} - C_{bulk,org}) \tag{B.2}$$

where V designates the slug and continuous phase volumes, while m is the experimentally derived partition coefficient between the two phases. The volumetric ratio can be expressed as:

$$\alpha = \frac{V_{aq}}{V_{org}} \tag{B.3}$$

Solving the system of Eqs. B.1, B.2 and B.3 yields the slug cap interfacial concentration:

$$C_{i,aq} = \frac{(ka)_{cap,aq}\alpha C_{bulk,aq} + (ka)_{cap,org} C_{bulk,org}}{(ka)_{cap,aq}\alpha + K_{partition}(ka)_{cap,org}} \qquad \text{(B.4)}$$

The rate of extraction from the aqueous slug is:

$$\frac{dC_{aq}}{dt} = -(ka)_{cap,aq}(C_{bulk,aq} - C_{i,aq}) \qquad \text{(B.5)}$$

Combining Eqs. B.4 and B.5

$$\frac{dC_{aq}}{dt} = -\frac{(ka)_{cap,aq}(ka)_{cap,org}}{\alpha(ka)_{cap,aq} + K_{partition}(ka)_{cap,org}} \cdot (K_{partition}C_{bulk,aq} - C_{bulk,org}) \qquad \text{(B.6)}$$

which can be rewritten as:

$$\frac{dC_{aq}}{dt} = -(ka)_{cap} \cdot (K_{partition}C_{bulk,aq} - C_{bulk,org}) \qquad \text{(B.7)}$$

The overall mass transfer coefficient is:

$$(ka)_{cap} = \frac{(ka)_{cap,aq}(ka)_{cap,org}}{\alpha(ka)_{cap,aq} + K_{partition}(ka)_{cap,org}} \qquad \text{(B.8)}$$

Nomenclature

a –surface-to-volume ratio, m^2/m^3
C –concentration, mol/m^3
h –slug cap height, m
k –reaction rate constant
$(ka)_{cap}$ –slug cap mass transfer coefficient, s^{-1}
$K_{partition}$ –partition coefficient
L –slug length, m
$N_{OH}{}^i$ –hydroxide ion surface coverage, mol/m^2
J –molar flux, mol/s
V –volume, m^3
R –slug radius, m
S –surface area, m^2
t –time, s

Greek letters
α- volumetric ratio
β- fraction of ions from the bulk covering the interface, -

Subscripts
aq – aqueous phase
i – interface
L-liquid
OH – hydroxide
org –organic phase
PAN –phenylacetonitrile
PAN^- –deprotonated phenylacetonitrile
$TEBA$ –benzyltriethylammonium chloride
$TEBA^+OH^-$ – benzyltriethylammonium-hydroxide complex
$TEBA^+PAN^-$ – benzyltriethylammonium- deprotonated phenylacetonitrile complex

Superscipts

i – interface

References

(1)   Jovanović, J.; Rebrov, E.V.; Nijhuis, T.A.; Hessel, V.; Schouten, J.C. Redispersion microreactor system for phase transfer catalyzed esterification, *Chem. Eng. Technol.*, 2011, submitted.

(2)   Ehrfeld, W.; Hessel, V.; Löwe, H. Microreactors: New Technology for Modern Chemistry, Wiley-VCH, Weinheim, 2000.

(3)   Jovanović, J.; Rebrov, E.V.; Nijhuis, T.A.; Hessel, V.; Schouten, J.C. Liquid-liquid flow in long capillaries: hydrodynamic flow patterns and extraction performance, *Ind. Eng. Chem. Res.* 2011, submitted.

(4)   Burns, J.R.; Ramshaw, C. The intensification of rapid reactions in multiphase systems using slug flow in capillaries. *Lab. Chip* 2001, *1*,10.

(5)   Kashid, M.N.; Agar, D.W. Hydrodynamics of liquid-liquid slug flow capillary microreactor: Flow regimes, slug size and pressure drop. *Chem. Eng. J.* 2007, *131*, 1.

(6)   Garstecki, P.; Fuerstman, M. J.; Stone, H.A.; Whitesides, G.M. Formation of droplets and bubbles in a microfluidic T-junction - scaling and mechanism of break-up. *Lab. Chip* 2006, *6*, 437.

(7)   Jovanović, J.; Rebrov, E.V.; Nijhuis, T.A.; Hessel, V.; Schouten, J.C. Phase-transfer catalysis in segmented flow in a microchannel: fluidic control of selectivity and productivity. *Ind. Eng. Chem. Res.* 2010, *49*, 2681.

(8)   Kiwi-Minsker, L.; Renken, A. Microstructured reactors for catalytic reactions. *Catal. Today* 2005, *110*, 2.

(9)   Zhou, G.; Kresta, S.M. Evolution of drop size distribution in liquid-liquid dispersions for various impellers. *Chem. Eng. Sci.* 1998, *11*, 2099.

(10) Hisamoto, H.; Saito, T.; Tokeshi, M.; Hibara, A.; Kitamori, T. Fast and high conversion phase-transfer synthesis exploiting the liquid-liquid interface formed in a microchannel chip. *Chem. Commun.* 2001, *24*, 2662.

(11) Ueno, M.; Hisamoto, H.; Kitamori, T.; Kobayashi, S. Phase transfer alkylation reactions using microreactors. *Chem. Commun.* 2003, *8*, 936.

(12) Borovinskaya, E.S.; Mammitzsch, L.; Uvarov, V.M.; Schael, F.; Reschetilowski, W. Experimental investigation and modelling approach of the phenylacetonitrile alkylation process in a microreactor. *Chem. Eng. Technol.* 2009, *32*, 919.

(13) Halpern, M. Increasing plant profits by phase-transfer catalysis retrofit. *PTC Comm.* 1996, *2*, 1.

(14) Makosza, M. Two-phase reactions in the chemistry of carbanions and halocarbenes: a useful tool in organic synthesis. *Pure Appl. Chem.* 1975, *43*, 439.

(15) Naik, S.D.; Doraiswamy, L.K. Phase transfer catalysis: chemistry and engineering. *AIChE J.* 1998, *44*, 612.

(16) Lednicer, D. The organic chemistry of drug synthesis, Vol. 7. Wiley-Interscience, New York, 2007.

(17) Starks, C.M. Phase-transfer catalysis. I. Heterogeneous reactions involving anion transfer by quaternary ammonium and phosphonium salts. *J. Am. Chem. Soc.* 1971, *93*, 195.

(18) Makosza, M.; Bialecka, E. Reactions of organic anions. LXXIII. Alkylation of phenylacetonitrile at the interface with aqueous sodium hydroxide. *Tetrahedron Lett.* 1977, *2*, 183.

(19) Rabinovitz, M.; Cohen, Y.; Halpern, M. Hydroxide ion initiated reactions under phase transfer catalysis conditions: mechanism and implications. *Angew. Chem. Int. Ed. Engl.* 1986, *25*, 960.

(20) Halpern, M.; Sasson, Y.; Rabinovitz, M. Hydroxide ion initiated reactions under phase- transfer-catalysis conditions. 5. Isomerization of allylbenzene via hydroxide ion extraction. *J. Org. Chem.* 1983, *48*, 1022.

(21) Calafat, S.V.; Durantini, E.N.; Chiacchiera, S.M.; Silber, J.J. Kinetics of the reaction between 2-phenylpropionitrile and 2-chloro-5-nitrotrifluoromethylbenzene under phase-transfer catalysis. *J. Org. Chem.* 2005, *70*, 4659.

(22) Starks, C.; Liotta, C.; Halpern, M. Phase-Transfer Catalysis: Fundamentals, Applications and Industrial Perspectives, Chapman & Hall, London, 1994.

(23) Starks, C. M. Interfacial area generation in two-phase systems and its effect on kinetics of phase transfer catalyzed reactions. *Tetrahedron* 1999, *55*, 6261.

(24) Jovanović, J.; Zhou, W.; Rebrov, E.V.; Nijhuis, T.A.; Hessel, V.; Schouten, J.C. Liquid- liquid slug flow: Hydrodynamics and pressure drop. *Chem. Eng. Sci.* 2011, *66*, 42.

(25) Dehmlow, E.V.; Slopianka, M.; Heider, J. Phase transfer catalysis in strongly alkaline media: notes on extractability of hydroxyl ions and on the stability of catalysts. Tetrahedron Lett. 1977, *18*, 2361.

(26) Landini, D.; Maia, A.; Montanari, F. Mechanism of phase transfer catalysis. *J. Chem. Soc. Chem. Commun.* 1977, 112.

(27) Solaro, R.; D'Antone, S.; Chiellini, E. Hetergeneous ethylation of phenylacetonitrile. *J. Org. Chem.* 1980, *45*, 4179.

(28) Sawarkar, C.S.; Juvekar, V.A. Kinetics of an interfacial reaction. Hydroxide ion catalyzed C-alkylation of phenylacetonitrile. *Ind. Eng. Chem. Res.* 1996, *35*, 2581.

(29) Albanese, D.; Landini, D.; Maia, A.; Penso, M. Key Role of Water for Nucleophilic Substitutions in Phase-Transfer-Catalyzed Processes: A Mini-Review. *Ind. Eng. Chem. Res.* 2001, *40*, 2396.

(30) Landini, D.; Maia, A.; Podda, G. Non-Hydrated Anion Transfer from the Aqueous to the Organic Phase: Enhancement of Nucleophilic Reactivity in Phase-Transfer Catalysis. *J. Org. Chem.* 1982, *47*, 2264.

(31) Landini, D.; Maia, A. Extraction of Highly Hydrophilic Anions in Low Polarity Media under Phase-Transfer Catalysis Conditions: Dramatic Enhancements of the OH- Reactivity by Reduction of its Specific Hydration. *J. Chem. Soc., Chem. Commun.* 1984, 1041.

(32) Wang, M.L.; Yang, H.M. Kinetic study of synthesizing 2,4,6-tribromophenol allyl ether by phase transfer catalytic reaction. *Ind. Eng. Chem. Res.* 1990, *29*, 522.

(33) Halpern, M.; Cohen, Y.; Sasson, Y.; Rabinovitz, M. Hydroxide ion initiated reactions under phase transfer catalysis conditions 8: notes on the interfacial mechanism. *Nouv. J. Chim.* 1984, *8*, 443.

Chapter 6. Redispersion microreactor system for phase transfer catalyzed esterification

Abstract

An interdigital mixer - redispersion capillary assembly was applied to prevent the liquid-liquid bubbly flow coalescence in microreactors. The redispersion capillary consisted of 1 mm long 0.25 mm inner-diameter constrictions, placed every 0.50 m along the channel length. The system was tested on the phase transfer catalyzed esterification to produce benzyl benzoate. The application of constrictions to prevent coalescence resulted in a reproducibility increase by a factor of 6, achieving 33.4 % conversion in 10 s, compared to the 18.8 % in a capillary without the constrictions. The bubbly flow generated by the interdigital mixer-redispersion capillary assembly was found to be independent of the redispersion capillaries inner-diameters (0.50 mm and 0.75 mm), while highly dependent on the flow rates. By controlling the total flow rate and the aqueous-to-organic ratio the bubbly flow surface-to-volume ratio could be increased up to 230700 m^2/m^3, more than 100 times higher than in conventional stirred tank reactors. The Increase of the redispersion capillary inner-diameter from 0.50 mm to 0.75 mm, allowed for the increase of the residence time to 67 s, resulting in product yield of 98 %. Compared to the conventional phase transfer catalyzed esterification, the continuous operation in the interdigital-redispersion capillary assembly, eliminated the use of solvents and bases, removing an energy intensive step of distillation, while increasing process safety.

6.1 Introduction

Microreactors today employ a wide range of mixing elements: from the simple T or Y geometries[1-4], to the more complex mixers such as the interdigital[5] and split and recombine[6] mixer. For the channel diameter from tens to hundreds of micrometers, the surface-to-volume ratio in the range of 10000 to 50000 m^2/m^3 is achieved[7]. Compared to microreactors, the maximal surface-to-volume ratios in the conventional stirred vessel are below 1000 m^2/m^3 [8, 9]. Consequently, significant intensification of mass and heat transfer can be reached, resulting in considerable reduction in operation times[10].

Phase transfer catalysis (PTC) is a chemical method employing catalysts with the ability to penetrate the interface between two immiscible phases, and transfer the immiscible reactants into the phase where the reaction takes place. The rate of a PTC reaction is most often limited by the rate of catalyst phase transfer, usually from an aqueous to an organic phase, which leads to long times needed to complete the reaction[11, 12]. PTC reactions are most commonly performed in stirred tanks where the inhomogeneous mixing often results in the loss of selectivity and product quality. The stirring of the phases in the conventional stirred tank multiphase reactor generates a wide range of drop sizes with diameters varying from tens of micrometers to millimeters, resulting in a considerable variation in interfacial surface area from one drop to another[13,14]. Consequently, different rates of reaction are obtained for different drops along with hot spot formation due to inhomogeneous mixing, resulting in a yield variation from one batch to another.

Microreactors, with the narrow drop size distribution and interfacial surface-to-volume ratios above 10000 m^2/m^3 have been shown to be an efficient tool for the intensification of PTC reactions, with successful applications in hydrolysis[15], diazo coupling[16], C-alkylation[1,17] and O-alkylation reactions[18]. The drawback of PTC microreactor applications is the small product throughput per channel (µl/min range, as shown in chapters 4 and 5), resulting in the need to scale-up via parallelization (numbering up).

In liquid-liquid microchannels, depending on the volumetric flow rates of the two immiscible liquids several flow patterns are achievable: slug, bubbly, annular and parallel flow[19]. Bubbly flow is of particular interest for mass transfer limited reactions such as the PTC reactions. In bubbly flow, the dispersed phase liquid generates bubbles from 25 µm to 60 µm in diameter[20], resulting in surface-to-volume ratios above 150000 m^2/m^3.

Bubbly flow can be achieved in a wide range of mixers from simple T or Y mixers to split and recombine and interdigital mixers. Interdigital mixers developed by the Institut für Mikrotechnik Mainz (IMM) function on the principle of multilamination whereby the stream of the two mixed fluids is split into thin lamellae, consequently generating small drops[21]. Application of the interdigital mixers in both gas-liquid[22] and liquid-liquid[23] systems resulted in highly reproducible bubbly flow, generating bubbles smaller than 60 µm in diameter. Furthermore, the principle of multilamination allows for millisecond range mixing times[24] while achieving surface-to-volume ratios above 100000 m^2/m^3. Last, they have been found to outperform the T and split and recombine mixers in mixing efficiency[25]. They have successfully been applied in extraction[26], as well as synthesis of caprolacatam[6], benzaldehyde[27] and ionic liquids[28].

One of the drawbacks of operating in the bubbly flow regime is the occurrence of coalescence[29] due to droplet collisions in the channel, resulting in decreased surface-to-volume ratio and poorer reactor performance. Bubble coalescence can occur at residence times as short as 0.12 ms[30]. The application of a channel constriction was found to be an efficient way to intensify mixing and redisperse the drops. Channel constrictions were found to increase the mixing by 90 %, and intensify internal circulations[31]. Consequently, redispersion reactor designs such as the foam microreactor have been developed in order to preserve the generated bubbly flow[32].

In this chapter a novel interdigital mixer-redispersion capillary assembly is developed aimed at preventing the coalescence in the bubbly flow. In order to achieve throughputs larger than of those described in chapters 4 and 5 while avoiding paralelization, an internal scaling up approach (via the capillary diameter increase) was chosen. The microreactor assembly was tested on a phase transfer catalyzed esterification of sodium benzoate (**1**) and benzyl bromide (**2**) into benzyl benzoate (**3**) (Scheme 1).

The target product, benzyl benzoate, is widely used as a plasticizer, food additive in artificial flavors, fixative in fragrances, solvent and insecticide. The PTC esterification is usually performed at temperatures below 85 °C[33 - 36], in the presence of sodium or potassium hydroxide in order to adjust the ionic strength and prevent the production of benzoic acid[37]. Kinetic studies of the PTC esterification in stirred batch reactors have shown that the reaction rate increases with increasing stirring speed exponentially even at stirring speeds above 1000 rpm[34,35,37]. The increase of stirring speed in batch reactors decreases the droplet size, thus increasing the specific surface-to-volume ratio[38]. The strong dependence of the reaction rate on the surface-to-volume ratio gives an indication that the reaction is mass transfer limited. Therefore, performing the PTC esterification in the bubbly flow regime in a capillary channel would significantly improve the mass transfer rate, and consequently the reaction rate.
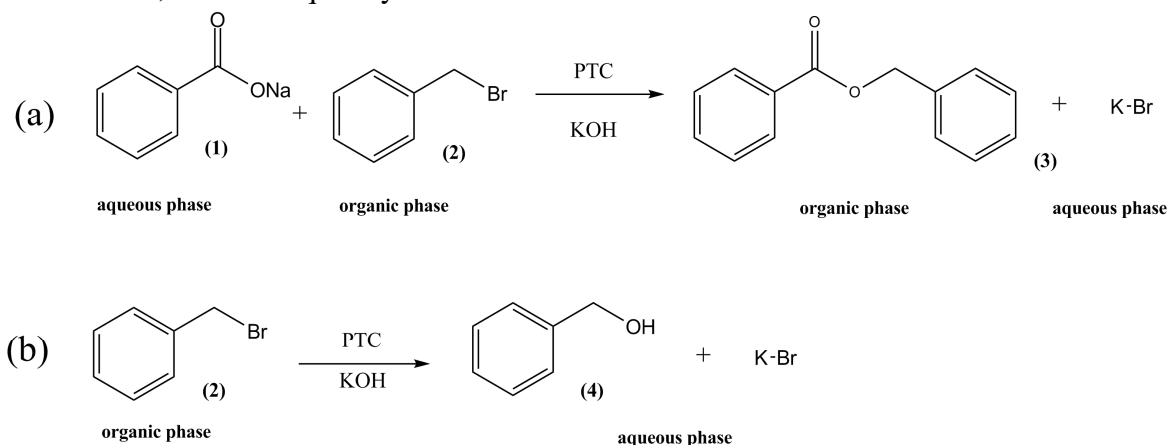
*Scheme 1: Phase transfer catalyzed esterification of sodium benzoate (**1**) with benzyl bromide (**2**) (a) and hydrolysis of benzyl bromide (**2**) into benzyl alcohol (**4**) (b).*

Last, in the PTC esterifications solvents such as toluene, benzene, chloroform, 1,2-dichloroethane[33,37] and chlorobenzene[34] are employed to suppress the side reaction of hydrolysis[33,35] into benzyl alcohol . In this study, the reaction was performed under solvent free conditions, in order to eliminate the expensive solvent removal step in the post reaction workup and with it, the environmental impact of the process. Although, benzyl

bromide has lower atom efficiency than benzyl chloride, it was used in order to demonstrate the increased safety features of the microreactor system. Benzyl bromide is a potent lachrymator agent (tear gas), with inhalation resulting in significant eye, skin and mucous membrane irritation and burns[39]. Continuous operation would significantly decrease the safety risk in the reactor filling, emptying and cleaning, as they can be easily performed via the pumps.

6.2 Experimental

Chemicals. All chemicals used in this work are commercially available and were obtained from Sigma-Aldrich. The organic phase solution consisted of benzyl bromide with the addition of decahydronaphthalene as the internal standard for the GC analysis, at a concentration of 0.92 mol/l. The aqueous phase was an aqueous solution of 5.75 wt% of potassium hydroxide, 11.2 wt% of tetra-n-butylammonium bromide (TBAB) and 27.8 wt% of sodium benzoate.

Experimental setup. A schematic view of the experimental set-up is given in Figure 1. The system consists of two HPLC pumps (Shimadzu LC-20AD) which feed the organic and aqueous phases to a stainless steel HPIMM interdigital mixer (IMM). The HPIMM mixer has an internal volume of 15 µl composed of 15 mixing channels with a cross section of 45x200 µm^2 mixing channels. The HPIMM was connected to a stainless steel redispersion capillary, with inner-diameters either of 0.50 or 0.75 mm. The length of the redispersion capillary was varied from 0.7 to 15.5 m. The constrictions with a length of 1 mm, 0.25 mm inner-diameter were placed in the redispersion capillary at every 0.50 m. The capillary outlet was connected to a transparent fused silica capillary with an internal diameter of 0.50 mm. In the experiments, the length of the redispersion capillary was varied from 0.7 to 15.5 m. The total flow rates were varied from 0.01 to 10.0 ml/min at aqueous-to-organic (AO) flow ratios of 1.0 – 9.0. Furthermore, experiments with fused silica capillary of lengths from 0.5 to 3 m at the aforementioned flow conditions were performed to observe the flow patterns without the constrictions.

Bubble size estimation. The liquid-liquid flow was visualized via a transparent fused silica capillary under a microscope (Zeiss Axiovert) and recorded by a high speed camera (Redlake MotionPro CCD) at 2500-7800 frames per second. Stable bubbly flow occurs at total flow rates above 2 ml/min, generating a large number of organic phase bubbles dispersed in the continuous phase, resulting in high diffraction of light. Consequently, the videos recorded with the high speed camera were blurred even at 7800 frames per second.

In the previous studies of liquid-liquid flows in the interdigital mixer, the analysis of the dispersions generated by the bubbly flow pattern was performed indirectly, by analyzing the samples collected at the capillary outlet [21]. Due to the significant coalescence present in the capillary, a direct method of bubble size estimation was needed. Therefore a so-called "stop flow" approach was taken, where the images were acquired immediately upon stopping the flow. It is important to note that by stopping the flow certain degree of coalescence occurred, however it did not significantly influence the bubble size

estimation. At total flow rates higher than 10 ml/min, the coalescence of the bubbles occurred immediately upon stopping the flow. Therefore a different approach was used, by injecting air over a period of 2 s without stopping the liquid flow. The air was injected by opening the purge valve on the HPLC pump while it is pumping the liquid, thus allowing for the suction of air into the liquid line. With the injection of air, annular flow was achieved where the dispersed bubbles were trapped between the wall and the gas annulus, thus allowing for visualization and bubble diameter estimation for the measurements at 12 ml/min. The estimation of the bubble diameters and the interfacial surface areas was performed via image analysis using the Matlab^{TM} software.

Analysis. The organic phase was quantitatively analyzed using a Varian CP-3800 gas chromatograph equipped with a 30 m x 0.25 mm CP-Sil 5 CB column and a FID detector.
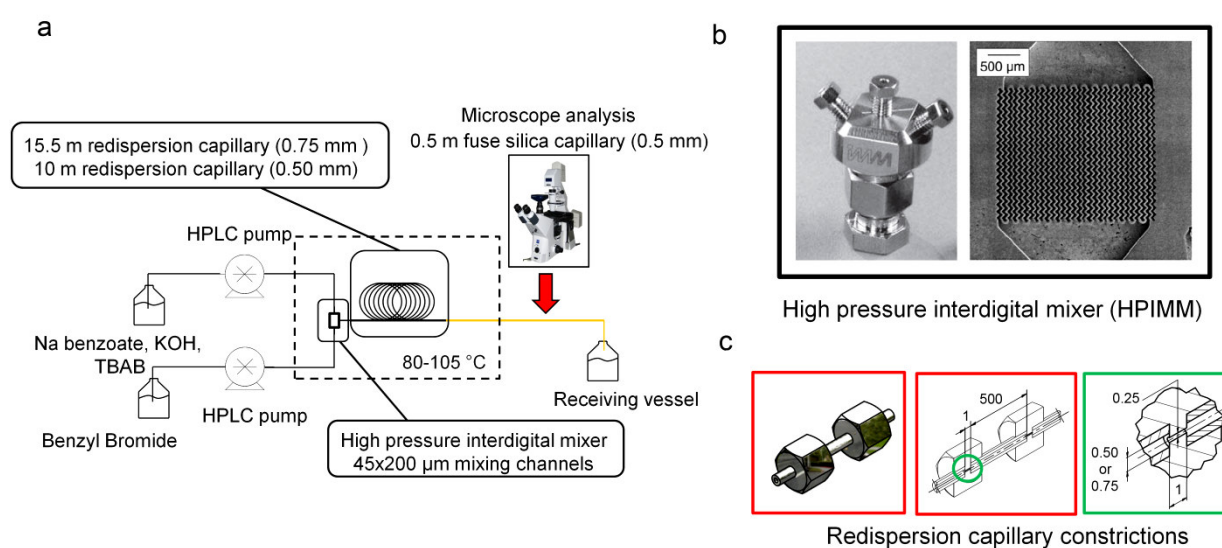
Figure 1: Experimental setup (a): Stainless steel high pressure interdigital mixer (HPIMM) (b) coupled with a 0.50 mm or 0.75 mm internal-diameter redispersion capillary. The redispersion capillary (c) consisted of 1 mm long 0.25 mm inner-diameter constrictions spaced 500 mm apart. The microscope observations were performed via the transparent fused silica capillary connected to the outlet of the redispersion capillary. Supply of the organic and aqueous mixtures was provided by two HPLC pumps (Shimadzu LC-20AD).

6.3 Results and Discussion

Image analysis in the 0.50 mm inner-diameter fuse silica capillary coupled to the interdigital mixer showed that significant bubble coalescence occurred after a length of ca. 1 m, at total flow as low as 2 ml/min, with bubbly flow coalescing into slug flow (Figures 2 a and b). With increasing flow rates the probability of bubble collision resulting in the coalescence increases[39], consequently at total flow rates above 3 ml/min the coalescence into larger slugs was observed already at 0.5 m of capillary length.

In order to study the performance of the redispersion capillary, image analysis at capillary lengths of 0.7, 10.2 and 15.2 m were performed. At a total flow rate of 6 ml/min and AO ratios of 1 and 5 the difference between mean bubble diameters was less than 10% for both the 0.50 mm and 0.75 mm inner-diameter capillary. Therefore, the redispersion capillary was deemed efficient for the prevention of the bubble coalescence (Figures 2 c and d).

6.3.1 Hydrodynamics

The flow patterns achievable in the interdigital mixer-redispersion capillary assembly were studied at flow rates from 0.01 to 10.0 ml/min in the capillary of 0.50 mm diameter. At flow rates lower than 1 ml/min, the flow patterns were observed at flow rate increments of 0.1 ml/min, while at flow rates higher than 1 ml/min, the increment was 0.5 ml/min. Four flow patterns were identified: slug, bubbly/slug, bubbly and bubbly/annular (Figure 3). By increasing the diameter of the redispersion capillary from 0.50 mm to 0.75 mm, no significant change in the flow pattern map was observed, indicating that the flow patterns are mainly determined by the interdigital mixer and the hydraulic resistance of the constrictions. Slug and bubbly flow were stable flows characterized by reproducible slug and bubble sizes. The bubbly/slug and bubbly/annular flows were characterized by succession of stable bubbly flow followed by intermittent annular or slug flow. The slug/bubbly flow pattern occurs as a transition flow pattern from the stable slug to bubbly flow. The bubbly/annular flow pattern is characterized by the occurrence of unstable liquid jets followed by bubbly flow. The bubbly/annular flow pattern was observed at two sets of conditions: at organic flow rates higher than 2 ml/min and AO ratios lower 0.02 and at organic and aqueous flow rates higher than 4 ml/min and approximately equal AO ratios (Figure 3).
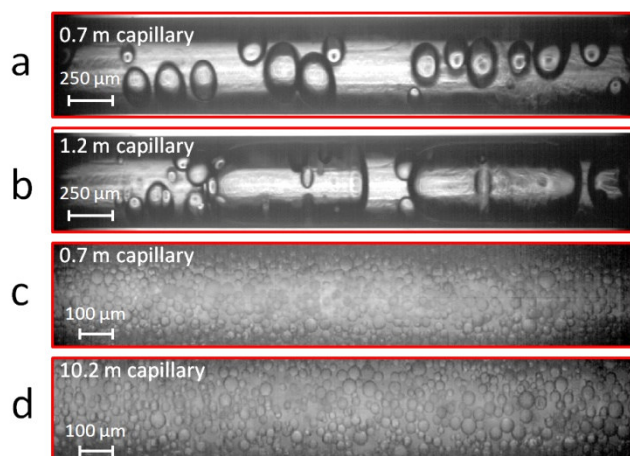

Figure 2: Bubble coalescence at 0.7 m (a) and 1.2 m (b) length in the 0.5 mm inner-diameter capillary at a total flow rate of 2 ml/min and the aqueous-to-organic (AO) ratio of 5. Preservation of the bubbly flow with the application of 0.7 m (c) and 10.2m (d) length of the 0.50 mm inner-diameter redispersion capillary at a total flow rate of 6 ml/min the AO ratio of 5.
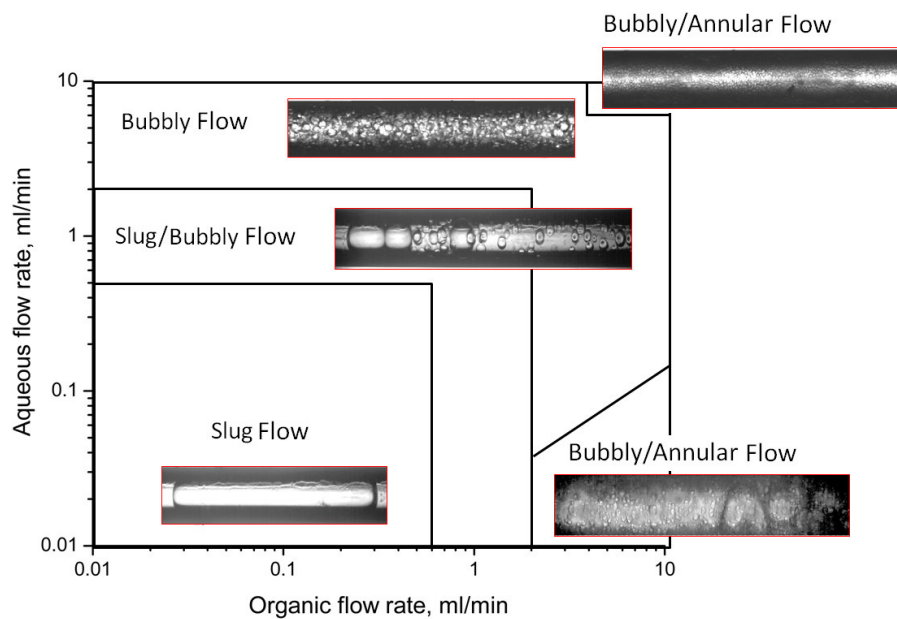
Figure 3: Flow pattern map for the 0.50 mm inner-diameter redispersion capillary with 2 stable (slug and bubbly) and 2 intermittent flow patterns (slug/bubbly and bubbly/annular).

The slug flow occurs at aqueous flow rates lower than 0.5 ml/min and organic flow rates lower than 0.6 ml/min, for both the 0.50 and 0.75 mm diameter capillaries. According to the IMM interdigital mixer specifications, flow rates higher than 0.80 ml/min should be used for its optimal performance. Therefore, it can be concluded that slug flow, a surface tension[2,15] dominated flow pattern, is occurring at flow conditions below the mixer efficiency range. The transition from the slug/bubbly flow to bubbly flow occurs at approximately the same aqueous and organic flow rates for both the 0.50 and 0.75 mm capillary, indicating that the flow pattern is determined by the mixer rather than the capillary. The bubbly flow pattern, which is the targeted flow pattern for this study, occurs at aqueous and organic flow rates higher than 2 ml/min (Figure 3). A comparison of the slug, slug/bubbly and bubbly flow patterns in terms of surface-to-volume ratios is shown in Table 1. By increasing the total flow rate from 0.1 to 6 ml/min, at an equal AO ratios, the transition from slug to bubbly flow occurs, resulting in a 43 times higher surface-to-volume ratio (Table 1). Furthermore, by increasing the total flow rate from 6 ml/min to 12 ml/min, the mean bubble diameter decreases by 59 % from 63 µm to 26 µm, consequently increasing the surface-to-volume ratio by approximately 2.4 times, from 95200 to 230700 m^2/m^3.

Varying the AO ratio in order to decrease the dispersed phase slug lengths and bubble diameters was found to be an effective method to increase surface-to-volume ratio[2,40]. By increasing the AO ratio from 1 to 6, the mean bubble diameter decreases by 57 %, from 63 to 27 µm (Figure 4). Consequently, the mean bubble surface-to-volume ratio increased approximately 2.3 times, from 95200 to 222200 m^2/m^3. The surface-to-volume ratios achieved in the bubbly flow regime are more than 100 times higher than the ones achieved in conventional stirred reactors (1000 m^2/m^3), therefore allowing for significant process intensification of mass transfer limited systems.
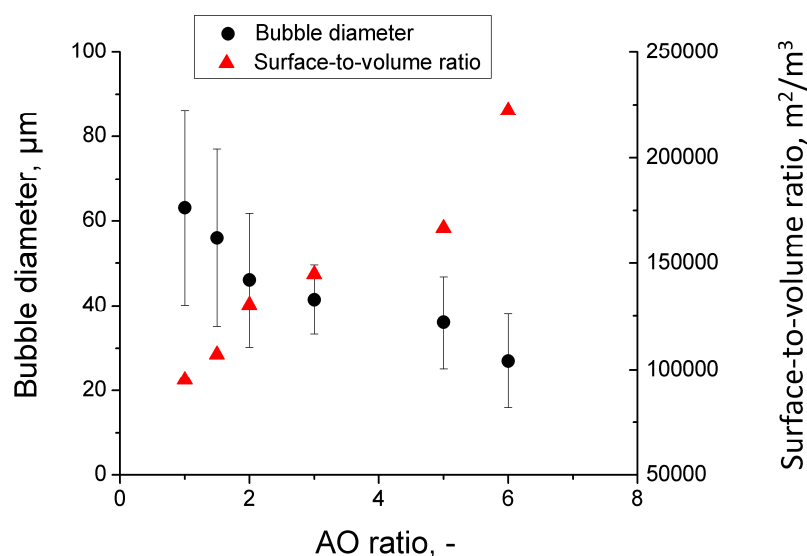
Figure 4: Bubble diameters and the estimated surface-to-volume ratios as a function of the aqueous-to-organic (AO) ratio at a total flow rate of 6 ml/min in a 0.50 mm inner-diameter redispersion capillary.

Table 1: Comparison of the slug, slug/bubbly and bubbly flow patterns

Total flow rate, ml/min	AO ratio, -	Flow pattern	Slug/bubble size, μm	Surface-to-volume ratio, m^2/m^3
0.1	1	Slug	1990	2200
1	1	Slug/bubbly	50-200	29000
6	1	Bubbly	63	95200
12	1	Bubbly	26	230700

6.3.2 PTC esterification

The performance of the interdigital mixer-redispersion capillary assembly was studied on a model reaction of PTC esterification of sodium benzoate (**1**) to benzyl benzoate (**3**) (Scheme 1). The reaction system consisted of two phases: an organic phase containing benzyl bromide (**2**) with the internal standard (decahydronaphthalene) and an aqueous phase containing sodium benzoate (**1**), potassium hydroxide and the phase-transfer catalyst (Tetra-n-butylammonium bromide, TBAB). Previous studies have shown that by increasing the concentration of TBAB, which acts as a mass transfer agent, the production of the benzyl alcohol (**4**) can be suppressed[33], thus increasing the selectivity. Therefore, all experiments were performed at the maximal TBAB solubility of 11.2 wt%.

The benzyl bromide conversion in the PTC esterification is highly dependent on the stirring speed, and therefore the bubble surface-to-volume ratio[34,35,37,38]. The coalescence of droplets in the bubbly flow results in the intermittent slug/bubbly flow pattern, reducing the surface-to-volume ratio (Table 1). Therefore, the coalescence in the capillary is expected to reduce the bubbly flow pattern reproducibility and decrease the conversion of benzyl bromide. The effect of the redispersion was studied by comparing the performance

of a 10 m long capillary with a diameter of 0.50 mm with redispersion constrictions and an empty capillary of the same length and diameter. The benzyl bromide conversion and conversion measurement reproducibility were studied at equal AO flow ratios and total flow rates ranging from 0.1 to 12 ml/min, corresponding to capillary residence times from 20 min to 10 s (Figure 5).
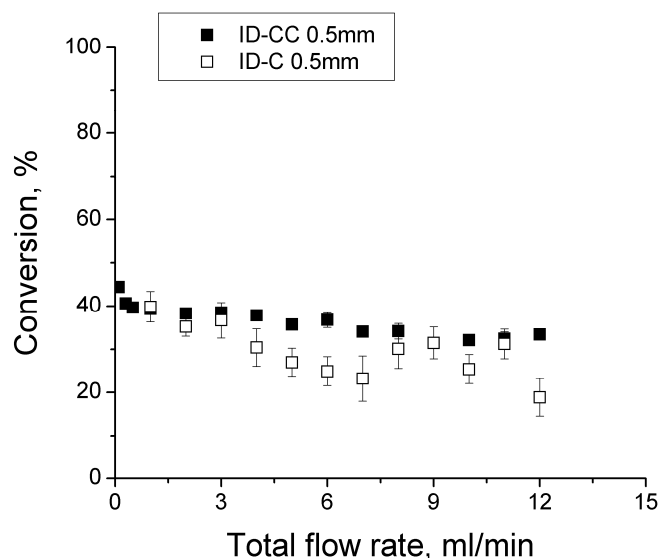

Figure 5: Comparison of the benzyl bromide conversion in the interdigital mixer coupled with a 0.50 mm inner-diameter capillary with (ID-CC) and without constrictions (ID-C) at total flow rates from 0.1 to 12 ml/min and an aqueous-to-organic (AO) ratio of 1.

In the empty capillary at total flow rates higher than 3 ml/min, the intermittent nature of the slug/bubbly flow resulted in decreased reproducibility and conversion as compared to the redispersion capillary (Figure 5). The mean standard deviation of the conversion measurements for the empty capillary was 13.6 %. In the redispersion capillary the use of redispersion capillaries prevented the coalescence of drops thus increasing the reproducibility to a mean standard deviation of 2.3 %. Furthermore, by increasing the flow rate from 0.1 to 12 ml/min, the surface-to-volume ratio of flow patterns generated by the interdigital mixer increases by a factor of 100 (Table 1), thus allowing for relatively constant conversions in the range of 33.4-40 % at residence times as low as 10 s (Figure 5). Due to the coalescence in the empty capillary, the conversion decreased with increasing flow rates. It is interesting to note that a slight increase in conversion was observed at flow rates higher than 7 ml/min, possibly due to redispersion caused by increased inertia of the flow. Last, at flow rates higher than 3 ml/min, the average conversion in the redispersion capillary was approximately 28 % higher than in the capillary without the constrictions.

Image analysis (Figure 2) and reaction studies (Figure 5) comparing the capillary with and without the constriction, clearly show that the redispersion capillary was effective in preventing the coalescence, thus yielding higher performance and bubbly flow reporducibility.

6.3.3 Microprocess optimization and scale-up

Previous liquid-liquid microreactor studies showed that the influence of the AO ratio, and consequently the surface-to-volume ratio, has much greater influence on the reaction than the residence time[29,40,41]. Consequently, the methodology of fluidic control, where the ratios of the aqueous and organic flow rates (i.e. AO ratios) are used to control the reaction rate, was found to be effective in reducing the time needed for achieving full conversion[2]. The influence of the AO ratio at total flow rates of 6 ml/min and 12 ml/min on the conversion and yield is shown in Figure 6. At a total flow of 6 ml/min, by increasing the AO ratio from 1 to 6, the conversion increased from 38 % to 95 %, representing a 2.5-fold increase at a constant residence time of 20 s. Furthermore, the surface-to-volume ratio increases 2.3 times, from 95 000 to 222 200 m^2/m^3 (Figure 4). Consequently, the rate of the interfacial hydrolysis of benzyl bromide to benzyl alcohol increases, decreasing the product yield at AO ratios higher than 3.5 (Figure 6). With the increase of the total flow rate from 6 to 12 ml/min, the decrease in residence time is balanced by the increasing surface area (Table 1), thus allowing for approximately the same conversions and yield.
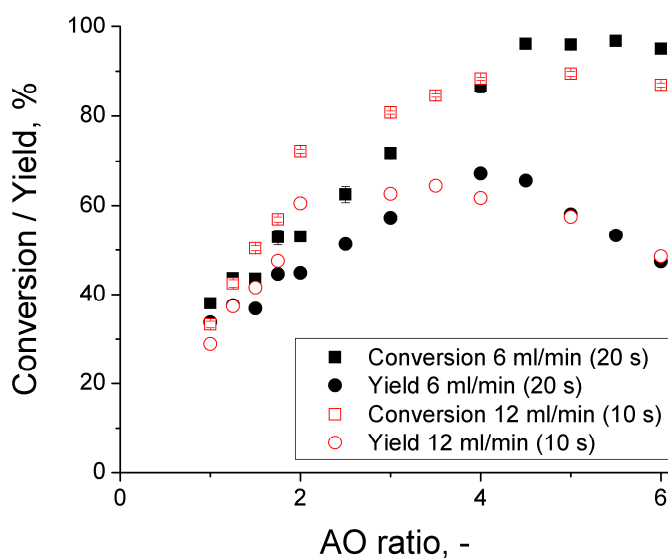

Figure 6: Conversion of benzyl bromide and benzyl benzoate yield in a 0.50 mm inner-diameter redispersion capillary at aqueous-to-organic (AO) ratios from 1 to 6, at total flow rates of 6 ml/min and 12 ml/min, corresponding to 20 s and 10 s residence times, respectively.

In order to optimize the benzyl benzoate yield, the effects of the temperature and the hydroxide ions on the reaction system at AO ratios from 1 to 6 were studied in the 10 m long, 0.50 mm diameter redispersion capillary. By decreasing the temperature from 105 °C to 80 °C both conversion and yield decrease (Figure 7 a). This indicates that the side reaction of base catalyzed hydrolysis of benzyl bromide to benzyl alcohol occurs at a higher rate relative to the esterification reaction, thus lowering the selectivity to the benzyl

benzoate product (Figure 8). Therefore, in order to increase the yield, the rate of the hydrolysis has to be decreased.
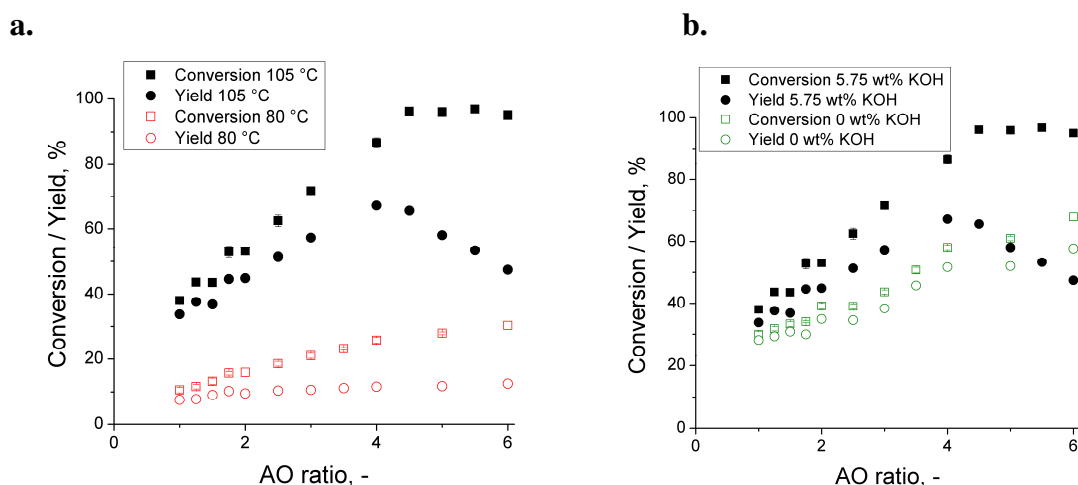
a.

b.

Figure 7: Influence of temperature (a) and presence of KOH (b) on the conversion of benzyl bromide and on the benzyl benzoate yield at aqueous-to-organic (AO) ratios from 1 to 6 in a 0.50 mm inner-diameter redispersion capillary.

The reaction is performed at a high pH to deprotonate the sodium benzoate so it can be transferred by the phase transfer catalyst into the organic medium. Furthermore, the presence of a base is often required to affect the catalyst-benzoate complex equilibrium between the organic and aqueous phases, lowering the solubility of the complex in the aqueous phase. The drawback of this approach is the intensification of the base catalyzed hydrolysis of benzyl bromide into benzyl hydroxide which occurs at the interface between the two phases, consequently lowering the selectivity of the reaction system. Wang et al. (1990) showed that under PTC conditions the rate of the benzyl halide hydrolysis is proportional to the OH$^-$ concentration[42]. In the absence of the base, the conversion was found to decrease (Figure 7 b), while the selectivity remained relatively constant at different AO ratios (Figure 8). The constant selectivity and increasing conversion at increasing surface to volume ratio (increasing AO ratio), indicate that the rate of the hydrolysis decreased compared to the rate of the esterification. The removal of the hydroxide decreased the conversion by approximately 32 %, while increasing the selectivity to benzyl benzoate by approximately 19 %. Furthermore, the negative impact of the increasing surface-to-volume ratio with increasing AO ratio (Figure 7 b and Figure 8) was eliminated.
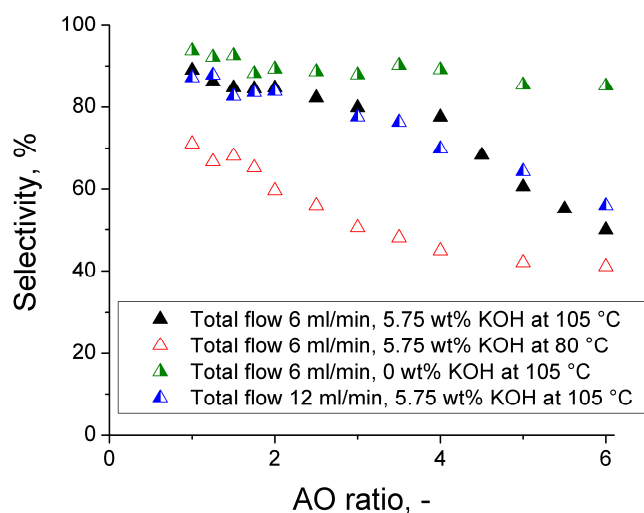
Figure 8: Influence of temperature, presence of KOH and total flow rate on the selectivity to benzyl benzoate at aqueous-to-organic (AO) ratios from 1 to 6 in a 0.50 mm inner-diameter redispersion capillary.

Finally, in order to reach a full conversion a higher residence time was provided by increasing the capillary inner-diameter from 0.50 to 0.75 mm and the redispersion capillary length from 10 to 15.5 m. In the 0.75 mm diameter redispersion capillary, by increasing the AO ratio from 1 to 4 the conversion increased from 34 to 97 % (Figure 9). The selectivity in the 0.50 and 0.75 mm diameter redispersion capillaries remained approximately the same, with an average value of 91 % for all observed AO ratios. Further process optimization showed that the conversion can be increased to above 99 %, with selectivity of 98.7 %, allowing for a benzyl bromide yield of approximately 98 %. Consequently, a product throughput of 79.5 g/h for the single capillary was achieved. The maximal achieved throughput of the microreactor system was 720 g/h.
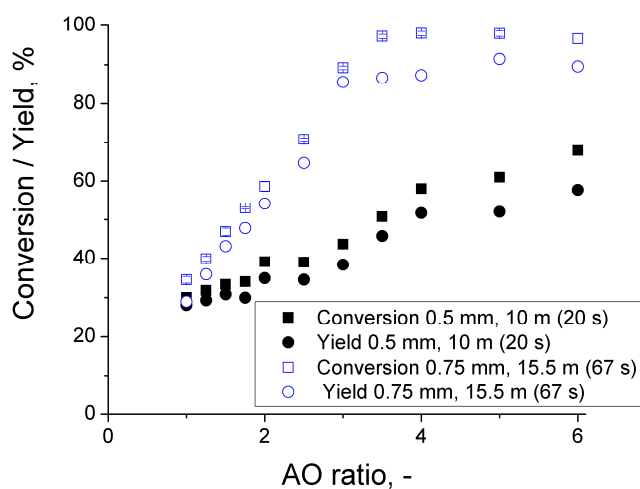

Figure 9: Conversion of benzyl bromide and benzyl benzoate yield at aqueous-to-organic (AO) ratios from 1 to 6, for the 0.50 mm and 0.75 mm inner-diameter redispersion capillary.

6.3.4 Process benchmarking: switching from batch to continuous

A comparison between the traditional esterification, conventional PTC and microprocess PTC esterification process in terms of yield, reaction time, process conditions and post reaction workup is shown in Table 2. Traditionally the production of benzyl benzoate is performed via the sodium benzoxide process, which requires the use of hazardous metallic sodium[43]. Furthermore, the process had to be performed below 60 °C, while the product yield differs from 10 to 90 % due to the formation of hot spots. The introduction of the PTC esterification, significantly improved the safety of the process by replacing the metallic sodium with bases such as sodium or potassium hydroxide. Furthermore, the selectivity of the process improved by removing the side products such as dibenzyl ether[43]. The conventional PTC process introduced the use of solvents such as toluene, benzene, chloroform, 1,2-dichloroethane[33,37] and chlorobenzene[34], which added an energy intensive solvent removal step via distillation. Furthermore, the PTC esterification is highly dependent on the stirring, where inhomogeneous stirring can result in yield variation. The conventional PTC process allowed for approximate same benzyl benzoate yield as in the traditional process, while increasing process safety and reducing the reaction times, from 5 to 3 h.

Table 2: Comparison of the traditional, the conventional PTC and microprocess PTC benzyl benzoate production process.

Process characteristics	Conventional	Conventional PTC	Microprocess PTC
Yield, %	10-90	90	98
Reaction time	5 h	3 h	67 s
Temperature	60 °C	<85 °C	105 °C
Base	PhCH$_2$ONa (metallic Na)	NaOH, KOH	none
Solvent	benzyl alcohol	Toluene, benzene, chloroform, 1,2-dichloroethane, chlorobenzene	none
Post reaction workup	Washing + distillation	Washing + distillation	Washing

By switching from the batch to the continuous process, significant improvement in process safety is achieved as the reactor fill/empty/cleanup process steps are eliminated, and with them the exposure to dangerous chemicals. All fluid handling is performed via pumps. The application of microreactors therefore allows for "novel process windows"[44,45], where reactions can be performed at higher temperatures than in the conventional processes. Consequently, the PTC esterification was performed at 105 °C, which is 30 °C higher than in the conventional PTC process (Table 2). The use of solvents and hydroxides was eliminated, significantly reducing the environmental impact of the process. Furthermore, by excluding the solvent recovery/distillation step, the process is significantly simplified requiring only a post reaction washing with water to remove the catalyst (TBAB) traces. Last, the intensification of mass transfer achieved in the bubbly flow, allowed for 99 %

reduction in reaction times, to approximately 1 min, while achieving throughputs of 79.5 g/h.

6.4 Conclusions

In this work the application of the interdigital mixer-redispersion capillary assembly for the prevention of the bubbly flow coalescence in microreactors was studied. The redispersion capillary consisted of 1 mm long 0.25 mm inner-diameter constrictions, spaced 0.50 m apart. The bubbly flow generated by the interdigital mixer-redispersion capillary assembly was found to be independent of the redispersion capillaries inner-diameters (0.50 mm and 0.75 mm), and highly dependent on the flow rates of the aqueous and organic phases. By increasing the total flow rate from 0.1 ml/min to 12 ml/min, the flow patterns transformed from slug to bubbly flow, yielding a 43 times increase in the surface-to-volume ratio, from 2200 to 230700 m^2/m^3. Furthermore, by controlling the aqueous-to-organic (AO) ratio the bubbly flow surface-to-volume ratio could be increased 2.3 times, from 95 200 to 222200 m^2/m^3, achieving surface-to-volume ratios more than 100 times higher than in conventional stirred tank reactors. The performance of the 0.50 mm inner-diameter redispersion capillary was compared to a capillary without constrictions on an example of phase transfer catalyzed esterification of benzyl bromide to benzyl benzoate. By applying constrictions to prevent coalescence the reproducibility increased by a factor of 6, achieving 33.4 % conversion in 10 s, compared to the 18.8 % in the capillary without the constrictions.

The fluidic control of the surface-to-volume ratio via the AO ratio, allowed for a 2.5-fold increase in conversion from 38 % to 95 %, at a residence time of 20 s. The increase of the surface-to-volume ratio, promoted the increase of the hydrolysis of benzyl bromide into benzyl alcohol, thus reducing the selectivity to below 70 %. By removing the hydroxide ions from the system, the side reaction of hydrolysis was suppressed, allowing for approximately constant selectivity of 91 %. By increasing the inner-diameter of the redispersion capillary from 0.50 mm to 0.75 mm, allowed the increase of the residence time to 67 s, resulting in a conversion of 97 %. Compared to the conventional PTC esterification, the continuous operation in the interdigital-redispersion capillary assembly eliminated the use of solvents and bases, removing the energy intensive step of distillation. Furthermore, the use of sub millimeter capillaries allowed for higher safety of operation, as the filling/emptying/cleaning steps were eliminated, thus reducing the exposure to the hazardous reactants.

References

(1)   Jovanović, J.; Rebrov, E.V.; Nijhuis, T. A.; Hessel, V.; Schouten, J.C. Phase-Transfer Catalysis in Segmented Flow in a Microchannel: Fluidic Control of Selectivity and Productivity. *Ind. Eng. Chem. Res.* 2010, *49*, 2681.

(2)   Dummann, G.; Quittmann, U.; Groschel, L.; Agar, D. W.; Worz, O.; Morgenschweis, K. The capillary-microreactor: a new reactor concept for the intensification of heat and mass transfer in liquid-liquid reactions. *Catal. Today* 2003, *79*, 433.

(3)   Nielsen, C.A.; Chrisman, R.W.; LaPointe, R.E.; Miller, T.E. Novel Tubing Microreactor for Monitoring Chemical Reactions.*Anal. Chem.* 2002, *74,* 3112.

(4)   Burns, J. R.; Ramshaw, C. The intensification of rapid reactions in multiphase systems using slug flow in capillaries. *Lab Chip* 2001, *1*, 10.

(5)   Hessel, V.; Hardt, S.; Löwe, H.; Schönfeld, F. Laminar mixing in different interdigital micromixers: I. Experimental characterization. *AIChE J.* 2003, *49*, 566.

(6)   Zuidhof, K.T.; de Croon, M.H.J.M.; Schouten, J.C.; Beckmann rearrangement of cyclohexanone oxime to ε-caprolactam in microreactors. *AIChE J.* 2010, *56*, 1297.

(7)   Hessel, V.; Hardt, S.; Löwe, H.*Chemical Micro-process Engineering – Fundamentals, Modeling and Reactions*, Wiley-VCH, Weinheim, 2004.

(8)   Ruiz, M.C.; Lermanda, P.; Padilla, R. *Hydrometallurgy* 2002, *63*, 65.

(9)   Perry, R. H.; Green, D. W. *Perry's Chemical Engineers Handbook*, 7th ed., McGraw-Hill, New York, 1997.

(10) Lomel, S.; Falk, L.; Commenge, J. M.; Houzelot, J. L.; Ramdani, K. The microreactor. A systematic and efficient tool for the transition from batch to continuous process? *Chem. Eng. Res. Des.* 2006, *84*, 363.

(11) Starks, C.; Liotta, C.; Halpern, M. *Phase-Transfer Catalysis: Fundamentals, Applications and Industrial Perspectives*, Chapman & Hall, London, 1994.

(12) Yadav, G. D.; Jadhav, Y. B. Kinetics and modeling of liquid–liquid phase transfer catalysed synthesis of p-chlorophenyl acetonitrile: Role of co-catalyst in intensification of rates and selectivity. *J. Mol. Catal.* 2003, *192,* 41.

(13) Pacek, A. W.; Chasart, S.; Nienow, A. W.; Bakker, A. The influence of impeller type on mean drop size and drop size distribution in an agitated vessel. *Chem. Eng. Sci.* 1999, *54*, 4211.

(14) Zhou, G.; Kresta, S. M. Evolution of drop size distribution in liquid–liquid dispersions for various impellers. *Chem. Eng. Sci.* 1998, *53*, 2099.

(15) Ahmed-Omer, B.; Barrow, D.; Wirth, T. Effect of segmented fluid flow, sonication and phase transfer catalysis on biphasic reactions in capillary microreactors. *Chem. Eng. J.* 2008, *135S*, S280.

(16) Hisamoto, H.; Saito, T.; Tokeshi, M.; Hibara, A.; Kitamori, T. Fast and high conversion phase-transfer synthesis exploiting the liquid–liquid interface formed in a microchannel chip. *Chem. Commun.* 2001, *24*, 2662.

(17) Okamoto, H. Effect of Alternating Pumping of Two Reactants into a Microchannel on a Phase Transfer Reaction. *Chem. Eng. Technol.* 2006, *29*, 504.

(18) Wurziger, H.; Pieper, G.; Schmelz, M.; Schwesinger, N. Use of a Microreaction Channel with a Piezo Element. *Patent WO0249737A1*, 2002.

(19) Zhao, Y.; Chen, G.; Yuan, Q. Liquid-Liquid Two-Phase Flow Patterns in a Rectangular Microchannel. *AIChE J.* 2006, *52*, 4052.

(20) Haverkamp, V.; Ehrfeld, W.; Gebauer, K.; Hessel, V.; Löwe, H.; Richter, T.; Wille, C. The potential of micromixers for contacting disperse liquid phases. *Fresenius J. Anal. Chem.* 1999, *364*, 617.

(21) Hessel, V.; Hardt, S.; Löwe, H.; Schönfeld, F. Laminar mixing in different interdigital micromixers: I. Experimental characterization. *AIChE J.* 2003, *49*, 566.

(22) Löb, P.; Pennemann, H.; Hessel, V. g/l-dispersion in interdigital micromixers with different mixing chamber geometries. *Chem. Eng. J.* 2004, *101*, 75.

(23) Löb, P.; Pennemann, H.; Hessel, V.; Men, Y. Steering of liquid mixing speed in interdigital micro mixers-from very fast to deliberately slow mixing. *Chem. Eng. Sci.* 2006, *61*, 2959.

(24) Löb, P.; Drese, K.S.; Hessel, V.; Hardt, S.; Hofmann, C.; Löwe, H.; Schenk, R. Steering of liquid mixing speed in interdigital micro mixers-from very fast to deliberately slow mixing. *Chem. Eng. Technol.* 2004, *27*, 340.

(25) Panic, S.; Loebbecke, S.; Tuercke, T.; Antes, J.; Boskovic, D. Experimental approaches to a better understanding of mixing performance of microfluidic devices. *Chem. Eng. J.* 2004, *10*, 409.

(26) Benz, K.; Jäckel, K.P.; Regenauer, K.J.; Schiewe, J.; Drese, K.; Ehrfeld, W.; Hessel, V.; Löwe, H. Utilization of Micromixers for Extraction Processes. *Chem. Eng. Technol.* 2001, *24*, 11.

(27) Pennemann, H.; Hardt, S.; Hessel, V.; Löb, P.; Weise, F. Micromixer based liquid/liquid dispersion. *Chem. Eng. Technol.* 2005, *28*, 501.

(28) Wilms, D.; Klos, J.; Kilbinger, F.M.; Löwe, H. Ionic Liquids on demand in continuous flow. Org. Process Res. Dev. 2009, *13*, 961.

(29) Okubo, Y.; Toma, M.; Ueda, H.; Maki, T.; Mae, K. Microchannel devices for the coalescence of dispersed droplets produced for use in rapid extraction processes. *Chem. Eng. J.* 2004, *101*, 39.

(30) Lee, J.; Kwon, S. Mixing efficiency of a multilamination micromixer with consecutive recirculation zones *Chem. Eng. Sci.* 2009, *64*, 1223.

(31) Rothstock, S.; Hessel, V.; Löb P.; Werner, B. Characterization of a Redispersion Microreactor by Studying its Dispersion Performance. *Chem. Eng. Technol.* 2008, *31*, 1124.

(32) Chang, J.; Yeh, M.Y. Kinetics of phase transfer catalytic preparation of benzyl benzoate. *J.Chin.Chem.Soc.* 1984, *31*, 185.

(33) Yang, H.M.; Lin, C.L. Phase-transfer catalyzed benzylation of sodium benzoate using aliquat 336 as catalyst in liquid-liquid system. *J. Mol. Catal. A: Chem.* 2003, *206*, 67.

(34) Lee, Y.S.; Yeh, M.Y.; Shih, Y.P. Phase-Transfer Catalytic Kinetics of the Synthesis of Phenyl Benzoate. *Ind. Eng. Chem. Res.* 1995, *34*, 1572.

(35) Hwu, D.H.; C. Hwang, M.Y. Yeh, H.M. Jung, Kinetics of the phase-transfer synthesis of benzyl esters using tertiary amines. *Ind. Eng. Chem. Res.* 1990, *29*, 2214.

(36) Asai, S.; Nakamura, H.; Tanabe, M.; Sakamoto, K. Synthesis of triphenyl phosphate and benzyl benzoate with phase-transfer catalyst in heterogeneous liquid-liquid reaction system. *Ind. Eng. Chem. Res.* 1994, *33*, 1687.

(37) Molag, M.; Joosten, G.E.H.; Drinkenburg, A.A.H. Droplet Breakup and Distribution in Stirred Immiscible Two-Liquid Systems. *Ind. Eng. Chem. Fundam.* 1980, 19 (3), 275-281.

(38) Lewis, R.J. Sax's Dangerous Properties of Industrial Materials. 9th ed. Volumes 1-3. Van Nostrand Reinhold , New York, 1996.

(39) Jovanović, J.; Zhou, W.; Rebrov, E.V.; Nijhuis, T.A.; Hessel, V.; Schouten, J.C. *Chem. Eng. Sci.* 2010, *66*, 42.

(40) Aljbour, S.; Yamada, H.; Tagawa, T.*Chem. Eng. Process.* 2009, *48*, 1167.

(41) Wang, T.T.; Huang, T.C. Benzyl ether form phase transfer catalyzed strongly alkaline hydrolysis of benzyl chloride. *J. Mol. Catal.* 1990, *57*, 271.

(42) Kamm O.; Kamm, W. F. Benzyl benzoate. Org. Syn., 1941, *1*,104

(43) Illg, T.; Lob, P.; Hessel, V. Flow chemistry using milli- and microstructured reactors- from conventional to novel process windows.*Bioorg. Med. Chem.* 2010, *18*, 3707.

(44) Hessel, V. Novel Process Windows - Gates to Maximizing Process Intensification via Flow Chemistry. Chem. Eng. Technol. 2009, *32*, 1655.

Chapter 7. Conclusions

7.1 Optimal flow patterns for microreactor design

The research carried out within this thesis focuses on the hydrodynamics, reaction applications and scale-up of liquid-liquid microreactors. One of the most important parameters in the multiphase reactor design is the choice of the hydrodynamic regime. Therefore, first the liquid-liquid hydrodynamics in microchannels has to be understood. Depending on the flow rates of the two phases, four stable liquid-liquid flow patterns can be distinguished in the microchannels: the slug, bubbly, parallel and annular flow pattern. The formation of the flow patterns was found to be determined mainly by the surface tension and inertia forces as described in chapter 2. The slug flow is fully dominated by surface tension, therefore achieving excellent reproducibility and allowing for high degree of control over the slug sizes. Bubbly flow is dominated by inertial force, whereby two streams of liquids are broken up to form droplets several times smaller than the microchannel diameter. In the parallel and annular flow, the inertial and surface tension forces are competing with each other, which often lead to flow instabilities and disruption of the interface. In annular flow the stability of the flow increased with increasing inertial force. Consequently, the parallel and annular flow were found to be stable in a narrow window of operation, determined by the channel length and flow rates, thus making their application limited in industrial environment. It is important to note that the choice of the microchannel material will affect the hydrodynamics of the system, particularly the slug flow. Depending on the polarity of the microchannel walls, the continuous phase will be the organic (in non polar, PTFE and PEEK channels) or aqueous phase (in polar, stainless steel and fused silica channels). The greatest influence of the microchannel wall polarity is seen on the slug flow pattern, where it influences the formation of the thin continuous phase film between the dispersed slug and the channel wall. The formation of the thin film was observed only in the case of polar walls, while in the case of non polar walls no observable film was noticed even at 100 x magnification.

The performance of the flow patterns in terms of interfacial areas and extraction application was studied on the example of 2-butanol extraction in a single microchannel. Slug and bubbly flow were found to be the best performing flow patterns, as both flow patterns exhibited a high degree of stability and could achieve surface areas above 10000 m^2/m^3 . Furthermore, it was possible to adjust the interfacial surface-to-volume ratios in both flow patterns by controlling the flow rates. The slug flow operates in the µl/min range and therefore it is suitable for high value, low volume chemical production and kinetic studies. Higher throughputs of microreactors operating in slug flow can be

achieved with scale-up via parallelization. The scale-up of multiphase reactors by numbering up of channels can bring about higher costs due to the scale-up factor of 1, as well as bottlenecks caused by maldistribution of the slug flow in the parallel microchannels. An alternative to the slug flow for high throughput operation is the bubbly flow, as stable bubbly flow can be achieved at ml/min to l/min throughputs in a single microchannel.
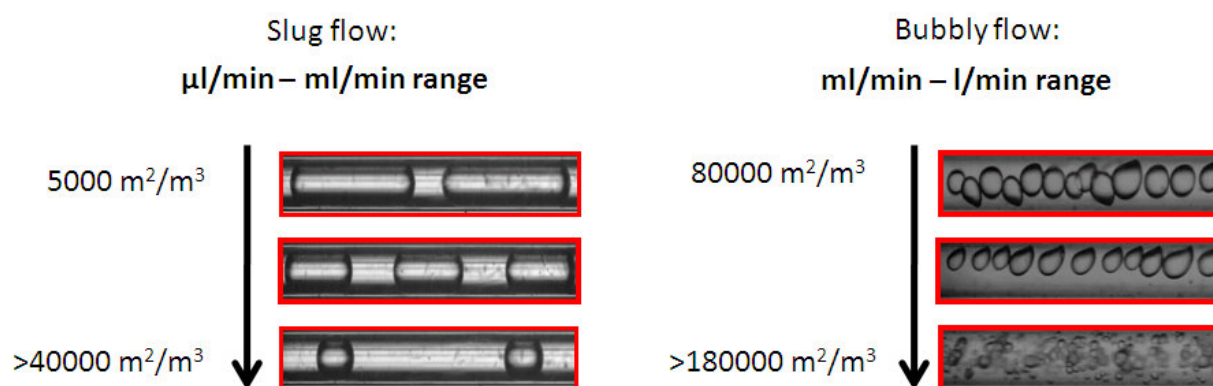

Figure 1: Slug and bubbly flow allow for control of interface surface-to-volume ratios via flow rate manipulation.

7.2 Slug flow microreactor design parameters: slug length and pressure drop

Stable slug flow can be achieved by employing various types of mixers: X, T or Y mixers. It is the author's opinion that the Y mixers represent the best choice, as the risk of back flow and consequent fouling is greatly reduced due to the Y geometry. When designing a slug flow reactor two important parameters must be observed –the slug length and the pressure drop. Slug length will determine the surface-to-volume ratio in the system, and with it the reaction performance. Knowledge of the pressure drop is crucial for the cost estimation and pump selection.

In the reactor design an initial estimate of the dispersed and continuous phase slug lengths of the can attained via the following equations:

$$\frac{L_{dispersed}}{D} = 1 + \frac{F_{dispersed}}{F_{continuous}} \tag{1}$$

$$\frac{L_{continuous}}{D} = 1 + \frac{F_{continuous}}{F_{dispersed}} \tag{2}$$

where L is the slug length, F the flow rate and D the diameter of the microchannel. It is important to note that the real slug lengths and their reproducibility are dependent on the mixer geometry, microchannel wall polarity and flow rates of the two phases.

In most cases, the thickness of the thin film between the dispersed slug and microchannel wall is usually below 15 µm. In cases where there is no catalytic reaction occurring on the microchannel walls, it is safe to assume that the thin film gets quickly saturated, and does not significantly contribute to the overall mass transfer. Consequently, the effective surface-to-volume ratio is determined mainly by the slug length and cap surface area. Therefore, initial design estimations of the dispersed and continuous phase slug flow surface-to-volume ratios can be provided via the following equations:

$$S/V_{dispersed} = \frac{2\pi\left(R^2+h^2\right)}{\pi R^2 L_{dispersed} + \frac{2}{6}\pi h\left(3R^2+h^2\right)} \tag{3}$$

$$S/V_{continuous} = \frac{2\pi\left(R^2+h^2\right)}{\pi R^2 L_{continuous} - \frac{2}{6}\pi h\left(3R^2+h^2\right)} \tag{4}$$

Where R is the microchannel diameter, L is the slug length and h is the slug cap height.

The slug flow pressure drop can be estimated using the model developed in chapter 3, which included the influences of the thin film, surface tension and slug length. The pressure drop was considered to consist of the continuous and dispersed phase frictional pressure drop and interface pressure drop contributions (Scheme 1).

$$\Delta P = \underbrace{L\frac{8v_d\mu_d\alpha}{(R-h)^2}}_{\Delta P_{Fr,d}} + \underbrace{L\frac{8v_c\mu_c(1-\alpha)}{R^2}}_{\Delta P_{Fr,c}} + \underbrace{\frac{L}{l_u}C(3Ca)^{2/3}\frac{\gamma}{d}}_{\Delta P_I}$$

$\Delta P_{Fr,d}$ = Dispersed frictional pressure drop
$\Delta P_{Fr,c}$ = Continuous frictional pressure drop
ΔP_I = Interface pressure drop

Scheme 1: Liquid-liquid slug flow model

The curvature parameter, C was found to be dependent on the balance of the inertia and surface tension forces, expressed via the We number. The developed model was tested on water-toluene and ethylene glycol/water-toluene multiphase system, yielding a good agreement with the experimental data with a relative error of 7 %. The thin film between the dispersed slug and hydrophylic wall was found to be of negligible influence on the pressure drop. The pressure drop over the slug interface was found to have a large contribution to the overall pressure drop, with more than 50 % of the overall pressure drop contribution in 250 µm diameter channels being attributed the interfacial pressure drop. Therefore, the information about the slug length and thus the total number of slug interfaces in the channel is crucial for the pressure drop estimation in the slug flow microreactors.

7.3 Fluidic reaction control

The high degree of control over the slug lengths, and with them the surface-to-volume ratios, was exploited to develop a novel methodology termed fluidic reaction control, described in chapter 4. By adjusting the flow rate ratios, the desired slug surface-to-volume ratio can be obtained, therefore allowing for fluidic control of the conversion and selectivity. The concept of fluidic reaction control was demonstrated on the example of the selective phase transfer catalyzed alkylation of phenylacetonitrile to the monoalkylated product. By increasing the aqueous-to-organic ratio from 1 to 6.1 while keeping the same residence time, the conversion increased from 40 to 99 % while the selectivity decreased from 98 % to 80 %, as a result of 97 % larger slug surface-to-volume ratio. Therefore, the optimum flow ratio was identified corresponding to the maximal productivity, while keeping the selectivity at 98 %. As compared to the slug flow microreactor, the batch reactor could yield maximal conversion of 26 %, with selectivity below 90 %. Furthermore, microreactor operated at solvent free conditions, thus eliminating the solvent removal steps from the process. The highly selective alkylation of phenylacetonitrile in slug flow microreactor opens doors for selective multistep synthesis of a large number of pharmaceuticals and agrochemicals (Figure 2).
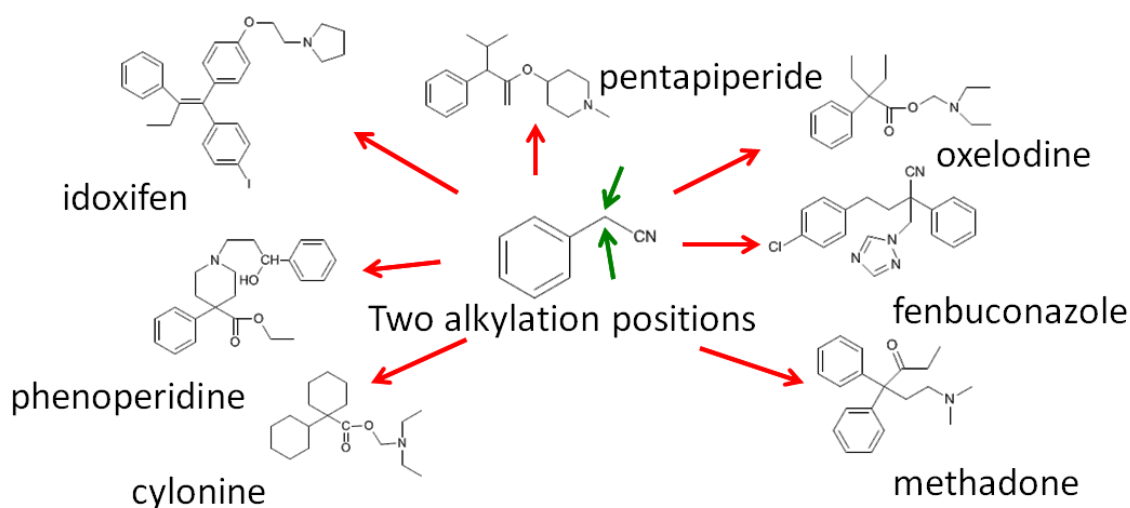
Figure 2: Multi step synthesis of pharmaceuticals and agrochemicals via selective phase transfer catalyzed alkylation.

The concept of slug flow fluidic control was applied on the kinetic study of phase transfer alkylation (chapter 5). Phase transfer alkylation of phenylacetonitrile is one of most complex reactions encountered in industry which combines catalyst mass transfer, interfacial reaction and consecutive reaction steps. The mechanism of the reaction was subject of discussion since 1977, with reaction being interpreted as mass transfer limited or interfacial reaction. Performing the reaction in a slug flow microreactor allowed for elimination of catalyst mass transfer limitations. Furthermore, by carefully choosing the reaction conditions, the reaction occurring at the interface was observed, allowing for the measurement of the interfacial reaction rate constant. The results showed a strong indication that the reaction proceeds via the interfacial mechanism. Therefore it was

demonstrated that performing kinetic studies in a slug flow microreactor allows for a level of reaction control unachievable in conventional stirred tank reactors.

7.4 Scale-up

An internal scaling-up approach was employed to develop a novel interdigital mixer - redispersion capillary microreactor assembly as shown in chapter 6. In single phase or gas-solid microreactors the effective surface-to-volume ratio is determined by the channel diameter. In gas-liquid and liquid-liquid microreactor systems, the effective surface-to-volume ratio is determined by the characteristic dimensions of the flow patterns under which the reactor is operating. For slug flow it is the slug length and the channel diameter, while for the bubbly flow is the diameter of the dispersed phase. By combining the interdigital mixer to generate highly disperse bubbly flow and redispersion capillary to prevent the liquid-liquid bubbly flow coalescence, surface-to-volume ratios as high as $230000 \, \text{m}^2/\text{m}^3$ were achieved, which are more than 1000 times higher than in conventional stirred tank reactors. The maximal throughput of the reactor was 720 g/h, showing that a single capillary reactor can achieve pilot scale production. The novel reactor was applied in the development of micrprocess of phase transfer catalyzed esterification to produce benzyl benzoate. When compared to the conventional process, microprocess phase transfer catalyzed esterification eliminated the use of solvents and bases, allowed for the removal an energy intensive step of distillation, while increasing process safety.

7.5 Future work recommendations

In order to develop more accurate equations for slug flow microreactor design, the complex relationship between the slug length, fluid and microchannel wall properties as well as pressure drop must be further investigated. Currently the effect of the slug cap curvature on the pressure drop is defined via the poorly understood curvature parameter. Furthermore, understanding of the slug cap curvature and its dependence on the surface tension and inertial forces is needed in order to develop better theoretical pressure drop models. Although it is clear that the liquid-liquid flow patterns in microchannels are mainly determined by the surface tension and inertial forces, there is a need for correlations for the flow pattern prediction.

In chapter 6 it was shown that smart design of the microreactor channels and micromixers provides an attractive alternative for the scale-up via parallelization. The application of micromixers such as the StarLaminator 30000 from IMM allows for throughputs up to 30 t/h, opening doors for microprocess bulk chemical production. It is the author's opinion that the combination of the high throughput micromixers and redispersion capillary principle described in chapter 6, would provide a promising alternative to conventional bulk chemical production. One of the bulk processes that is expected to significantly benefit from high throughput microreactor application is the phase transfer catalyzed polycarbonate production, which has a volume of more than 1 million tones per annum. However, in order to achieve microprocess bulk chemical production, further research is needed on the redispersion residence time units, low pressure drop mixers with high

throughput as well as process control. Furthermore, the potential application of microstructured internals such as catalytic solid foams needs to be investigated. Additionally, the cost and accuracy of the current microchannel fabrication methods needs to be improved. Manfucaturing tolerances up to 10 % are common, which can affect the reproducibility of the process performance. Last, significant capital commitment for the industrial micrprocess development is essential due to the high material and equipment costs of microreactor research at t/h throughputs.

List of publications

Journal publications:

Jovanović, J., de Beer, M., Rebrov, E. V., Nijhuis, T.A., Hessel, V., Schouten, J. C. Microreactors as a powerful tool for reaction mechanistic studies: control of liquid-liquid interface of a phase transfer catalysed alkylation. ChemSusChem 2011, submitted.

Jovanović, J., Rebrov, E., Nijhuis, T.A., Hessel, V., Schouten, J.C., Liquid-liquid flow patterns and their extraction application in long capillary microreactors, Industrial & Engineering Chemistry Research, submitted, 2011

Jovanović, J.; Hengeveld, W.; Rebrov, E.V.; Nijhuis, T.A.; Hessel, V.; Schouten, J.C. Redispersion microreactor system for phase transfer catalyzed esterification, Chemical engineering and technology, 2011, 34, 1691.

Jovanović, J.; Rebrov, E.V.; Nijhuis, T.A.; Hessel, V.; Schouten, J.C. Redispersions-Mikroreaktorsystem für eine phasentransfer-katalysierte Veresterung, Chemie Ingenieur Techink, 2011, 83, 1096.

Jovanović, J., Zhou, W., Rebrov, E., Nijhuis, T.A., Hessel, V., Schouten, J.C., Liquid-liquid slug flow: hydrodynamics and pressure drop, Chemical Engineering Science 2010, 66, 42.

Jovanovic, J., Rebrov, E., Nijhuis, T.A., Hessel, V., Schouten, J.C., Phase transfer catalysis in segmented flow in a microchannel: fluidic control of selectivity and productivity, Industrial & Engineering Chemistry Research 2010, 49, 2681.

Conference proceedings:

Jovanović, J., Rebrov, E., Nijhuis, T.A., Hessel, V., Schouten, J.C., Hydrodynamics and pressure drop of the liquid-liquid slug flow in microreactors, Proc. Netherlands Process Technology Symposium, Veldhoven, the Netherlands, 2010.

Jovanović, J., Rebrov, E., Nijhuis, T.A., Hessel, V., Schouten, J.C., Phase transfer catalysis in microchannels: fluidic control of conversion and selectivity, Proc. ISCRE-21, Philadelphia, United States, 2010.

Jovanović, J., Rebrov, E., Nijhuis, T.A., Hessel, V., Schouten, J.C., Phase transfer catalysis in microchannels: fluidic control of conversion and selectivity, Proc. IMRET-11, Kyoto, Japan, 2010.

Jovanović, J., Rebrov, E., Nijhuis, T.A., Hessel, V., Schouten, J.C., Alkylation of benzyl cyanide in a microreactor - Effect of hydrodynamics on reaction rate and selectivity, Proc. NCCC-X, Noordwijkerhout, Netherlands, 2009.

Jovanović, J., Rebrov, E., Nijhuis, T.A., Schouten, J.C., Smart microreactors for phase transfer catalysis, Proc. Netherlands Process Technology Symposium; Veldhoven, Netherlands, 2008.

Jovanović, J., Smart microreactors for phase transfer catalysis, in Young Scientists' Workshop, Mainz, Germany, 2008.

Acknowledgements

About the author

Jovan Jovanović was born on 03-09-1982 in Belgrade, Yugoslavia. After finishing high school in 2001 at 1st Belgrade High School, he pursued his MSc. studies in Organic Chemical Technology and Polymer Engineering at the Faculty of Technology and Metallurgy in the University of Belgrade. In 2005 he graduated within the Oil and Petrochemistry group at the University of Belgrade on the subject of LDPE process development and scale-up. He moved to the Netherlands in 2005, where he obtained his MSc. in Chemical Process Engineering from the Eindhoven University of Technology, on the topic of carbon solid foam catalyst development within the Laboratory of Chemical Reactor Engineering. From 2007 he started a PhD project at the University of Eindhoven in the Netherlands of which the results are presented in this dissertation. Since 2011 he is employed as a process development engineer at Royal Dutch Shell.